Dissertation presented to the Instituto Tecnológico de Aeronáutica, in partial fulfillment of the requirements for the Degree of Master of Science in the Program of Aeronautics and Mechanical Engineering, Materials and Manufacturing Processes Area.

Patrícia Helena de Oliveira Teixeira

APPLICATION OF THE HALL EFFECT FOR THE ASSESSMENT OF THERMAL DAMAGE DUE TO THE GRINDING PROCESS OF GEARS

Dissertation approved in its final version by the signatories below:

Prof. Dr. Jefferson de Oliveira Gomes
Advisor

Prof. Dr. Maria Margareth da Silva
Co advisor

Prof. Dr. Luiz Carlos Sandoval Góes
Prorector of Graduate Studies and Research

Campo Montenegro
São José dos Campos, SP – Brasil
2017

BIBLIOGRAPHIC REFERENCE

DE OLIVEIRA TEIXEIRA, Patrícia Helena. **Application of the Hall effect for the assessment of thermal damage due to the grinding process of gears**. 2017. 113p. Dissertation of Master of Science in Manufacturing Technology – Instituto Tecnológico de Aeronáutica, São José dos Campos.

CESSION OF RIGHTS

APPLICATION OF THE HALL EFFECT FOR THE ASSESSMENT OF THERMAL DAMAGE DUE TO THE GRINDING PROCESS OF GEARS

Patrícia Helena de Oliveira Teixeira

Thesis Committee Composition:

Prof. Dr.	Gilmar Patrocínio Thim	Chairperson	-	ITA
Prof. Dr.	Jefferson de Oliveira Gomes	Advisor	-	ITA
Prof. Drª.	Maria Margareth da Silva	Co Advisor	-	ITA
Prof. Dr.	Anderson Vicente Borille		-	ITA
Dr.	Fábio Wagner Pinto		-	Eins

ITA

To my family

Acknowlegments

To my parents, Roseli and Teixeira, for their inconditional love and guiding hand. For sharing all my dreams. And to my sister, Ana, for the love and laughs in every moment.

To my dearest Anna-Lisa, for her unshakable companionship and all the soothing words during hard times. For making my days lighter. For all the love.

To my advisor, Prof. Jefferson Gomes, for the support and for trusting me on carrying out this research.

To Ronnie Rego, for his constant valuable guidance, technical support and Indiana Jones motivational quotes at the right moments.

To Fábio Pinto, for introducing the opportunity for this research. For the constant guidance and rich technical discussions.

To Christoph Löpenhaus for disposing the facilities of the Werkzeugmaschinenlabor der RWTH Aachen for experimental tests, and for his technical advices along the research.

To Prof. Anderson Borille for his valuables advices.

To the coleagues of the Fraunhofer Institute for Production Technology, Kai Winands and Stefan Gräfe, for disposing their facilities for the laser tests and for their enriching technical discussions and ideas on the subject.

To the Instituto Senai Santos Dumont – São José dos Campos, for kindly disposing their facilities for the grinding tests. In special, to the Prof. Fabiana Passador and Prof. Bosco, for their pacient technical support and openess to the challenges of the task.

To Artur Facciolla, for kindly disposing the facilities of the Companhia Industrial de Peças (CIP) for the workpieces heat treatment. And to Gustavo Camara, for the technical support on the process performance.

To the coleagues of the Inovation Gear Group: André D'Oliveira, Lucas Robatto, André Maia and Nathianne Andrade, for their amazing support and companionship. And to José Luis Moreira, for his significant support, commitment and partnership during the entire research.

To the coleagues of WZL, Deniz Sari, Matthias Ophey, Marco Kampka and Felix Kühn, for the support, advices and technical discussions during the research.

To the dear friends Tabata, Hamilton, André, Eva, Mubarik who, through good laughs and beautiful memories, made difficult moments do not seem so difficult after all.

To CNPq for the financial support.

"But it ain't about how hard ya hit. It's about how hard you can get hit and keep moving forward. How much you can take and keep moving forward!".

(Rocky, Rocky Balboa)

Resumo

Engrenagens são componentes chaves em um sistema de transmissão. Durante seu funcionamento, elas trabalham sob altas condições de carregamentos, e devem suprir requisitos de baixo ruído e alta resistência à fadiga. Tais características funcionais são diretamente afetadas pela integridade superficial, gerada depois do processo de acabamento. Na fabricação de engrenagens, retífica é o processo mais utilizado para acabamento. Entrentanto, o teor abrasivo do processo induz um aumento de temperatura na zona de corte, que, se não controlado, pode gerar queima de retífica. A queima de retífica é um dano gerado pelas altas temperaturas do processo, deteriorando propriedades superficiais. A temperatura atingida no processo define a severidade do dano; a partir de certa temperatura, a integridade superficial é invariavelmente afetada. Ataque de nital e ruído de *Barkhausen* são métodos atualmente utilizados pela indústria para detecção desses danos, por exemplo. Entretanto, tais métodos apresentam significativas desvantagens para a aplicação industrial. Devido a essa lacuna tecnológica, este trabalho investiga a proposta de um método de escaneamento magnético superficial através do efeito Hall, sem a utilização de magnetização do componente. Para a investigação do método, um protótipo foi construído. Em uma primeira fase, a influência do protótipo nas medições é investigada, a respeito da precisão de posionamento, perfil de contato entre a sonda Hall e a superfície medida e influência de sinais externos. Em seguida, o método é investigado em relação à habilidade de detectar queima de retífica. Três níveis de dano são simulados pelo processo a laser, entre eles danos com e sem transformação de fase do material. A medição dos danos com mudança de fase usando o novo método mostram uma alteração no sinal do campo magnético remanescente, devido a presença da diferente fase do material. Essa alteração no sinal magnético destaca a posição do dano, indicando sua presença na superfície da peça; além disso, a alteração detectada pela sonda Hall está de acordo com a teoria micro-magnética, que estabelece uma correlação entre o campo magnético remanescente e a dureza do material. O dano sem transformação de fase apresenta alteração no estado de tensão residual, de compressivo para trativo. O método *Hall* detecta uma alteração no sinal magnético da peça, atribuída à presença do novo estado de tensão residual. O sentido dessa alteração não segue a teoria micro-magnética estabelecida, comportamento parcialmente explicado pelo sentido de magnetização favorável ao sentido do estado de tensão residual compressivo. O estudo mostrou que o novo método *Hall* é robusto o suficiente para detecção de queimas de retífica com e sem transformação de fase.

Abstract

Gears are a key component of a transmission system, and have been widely employed in motion transmission systems. During operation, they face heavy loads conditions, low noise and long-life requirements. These functional characteristics are highly affected by the surface integrity, generated after the finishing process. In most gears manufacturing chain, finishing is performed by the process of grinding. However, the process abrasive characteristic induces an increase of temperature in the working zone, which, under non-controllable conditions, might lead to grinding burn. Grinding burn is a damage generated by high temperatures, which induces surface properties deterioration. Based on the temperature reached in the process, the damage is more or less severe, but, ultimately, it will affect the material surface integrity. Methods for grinding burn detection have been used in the industry, such as nital etching and *Barkhausen* noise. However, these methods present significant disadvantages that, at a certain extent, make them non-reliable for industrial application. Due to this technical gap, a method of magnetic surface scanning by means of Hall effect and without the use of magnetization, is proposed. For the analysis of the new method, a prototype was built. On a first phase, the influence of the prototype on the measurements is investigated, regarding the equipment positioning precision, Hall probe contact profile and environmental factors. Next, the ability of the new method to detect grinding burn is evaluated. Three degrees of thermal damage are simulated by laser process, including damages with and without phase alteration. The Hall method scanning of damages with phase transformation shows an alteration in the remanence magnetic signal in the workpiece due to the presence of the new microstructure phases. This signal alteration highlights the position of the damage, indicating its presence in the workpiece surface; in addition, the alteration detected by the probe is in accordance with the micro-magnetic theory, which establishes a correlation between the remanence magnetic field and material hardness. The damage without phase transformation presents an alteration in the residual stress state, from compressive to tensile. The new *Hall* method detects an alteration in the workpiece magnetic signal, attributed to the presence of the new residual stress state. The direction of this alteration is not in accordance to the established micro-magnetic theory, which is partially explained by the magnetization direction in favor of compressive residual stresses direction. The research showed that the new *Hall* method is robust enough for measurements of grinding burn with and without phase transformation.

List of Figures

List of Tables

Contents

1 Introduction

The continuously increasing claims of the transmission market over the years are responsible for the increase in the requirements for gears, leading to the need for improvements in manufacturing processes (GORGELS; SCHLATTMEIER.; KLOCKE, 2006). Gears have been widely used in mechanical power and motion transmissions, due to its key role in the transmission system (QIAO *et al*, 2017). The demands for higher manufacturing and surface quality by the advancing technical and precision aspects of modern gears, increase the number of gears to be finished (COMLEY, 2005; GORGELS; SCHLATTMEIER.; KLOCKE, 2006).

Surface finishing in gears can be performed by several processes, such as shaving, lapping, honing and grinding. Each of them contains advantages and limitations that make them suitable according to the gears specifications (HASHMI, 2017). Grinding is the most commonly used finishing processes, due to its unique main characteristics, such as (1) High performance with high stock removal rate; (2) high dimension and contouring accuracy in profile and lead; (3) correction of thermal distortions; (4) improvement of surface quality and micro-geometry (SHAH, 2012; HASHMI, 2017).

Regarding surface quality, it is well recognized that surface integrity of machined components has a significant impact on their service performance (ZHOU *et al*, 2016; QIAO *et al*, 2017). The nature of the surface determines the performance of the gear, directly impacting on crucial operational characteristics, as shown in Figure 1.1
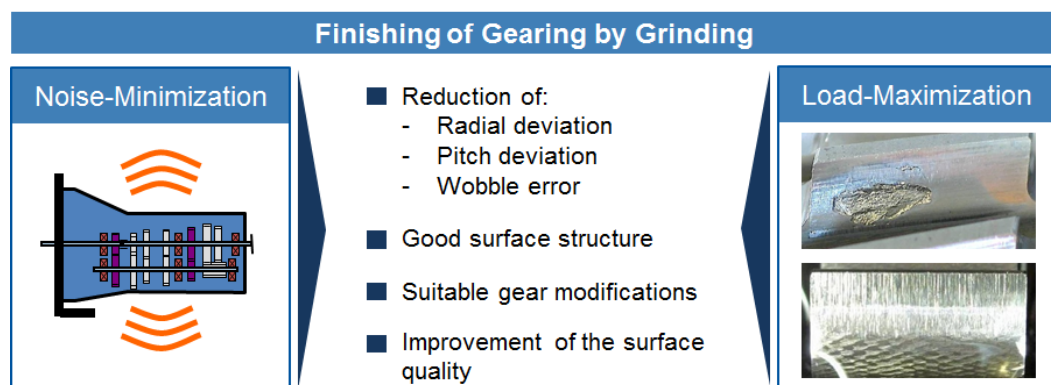
Figure 1.1 - Operational characteristics of gears due to finishing process (AHMAD, 2017; KAMPKA, 2017; KONOWALCZYK, 2017).

The concept of surface integrity was first introduced by Field and Kahles (1964), defining it as the 'inherent or enhanced condition of a surface produced by machining processes or other surface generation operations'. Along the years, surface integrity is associated with mechanical and phase alterations of the surface layers (MALKIN; GUO, 2008; ZHOU *et al*, 2017). For grinding, the aspects of surface integrity are partially correlated to the thermal damage caused by the high temperatures that can be induced during process (MALKIN; GUO, 2008). Due to the nature of the grinding kinematics, nearly the whole consumed energy during the process is frictional. The distribution of this energy and heat during the abrasive cutting is mainly divided into four parts: (1) grinding wheel; (2) lubricant; (3) chip; (4) workpiece (KARPUSCHEWSKI; BLEICHER; BEUTNER, 2011; KONOWALCZYK, 2017). For the research developed by this study, the fraction of energy going to the workpiece is the only relevant one. This energy generates heat in the work zone, increasing the temperature of the workpiece surface. If the temperature achieves critical high values, the surface properties deteriorate, leading to the thermal damage known as grinding burn (MAYER *et al*, 2002; MALKIN; GUO, 2008; KARPUSCHEWSKI; BLEICHER; BEUTNER, 2011). Based on the temperature reached during grinding, thermal damage can be classified into 4 categories: (1) Oxidation; (2) Thermal softening; (3) Tensile residual stresses; (4) Re-hardening, where the fourth topic is the most severe one (OPOKU, 2005; SUNDERRAJAN, 2012). Each degree of burn will introduce a specific alteration in the material surface property, which will affect the gear's operation, which often subjected to severe working conditions and under repeated loading and vibrations (SHAH, 2012).

Ultimately, grinding burn is a big concern to manufacturers since it might reduce the fatigue life of the gears by the introduction of tensile residual stresses, change of material phase, introduction of micro-cracks and change the material hardness (DAVIS, 2005; OPOKU, 2005; MALKIN; GUO, 2008; ROWE, 2014). These phase alterations caused by the thermal damage are highly unwanted, since they can lead to component malfunction and, eventually, breakage during operation. In his work, Klocke (2004) stated that the number of failures in gears has increased, especially in case hardened and large module gears. In the field of wind turbines, the main cause of damage is concentrated in the main gear transmission (KONOWALCZYK, 2017). For both examples, the damages are partially related to the grinding process in which the gears are submitted to (KLOCKE; SCHLATTMEIER, 2004). Therefore, in order to avoid the component failure, any phase alteration in the material caused by grinding must be detected by any kind of suitable testing (KARPUSCHEWSKI; KNOCHE; HIPKE, 2008; SANTA-AHO *et al*, 2012).

However, due the process kinematics, it is not trivial to predict the presence of thermal damage during grinding. Therefore, in the face of the possibility of these damages to happen, a robust quality and process control is required (KARPUSCHEWSKI; BLEICHER; BEUTNER, 2011). The methods for grinding burn detection must be not only efficient, but suitable to the industrial environment. Nowadays, the most used method for this application is the nital etching (DAVIS, 2005; KARPUSCHEWSKI; KNOCHE; HIPKE, 2008). Although the method is widely used in the industry, it presents main disadvantages such as destructive and high subjectivity character, which might lead to false results (KARPUSCHEWSKI; BLEICHER; BEUTNER, 2011). Several other methods, shown in Figure 1.2, can also be applied for detecting grinding burn; however, in general they always present drawbacks such as cost, time, complexity, subjectivity or the use of hazardous chemicals (CEURTER; SMITH; OTT, 2002).
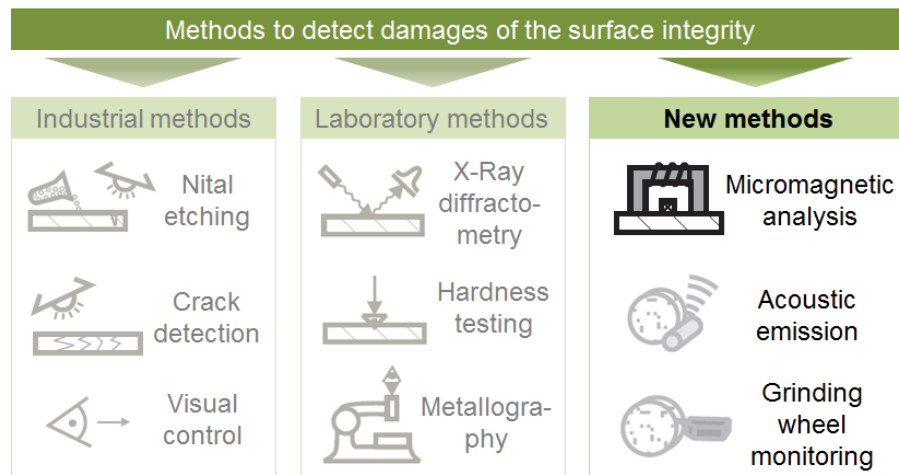
Figure 1.2 - Usual and new methods to detect damages of the surface integrity (KARPUSCHEWSKI; BLEICHER; BEUTNER, 2011).

The disadvantages of the current measurement techniques bring the necessity of a new method that could better support the requirements of the grinding burn detection for the industry. Between the possibilities of new methods, highlighted in Figure 1.2, the micro-magnetic methods are the most interesting ones, due to characteristics such as objective, fast and relatively non-destructive measurements (NESLUSAN *et al*, 2017). For these reasons, the magnetic *Barkhausen* noise (MBN) technique has become widely employed and many researches have been conducted to understand its advantages and limitations (KARPUSCHEWSKI; BLEICHER; BEUTNER, 2011; NESLUSAN *et al*, 2017). Although

the MBN technique possess interesting characteristics, it also faces some challenges, since the signal is very sensitive to all material properties like hardness, structure and residual stresses. This makes the calibration and analysis of results a very time consuming and delicate process (KARPUSCHEWSKI; KNOCHE; HIPKE, 2008). Due to these technical gaps left for the current methods, a new micro-magnetic measurement technique is presented in the current work. By means of the *Hall* effect, the method aims to fulfill the gaps left for other methods, for the case of grinding burn detection in gears.

Fundamentally, the *Hall* effect is a phenomenon that describes physical effects arising in matter carrying electric current in the presence of a magnetic field (POPOVIC, 2004). Due to this, when a magnetic field is applied perpendicularly to the *Hall* probe, a small voltage appears across the probe. The small voltage detected by the probe can be correlated to the magnetic field applied, making the *Hall* effect a phenomenon able to measure the magnitude of magnetic fields. This possibility is very interesting for the measurement of electromagnetic properties of materials (KARIMIAN *et al*, 2014). Such properties are highly influenced by factors such as material structure, mechanical stresses, residual stresses, presence of impurity atoms, dislocations, etc. (YIN; PEYTON; STRANGWOOD, 2007; KARIMIAN *et al*, 2014). Consequently, any alteration in these factors will cause a variation in the electromagnetic properties of a certain material, which could be detected by a magnetic method, such as a *Hall* probe.
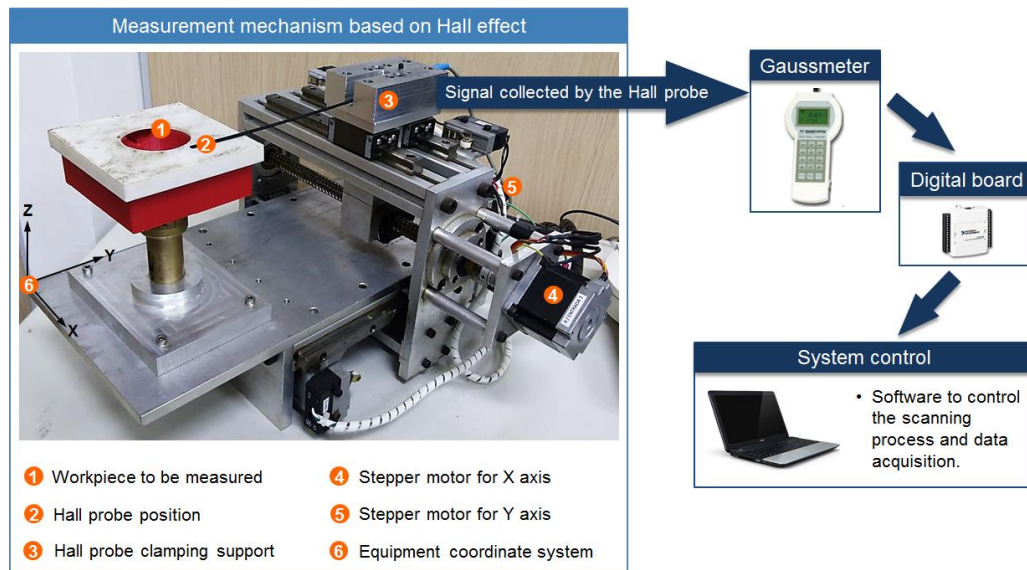
Figure 1.3 - Measurement equipment of scanning with a *Hall* probe developed for this study.

As already stated, a thermal damage on the surface of a component might cause phase alteration and change from compressive to tensile residual stresses. Therefore, the presence of grinding burn causes an alteration in the electromagnetic properties. It is assumed this alteration is measurable by means of an electromagnetic method, and for the current work, a *Hall* probe is used. However, the correlation between electromagnetic properties of a material and its microstructure is a very complex subject (YIN; PEYTON; STRANGWOOD, 2007). In order to use this phenomenon for detection of grinding burn, a careful study must be conducted. The study aims to understand the role of specific alterations in the material generated by the thermal damage, on the magnetic signal measured by the *Hall* probe on the component surface.

The first step for the conduction of the study was the construction of a measurement mechanism, allowing the *Hall* probe to move regularly along the workpiece surface, scanning it. The mechanism is shown in the Figure 1.3, with a description of its main components. The gear flank is represented by the surface of a steel cylinder, where the grinding burn is inducted.

The current research aims to analyze the advantages and limitations of the new method for the detection and characterization of different degrees of grinding burn. For this goal, a complete analysis of the method must be performed, covering not only the analysis of surface integrity, but also the role of the measurement mechanism built on the results measured.

2 Objective

2.1 General

To investigate which material properties arise from the thermal damage caused during grinding process, influencing the magnetic flux of a metal workpiece, by means of *Hall* effect.

2.2 Specific

- (1) *System robustness*: To investigate the influence of the measurement mechanism architecture and environmental factors on the measurement results;
- (2) *Thermal damage with phase transformation*: To determine if different material structures, representing different thermal damage levels, can modify the magnetic flux of the material to a point where the variation is detectable with a *Hall* probe;
- (3) *Thermal damage without pahse transformation (residual stresses)*: To determine if a thermal damage with same microstructure can modify the magnetic flux of the material to a point where the modification is detectable with a *Hall* probe;

3   Literature Review

3.1   Gears manufacturing processes

In several areas, the use of gears is the most suitable solution available for movement transmission due to its relatively low costs and high accuracy (DAVIS, 2005). During operation, they can be exposed to extremely high loads, which requires a careful control of their quality. In this context, the surface layer plays a main role in the component fatigue life, since it is the region which directly interacts with most loads, and, therefore, where fatigue failure begins (KARPUSCHEWSKI; BLEICHER; BEUTNER, 2011; SANTA-AHO *et al*, 2012).

Along the manufacturing chain of gears, several processes can be used. Each of them, according to its own technical limitations, generates a different surface quality, more or less refined. In a manufacturing chain, the processes which provide more refined surface quality are performed last (KLOCKE, 2009)

The Figure 3.1 describes an example of a manufacturing process chain for a general gear, highlighting the finishing processes in the end of the chain.
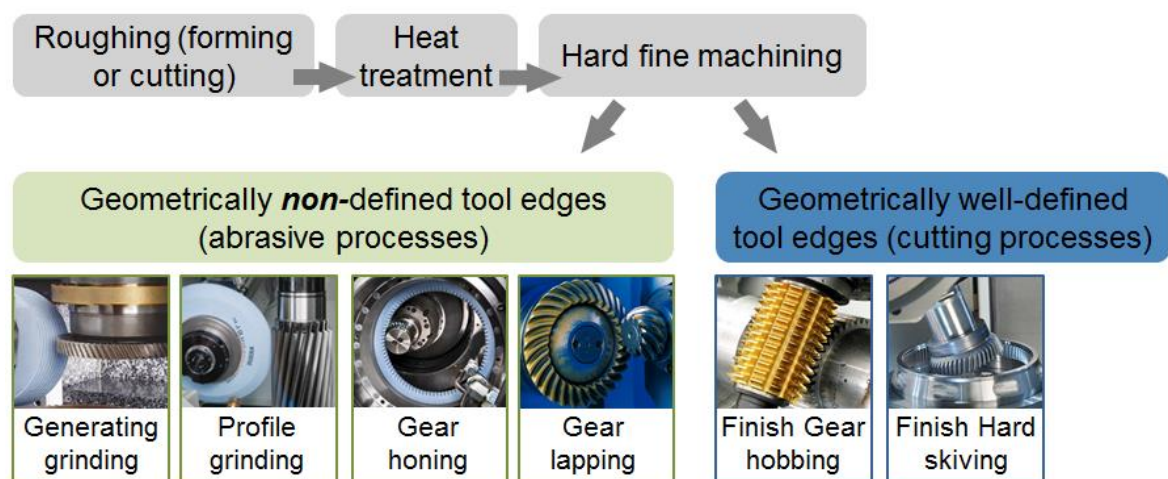
Figure 3.1 - Gear manufacturing process chain (KARPUSCHEWSKI; KNOCHE; HIPKE, 2008).

The processes in the manufacturing chain of gears can be divided into two general categories: rough machining (gear cutting) and finishing (high precision machining). These steps are, within the manufacturing chain, divided by the heat treatment (DAVIS, 2005).

The rough machining processes are responsible to cut the material, leaving the desired teeth profile. Next, most steel gears go through the process of heat treatment, which is used in order to enhance its surface properties such as hardness and residual stress. However, undesirable diametric changes occur during the process, as an outcome of the high thermal loads and the consequent phase transformations (DAVIS, 2005; BUGLIARELLO *et al*, 2010). Finishing processes are located at the end of the manufacturing chain because they are responsible not only for correcting the form errors induced by previous processes, such as the heat treatment, but ultimately for improving the surface finishing and accuracy of the gear (DAVIS, 2005). The grinding process, which is the main topic of the current study, is categorized as a finishing process. The next topics will describe important aspects of this process regarding gears.

3.2   Gears grinding processes

By definition, grinding is an abrasive machining process which uses high-speed abrasive wheels to remove small layers of material, which can amount only several hundredths of a millimeter (ROWE, 2014; DAVIS, 2005).

According to Davis (2005), grinding is recommended when the material has hardness higher than 40HRC and dimension accuracy is required for the component. For the case of gears in general, after heat treatment the surface hardness in the flanks reaches values between 58HRC and 62HRC (DAVIS, 2005). Since dimension accuracy is an important requirement in gears manufacturing, grinding becomes a suitable finishing process. The geometry of the teeth flank of a gear can be very complex, which demands a specific grinding process kinematics. Nowadays, the process of grinding for gears can be distinguished primarily in two categories: generating and profile grinding. Inside these two categories, other sub categories such as continuous and discontinuous process are done (KARPUSCHEWSKI; KNOCHE; HIPKE, 2008). Figure 3.2 describes each of these categories.

The gear grinding processes described in Figure 3.2 are distinguished from one another by geometry and kinematics. However, they still hold several similarities, such as

working with high cutting speeds and always with intensive use of lubricants (KARPUSCHEWSKI; KNOCHE; HIPKE, 2008).

- **Generating grinding**

For this type of grinding, the movement is tangencial to the gear evolvente.

Continuous: the grinding worm tool moves back and forward in the direction parallel to the gear axis. It grinds the teeth flanks, providing position (steps) and teeth profile according to the quality requirements specified. The advantage of this method is to be able to grind large lots. On the other hand, the tool costs are high, comparing to other methods (MAZZO, 2013).

Discontinuous: In this process, the tooth flank of a spur gear is approximated stroke by stroke with a double conical grinding wheel, by means of polygonal small cuts. Although it is a flexible process, it is less productive compared to other more competitive methods (KARPUSCHEWSKI; KNOCHE; HIPKE, 2008).
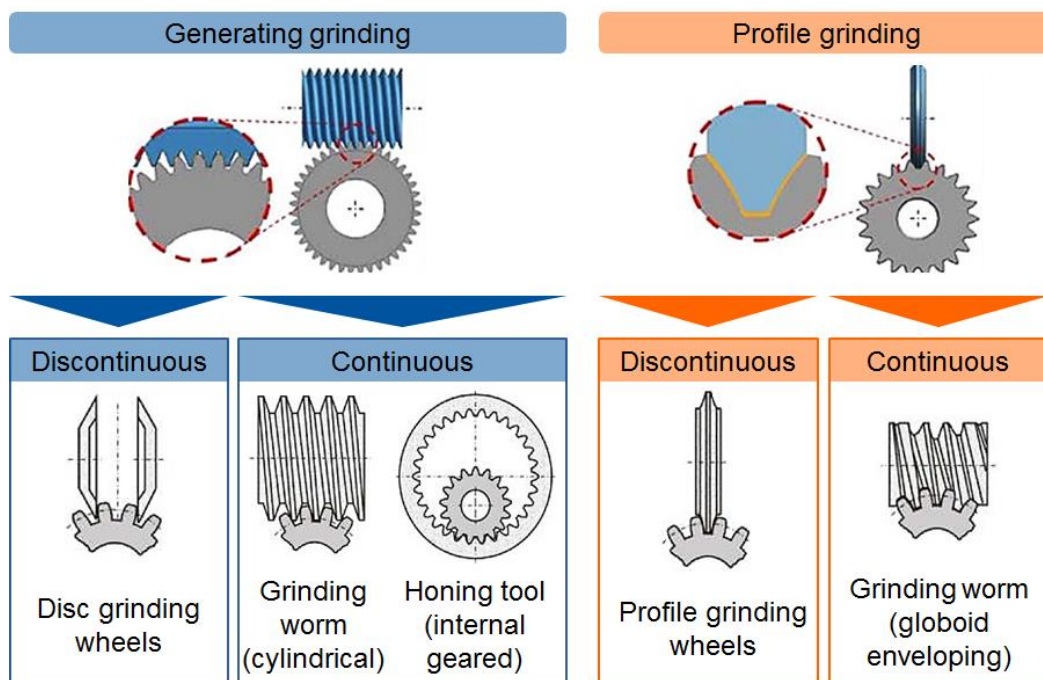
Figure 3.2 - Classification of grinding processes for hard gear finishing (KARPUSCHEWSKI; KNOCHE; HIPKE, 2008; BRECHER *et al*, 2014).

- **Profile grinding**

For this type of grinding, the tool has the shape of the space between the teeth, and the movement is perpendicular to the gear evolvente. The operation is made tooth by

tooth, and an index system is responsible for the position of the tool in the space to be ground. Although this is a slower method compared to the generating grinding, it provides better quality in the teeth profile and low costs of the working tool (MAZZO, 2013). This type of grinding is divided into continuous and discontinuous.

Continuous: for this type of grinding, a globoid worm shaped grinding wheel, surrounding a part of the workpiece is used. This tool can only be used for one specific kind of gear geometry, which makes the process only suitable for serial or mass production (KARPUSCHEWSKI; KNOCHE; HIPKE, 2008).

Discontinuous: the tool in this case has usually the profile identical to the profile of the workpiece in normal section, and the tooth flanks can be either ground separately or joint, depending on the number and set-up of the wheel (KARPUSCHEWSKI; KNOCHE; HIPKE, 2008).

More important than the type of grinding used for gears manufacturing, it is important to understand that grinding is a finishing process which ultimately provides significant functional aspects that will have an impact on their operation (ZHOU *et al*, 2016; QIAO *et al*, 2017).

3.2.1 Ground surface

Fundamentally, grinding process can ensure superior quality regarding accuracy of dimensions, form and surface texture (ROWE, 2014). For the current work, another aspect of the ground surface is more important: surface quality.

The integrity of the material at the machined surface is of vital importance in many situations (ROWE, 2014). The characteristics of the surface integrity after grinding can influence the functionality of the gears mainly in two aspects: noise level and load capacity. Characteristics such as type and magnitude of residual stresses, plastic deformation, hardness alterations and teeth microgeometry, that can come from the grinding process, have direct influence on the loading capacity, wear behavior and fatigue resistance (SOSA *et al*, 2007; KLOCKE, 2009). The grinding also influences characteristics such as surface roughness and pitch deviation, which are directly correlated to the noise excitation behavior. (KLOCKE, 2009).
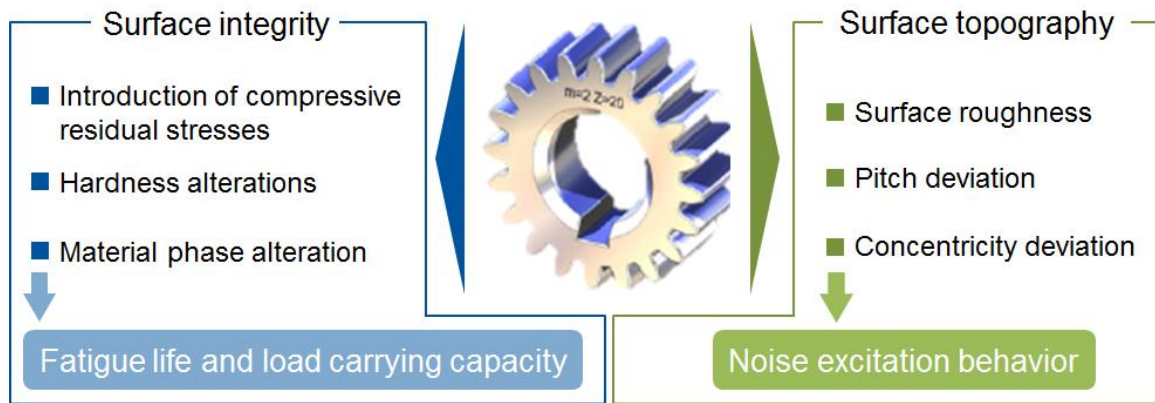
Figure 3.3 - Gear functional characteristics due to grinding finishing (KLOCKE, 2009).

Figure 3.3 shows in more details the two main operational characteristics relevant in the gears performance, and how they are affected by surface integrity and surface quality. Surface integrity and surface topography are two characteristics used to define the surface quality (MALKIN; GUO, 2007). For gears, each of them influences different operational functions and, therefore, it is important to have these parameters under control during grinding process. A brief description of topography is required and presented in the next topic. Since this study aims to study a new method of the assessment of surface integrity, this subject will be explained in detail in the topics in the pages ahead.

3.2.2 Surface Topograph

Surface topography is usually characterized by roughness, and it relates to the geometry of surfaces (MALKIN; GUO, 2008). In the case of grinding, surface is formed mostly of overlapping scratches caused by the performance of the abrasive wheel into the workpiece surface.

Measurements of surface topography are made along and across the grinding direction.

Roughness across grinding direction can be referred to as macro-roughness, and it suffers the influence of possible defects in the abrasive wheel. Normally, adjacent peaks and valleys, across grinding direction are closer to each other in comparison to measurements made in grinding direction. Roughness measurements taken along the grinding direction are referred to as micro-roughness, it provides information relating to grit material interface and, ultimately, the capability of the grinding process (COMLEY, 2005; MALKIN; GUO, 2008).

In gears, there are two main regions where roughness should be measured: teeth flanks and root. The parameters normally used to characterize roughness are Ra and Rz.

The profile of surface topography is mainly defined by the needs and operational characteristics of the gears application (MAZZO, 2013). Parameters of grinding process, such as type of wheel, wheel and workpiece speed and feed rate, play an important role in the workpiece final topography. These parameters are defined according to the topography requested by the gear project. DIN 3961

The quality of the teeth regarding to its roughness is expressed by indexes, according to the DIN norm (MAZZO, 2013). The indexes have values which go from 1 to 12, the smaller means the better quality and tighter tolerances (DIN 3961). Usually, the indexes can be classified according to gears operation or finishing processes, according to the Figure 3.4.

Operation	Examples	DIN Quality number	Manufacturing / Finishing process
Comercial applications	• Pumps • Clocks • Slow speed machineries	12	Investiment casting, Injection molding, Extrusion
		11	Die casting
		10	Milling, cold drawing, Stamping, powder mettalurgy
Precision applications	• Aircraft engines • Turbines • Cameras • Automatic transmission system • High speed machineries	9-10	Rolling, Shaping, Hobbing
		8-9	Rolling, Shaving, Honning, Lapping, Grinding
		7-8	Shaving, Honing. Lapping, Grinding
		6-7	Shaving, Grinding
		4-6	Grinding
Ultra-precision applications	• Precision instruments • Military navigations	3-4	Grinding
		1-2	Grinding with extra care

Figure 3.4 - Quality indexes according to the gears operational functions (MAZZO, 2013).

Surface integrity is the second surface quality characteristic, and it is associated with mechanical and microstructure alterations at the surface layer (MALKIN; GUO, 2008). In grinding, this characteristic is associated to thermal damage caused by the high temperatures in the process (MALKIN; GUO, 2007).

3.2.3 Surface integrity: thermal damage – grinding burn

The grinding process not only generates a more refined surface and corrects geometry errors. Also, when performed under low-temperature regime, it produces compressive residual

stresses, which is highly required for its characteristic of improving fatigue life (ROWE, 2014). However, if the grinding conditions are not correctly defined, the process can achieve high temperatures, compromising the surface integrity of the part. Depending on the temperature achieved, thermal damages occur, which are known, in this situation, as grinding burn (MALKIN; GUO, 2008).

At first, heat is generated because almost the whole consumed energy is frictional, due to the nature of the grinding process kinematics (KARPUSCHEWSKI; BLEICHER; BEUTNER, 2011). The heat generated by the process will be partitioned into four directions: lubricant (if the process is not performed under dry conditions), tool (wheel), chip and the workpiece (LIAO; LUO; YANG, 2000; COMLEY, 2005). For the purpose of this work, the fraction of energy that goes into the workpiece is the main concern, since it is the responsible for the gear surface integrity. In definition, grinding burn is an overheated localized area in the surface of the work zone (KARPUSCHEWSKI; BLEICHER; BEUTNER, 2011; SUNDARRAJAN; 2012). The visible burn is characterized by bluish temper colors on the workpiece surface, a consequence of oxide-layer formation. Usually, the temper colors are removed by spark-out at the end of the grinding cycle. However, the absence of temper colors on the ground surface does not mean that workpiece burn did not occur (MALKIN; GUO, 2008).

Depending on the temperature reached in the process, the burn will present a specific characteristic. The degree of burn can be characterized in four diferent categories, as specified below. As the temperature increases, the degree of burn becomes more severe, iniciating with the degree of Oxidation, until the most severe, named Re-hardening (SUNDARRAJAN, 2012).

1. *Oxidation burn*
2. *Thermal softening*
3. *Residual tensile stress*
4. *Re-hardening burn*

1. *Oxidation burn*

It is considered the first stage of burn, where a discoloration of workpiece appears due to a thin surface layer of oxidized metal and coolant (SUNDARRAJAN, 2012). Although a bluish temper color might appear at the surface, the part does not suffer from any metallurgical damage, and the layer can be removed by spark-out at the end of the grinding cycle (MALKIN; GUO, 2008; SUNDARRAJAN, 2012).

2. Thermal softening

The grinding in gears is performed when the material is already at hardened state. Excessive temperatures may induce transformations including tempering, also known as thermal softening or temper burn (WOJTAS; SUOMINEN; SHAW, 1998; MALKIN; GUO, 2008). At one point, the temperature increases up to a value sufficiently high to cause diffusion of the carbon in the steel (ROWE, 2014). Although workpieces do not always show burn marks or temper colors at the surface, it is possible to detect this damage by the alteration it causes in surface hardness, as shown in Figure 3.5 (ROWE, 2014). According to Figure 3.5, the damage affects the surface until a certain point in depth, where, from there on, the hardness is maintained to its original value.
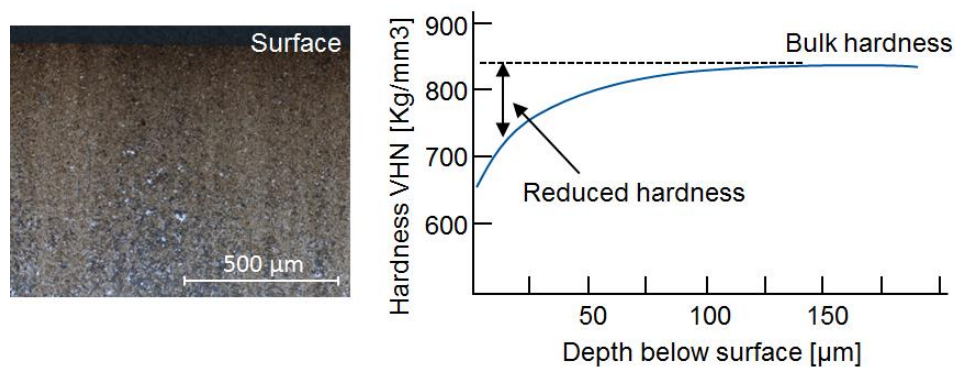
Figure 3.5 - On the left, the section showing temper damage to a hardened and tempered steel and on the right, sub-surface softening due to temper damage (ROWE, 2014).

The minimum temperatures to cause temper damage depends on the gear material alloy as well as the heat treatment which the material has been through. Rowe (2014) affirms that temperatures of the order of 450ºC are sufficient to cause temper damage. In general, the range of temperature for this damage is between 400 and 700°C. As an example, the temperature required to cause temper burn in hardened steels must be higher than the tempering temperature (WOJTAS; SUOMINEN; SHAW, 1998). The depth affected by the damage will highly depend on the temperature reached during grinding, but it is usual that this depth goes from a minimum of 100µm to higher values (ROWE, 2014). In opposite to the oxidation burn damage, where the affected layer can be removed during spark-out, the affected layer of thermal softening damage is too big to perform the same. The characteristic of temper burn is an alteration in the material properties, even though the workpieces do not

necessarily exhibit mark or temper colors at the surface (ROWE, 2014). The responsible factor for this material alteration is the diffusion of carbon into the material and, in the case of hardened steels, the transformation of tempered martensite into overtempered martensite.

3. *Residual stresses*

   In its definition, residual stress is the stress which exists in a solid body without the application of external forces or any other sources of load (BHADESHIA; WITHERS, 2001; TOTTEN; HOWES; INOUE, 2002). The phenomenon was first defined by Prof. Heyn, in 1914, where he referred to residual stresses as ''internal strains'' (REGO, 2016). The grinding process will always lead to residual stresses in the vicinity of the finished surface, since they are induced by non-uniform plastic deformation near the workpiece surface (MALKIN; GUO, 2008). The final state of residual stress in a ground surface is the result of the interaction between thermally induced stress and deformation. The contribution of temperature in the process, as well as the mechanical deformation will define the profile of the residual stress state of the part (MALKIN; GUO, 2007; ROWE, 2014).
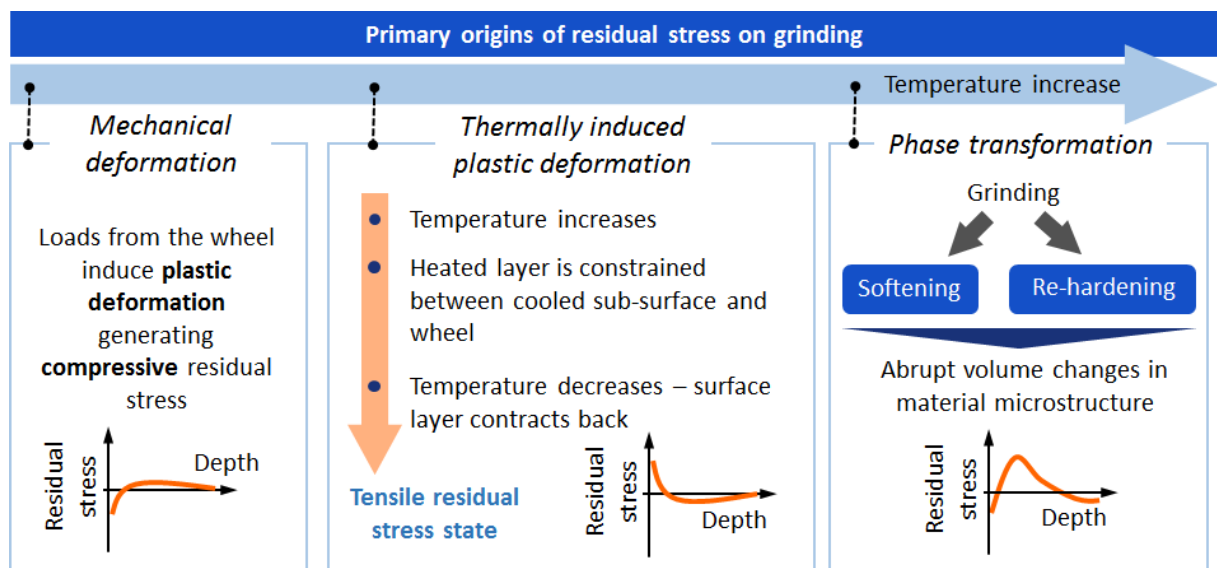
Figure 3.6 - Steps of formation tensile residual stress induced by mechanical and thermal inputs (CHEN; ROWE; McCORMACK, 2000; BALART *et al*, 2004; MALKIN; GUO, 2008).

   Figure 3.6 describes the steps in the formation of the residual stress states of ground gears, taking into consideration the contribution of temperature.

(I) **Mechanical deformation:** Hertzian loads coming from the wheel induce plastic deformation to the piece, giving compressive residual stresses. At this point, there is no influence of temperature, and the final effect can be linked to that of shot peening. At the bottom left of Figure 3.6 stands a graphic with the predicted residual stress profile. The area under the curve, below the X axis represents the compressive residual tension expected for this mechanical input (CHEN; ROWE; McCORMACK, 2000; BALART *et al*, 2004; MALKIN; GUO, 2008).

(II) **Thermally induced plastic deformation:** At this point, the temperature input is considered. When grinding at high temperature, the surface layer is rapidly heated but the expansion of the hot material is partially constrained by cooler subsurface material. With increasing temperature, the material yield stress reduces, leading to plastic deformation. During the cooling, after the grinding heat passes, the plastic deformed material contracts, generating the final tensile residual stress state. Residual compressive stresses arise deeper in the material, to ensure mechanical equilibrium, but in much smaller magnitude than the residual tensile stresses. This profile is shown on the graphic at the bottom left of the second box in Figure 3.6 (CHEN; ROWE; McCORMACK, 2000; BALART *et al*, 2004; MALKIN; GUO, 2008).

(III) **Phase transformation:** transformation from softening to re-hardening, involving abrupt volume of changes, generating tensile stresses in the untempered martensite surface layer (CHEN; ROWE; McCORMACK, 2000; BALART *et al*, 2004).

The control of the residual stress state is made if the maximum grinding temperature is kept under the transitional temperature from compressive to tensile residual stress, depending on the workpiece material (CHEN; ROWE; McCORMACK, 2000).

4. Re-hardening

The damage is characterized by a thin layer of hard, brittle material and it occurs when the grinding temperature exceeds the austenizing temperature. During the process, the reaustenized material is rapidly cooled, and untempered martensite is formed, a brittle and hard material (MALKIN; GUO, 2008; SUNDARRAJAN, 2012; ROWE, 2014).
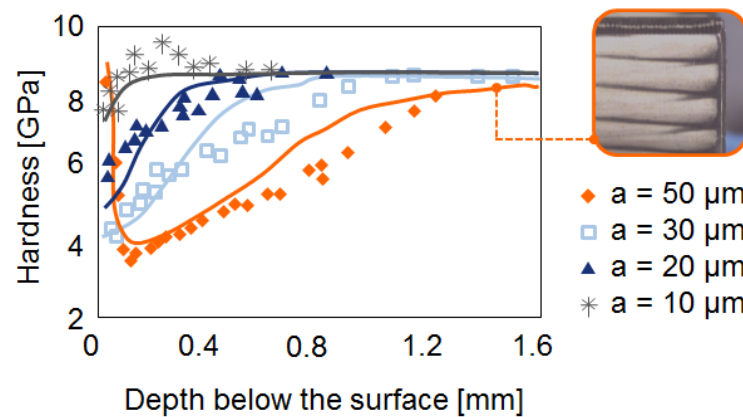
Figure 3.7 - Hardness profile through depth for different grinding parameters (MALKIN; GUO, 2008; SCHWIENBACHER, 2008).

Figure 3.7 shows hardness curves for materials grounded under four different values of feed rate, represented by a. In the maximum feed rate, a = 50 µm, the process is aggressive and the temperature rises until a point where re-hardening occurs. In this case, it is possible to see that the hardness is greater than in the other parameters, but only at the surface, where the phase transformation happens.

3.3 Correlation between material ferromagnetic properties and thermal damage

3.3.1 Magnetic domains

Currently, well-known measurement techniques based on ferromagnetic properties are being used, as a non-destructive alternative to measure specific material characteristics, such as *Barkhausen* noise, Eddy Current and 3MA (GOLDMAN, 1999). For the application of grinding burn detection, *Barkhausen* noise technique is the most commonly used and it will be better explained further in the current study. The usage of magnetic techniques to detect thermal damage is significantly depended on the ferromagnetic characteristics as well as the microstructure of the material.

The development of the understanding of ferromagnetic properties, especially in micro-magnetic fields, gives a powerful tool for the explanation of interaction between lattice imperfections and internal stresses with *Bloch*-walls (THEINER, 1997). In order to understand this relation, first it is necessary to explain some basic important concepts about

the micro-magnetism in materials. The micro-magnetic theory purposes the existence of *Bloch* walls, and correlates it to lattice imperfections, internal stresses and microstructure characteristics, a very important point for the understanding of the new method proposed in this work. (THEINER, 1997; HÜBSCHEN *et al*, 2016).
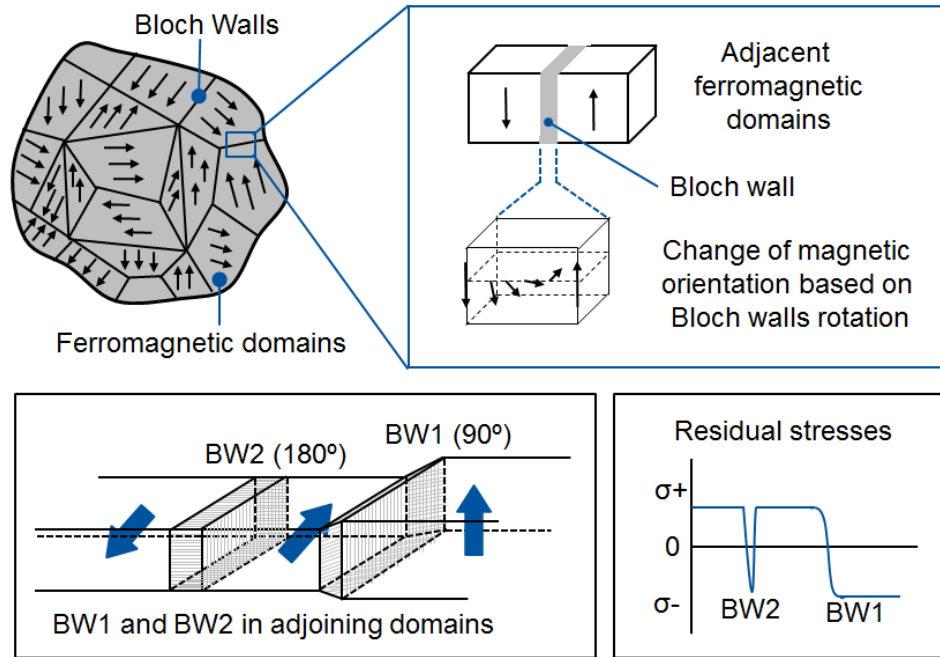
Figure 3.8 - Upper, description of micro-magnetic grains and the *Bloch* walls; lower, visualization of the magnetic characteristics of each type of *Bloch* walls (THEINER, 1997; KARPUSCHEWSKI; BLEICHER; BEUTNER, 2011).

The micro-magnetic theory explains that ferromagnetic materials consist of small finite regions, spread in the material volume, with uniformly oriented magnetic moments, called magnetic domains (DOBMANN, 2011; KARPUSCHEWSKI; BLEICHER; BEUTNER, 2011, TAGLIARI, 2012). The left side of Figure 3.8 shows an example of magnetic domains. Each of these domains becomes a magnet formed of smaller magnets, and their dimensions are in the order of micrometers. They are formed primarily to reduce magneto static energy, which is the potential energy contained in the field lines connecting north and south poles of the material. Size and shape of a domain are determined by the minimization of several types of energies, such as: (1) Magnetostatic; (2) Magnetocrystalline anisotropy; (3) Magnetostrictive and (4) Domain wall (GOLDMAN, 1999). The change of magnetization of a domain and, therefore, changing of magnetization of a material, acts by two general mechanisms. The first mechanism rotates the magnetization towards the direction

of the field and, in some cases, requires a certain amount of anisotropy energy. For the second mechanism of changing the domain magnetization, the direction of magnetization remains the same, but the volumes of different domains may change. In this process, those domains where magnetizations are in a direction closest to the field direction grow larger while those that are more unfavorably oriented become smaller in size (GOLDMAN, 1999).

The upper panel of Figure 3.8 shows two adjacent domains, divided by a wall, called *Bloch* wall. The *Bloch* wall encases the ferromagnetic domains like a shell, rotating their magnetic vector. The rotation is constant from one domain to another and it is performed orthogonally in the plane of the wall (THEINER, 1997; KARPUSCHEWSKI; BLEICHER; BEUTNER, 2011).

In order to better understand the influence of *Bloch* walls in the material magnetic behavior, different types of walls as well as their major characteristics will be explanained. Basically, *Bloch* walls are divided into two types, 1st and 2nd kind, described as BW1 and BW2, respectively (RABUNG *et al*, 2012). BW1, which can be seen in the bottom left of Figure 3.8, can be described in simple words as the walls where the magnetic spin from one domain is 90° in relation to one adjacent domain. Due to this, these walls have great interacting volumes. If a BW1 is moved, the elastic energy density will be affected in dependence of the wall position. The walls of 1st kind can only be moved from their position if an external energy is applied to the material, causing alteration in the magnetic field strength or elastic energy density (THEINER, 1997; TAGLIARI, 2012).

The *Bloch* walls of 2nd type, BW2, are the walls where the magnetic spin from one domain is 180º in relation to one adjacent domain, as shown in the bottom left of Figure 3.8. Since BW2 separates domains with the same magnetostrictive behavior, no alteration in the elastic energy will be detected during their movement. One important characteristic of these type of walls is that they only produce residual stresses within the *Bloch* wall itself, exemplified in the bottom right of Figure 3.8. Furthermore, they do not interact with macrostresses and microstresses within grains which are larger than the walls dimension (THEINER, 1997; TAGLIARI, 2012).

3.3.2 Hysteresis loops

Another property of ferromagnetic materials is the hysteresis loop, which characterizes the relationship between the magnetic field H [A/m] and the magnetic flux density B [T] (GAO *et al*, 2010; KARPUSCHEWSKI; BLEICHER; BEUTNER, 2011). The complete

curve is shown in Figure 3.9 f), and it determines how much induction a certain applied field creates on a determined material (GOLDMAN, 1999). An external magnetic field forces the alternation of the domains orientation, where the unfavorable magnetic orientation increases over areas with less favorable orientation. In this case, domains with direction parallel or nearly parallel to the external magnetic field increase, while the others are eliminated (KARPUSCHEWSKI; BLEICHER; BEUTNER, 2011; DOBMANN, 2012).

According to Figure 3.9, the increase of H generates a response in the induced magnetic field, B, and the relation between both factors is represented in the hysteresis curve. When a high magnetic field, H_m, is applied, the induction curve is flattened, as shown in Figure 3.9 a). After the material achieves the saturation zone, if the external magnetic source is constantly removed, a different relation between B and H is obtained, as shown by the curve in Figure 3.9 b). Even with H reduced to zero, a flux density remains in the material, called remanence magnetism, B_t. In order to reduce the flux density to zero, a magnetic force, $-H_m$, opposite to the first one, must be applied. As H becomes more negative, it reaches the saturation zone in the opposite side, as shown in Figure 3.9 d) (GOLDMAN, 1999; KAUFMANN et al; 2000).
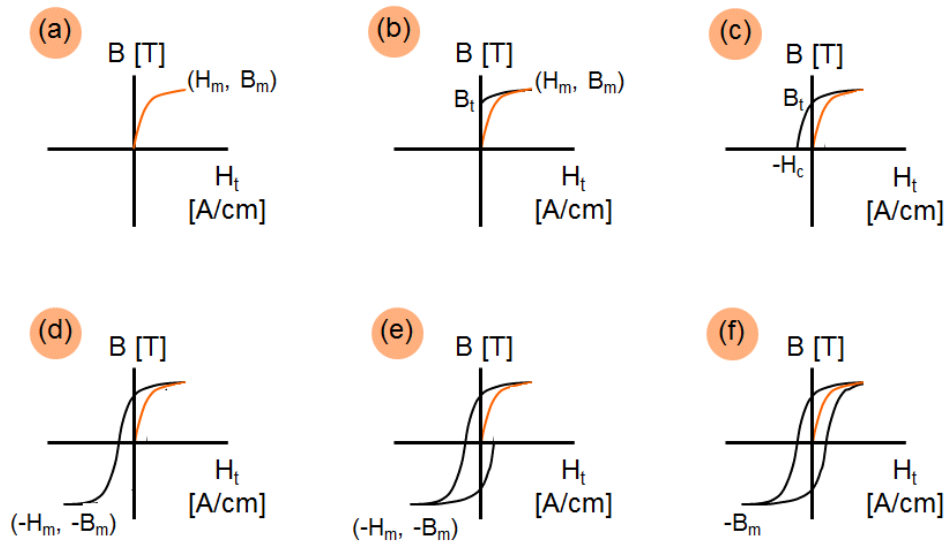
Figure 3.9 - Steps of the development of a hysteresis curve of a ferromagnetic material (KAUFMANN et al, 2000).

If H is alternated between the saturation limits, $-H_m$ and H_m, the relation between B and H follows a fixed closed loop, represented by the hysteresis curve, in Figure 3.9 f) (GOLDMANN, 1999; KAUFMANN et al, 2000).

The hysteresis curve is a way to represent the magnetic behavior of a material. In addition, important properties can be analyzed, such as:

(a) *Remanence*: magnetic induction that remains in the material after the external magnetic force H is removed.

(b) *Residual flux density or residual induction*: magnetic induction that remains in the material when H is zero, for the condition when the material is being symmetrically magnetized in a cycle.

(c) *Retentivity:* the flux density that remains in the material after a magnetizing external force H strong enough to cause saturation, is removed (KAUFMANN *et al*, 2000).

The characteristics described above, although seeming very similar at first sight, carry fundamental conceptually differences. The clear understanding of each of them will be important in the future application of the method under investigation.

In general, the form of the hysteresis loop of any ferromagnetic material is very similar to the curve shown in Figure 3.9 f). However, the proportions of the curve can alter among different materials, and, for a determined material, it also varies due to the heat treatment and/or mechanical working to which the material is subjected. This is due to the fact that any microstructural variation in the material leads to a change in its magnetic properties (YIN; PEYTON; STRANGWOOD, 2007; KARIMIAN *et al*, 2014).

Figure 3.10 b) shows the research conducted by Ikhmayies (2017), regarding the magnetic characterization of determined materials. In his studies, two phases of the steel alloy SAE 4140 were studied, quenched and tempered phases, and its hysteresis curve calculated. The diagram in Figure 3.10 b) shows a correlation between the hardness of each phase and its magnetic hysteresis. The coercivity values shown in the curve reflect the magnetic hardness of the material, which, in turn, is a form to indicate the material hardness. The quenched steel presents higher hardness, due to its small needles martensite structure. This form of structure results in very small domains, and therefore, high dislocation density, which acts like obstacles to the domain wall movement. Due to this, magnetization processes will take place under a large range of H field (THEINER, 1997; KARIMIAN *et al*, 2014; ZHOU *et al*, 2014; IKHMAYIES *et al*, 2017).

The structure of the alloy tempered at 600°C consists of cementite and spheroidize carbides, and the crystal structure, initially of martensite, loses its tetragonality by the recrystallization of ferrite. This leads to a remarkable reduction of dislocation density, and

consequently, the material magnetization occurs under a smaller range of H compared to the quenched phase (THEINER, 1997; ZHOU *et al*, 2014; IKHMAYIES *et al*, 2017).
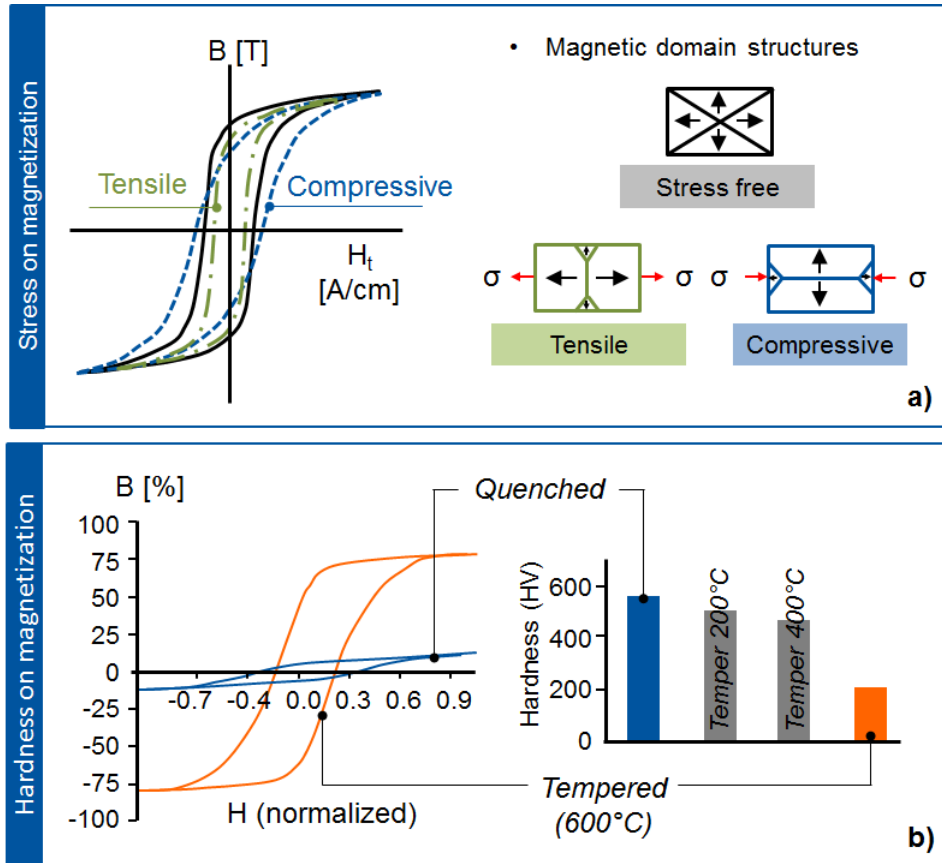
Figure 3.10 - Influence on the magnetic hysteresis curve of a material due to a) residual stresses state; b) material microsctrure alteration (THEINER, 1997; DESVAUX *et al*, 2004; IKHMAYIES *et al*, 2017).

Similar to the magnetic behavior of the material for different phases, when the material is under residual stresses, the hysteresis curve also undergoes alteration depending on the stress characteristics. Macro stresses interact to the material domains, BW1 and RP, in a way that BW1 must to move in order to reduce the elastic energy density (THEINER, 1997). During the process, the average orientation of the material magnetic domains is aligned parallel or perpendicular to the direction of a determined external magnetic field applied. If the material is under tensile resisual stress, and the applied magnetic field is parallel to its domains, the direction of the tensile stress increases at the expense of the other domains. As the H continuously increases, the domains gradually take over the total available volume (THEINER, 1997; DESVAUX *et al*, 2004).

Whenever a magnetic field is superimposed in a stress field direction, this direction becomes the preferred magnetization direction, and, therefore, the direction of lower energy (THEINER, 1997). This is reflected in the hysteresis curve, as shown in Figure 3.10 a); in the case shown in the diagram, the tensile stress direction is favorable to the magnetized direction, which causes the material to be easier magnetized (narrowing of the curve) in comparison to material under compression stresses (DESVAUX *et al*, 2004). This behavior brought to the hysteresis curve by the residual stresses makes a magnetic method an important technique to detect different states of superficial residual stresses.

The effect of microstructure and / residual stresses profile on the hysteresis curve is evident by means of important factors which are responsible for characterizing the magnetic profile of a material. One of these factor is permeability.

3.3.3 Permeability

Magnetic permeability (µ) is an important parameter which represents the ratio of induction, B, to the magnetized field, H, according with Equation (3.1) It is one of the most important parameters used for the evaluation of magnetic materials, since it is directly responsible for the value of the magnetic field induced in the material by an external magnetic field. However, due to the non-linearity of general magnetic materials, the permeability must be calculated at a determined value of either B or H (GOLDMAN, 1999; KAUFMANN *et al*, 2000).

$$\mu = \lim_{B \to 0} (\frac{B}{H})$$

(3.1)

Permeability is highly influenced by the chemical composition, microstructure, temperature, stress and several other factors related to the bulk material. (GOLDMAN, 1999). This influence can be demonstrated in the hysteresis curve, as shown in Figure 3.10. Figure 3.10 a) shows the influence of different microstructures in the induced magnetic field. Due to the difference between the microstructure, when they are subjected to the same external magnetic field, each of them have a distinguish response. In addition, Figure 3.10 b) shows that the presence of mechanical stresses can also influence the response of the material to an external magnetic field.

3.3.4 *Barkhausen* noise method

As already stated, when a ferromagnetic material is exposed to an external magnetic field, the process of magnetization occurs, where *Bloch* walls move, and the material starts its magnetization process. The movement of the *Bloch* walls, however, is not continuously and as it happens, it changes the magnetization state locally, emitting an electrical pulse. The compilation of these electrical pulses is known as *Barkhausen* noise, as shown in Figure 3.11 a). (KARPUSCHEWSKI; BLEICHER; BEUTNER, 2011; DOBMANN, 2012). The microstrucuture plays an important role in the movimentation of the walls; the presence of impurity atoms, inclusions and vacancies, dislocations, phase or grain boundaries, for example, constrain the movement of the *Bloch* walls, acting like obstacles to magnetization change of the domain (KARPUSCHEWSKI; BLEICHER; BEUTNER, 2011; DOBMANN, 2012). As a consequence, an alteration in the electrical pulse is detected. In addition, mechanical stresses also affect the change in the magnetic structure. The resistance against the mobility of the wall is decreased or increased by the presence of tensile or compressive residual stresses, causing an alteration in the *Barkhausen* signal amplitude, as shown in Figure 3.11 b) (KARPUSCHEWSKI; BLEICHER; BEUTNER, 2011; DOBMANN 2012).
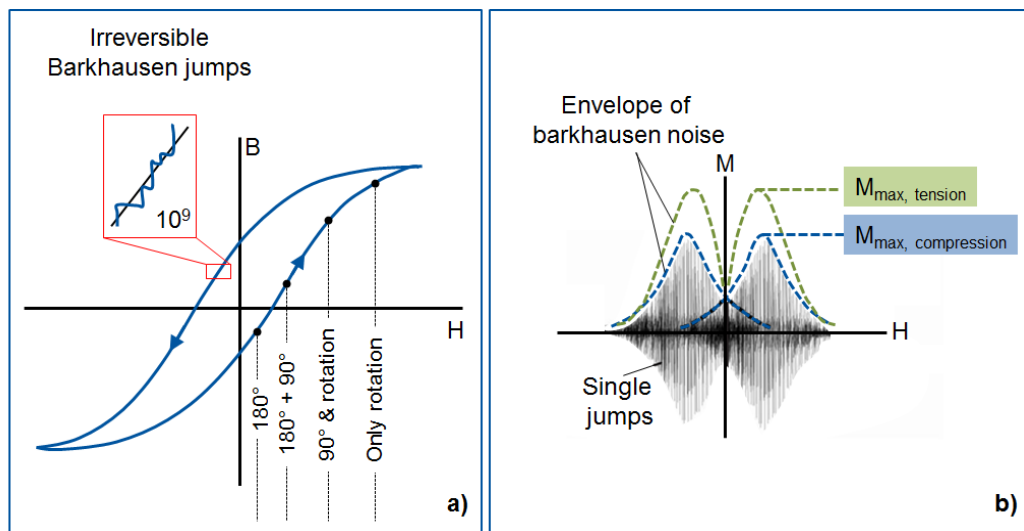
Figure 3.11 - a) Hysteresis curve and b) magnetic *Barkhausen* noise profile M(Ht) (GOLDMAN, 1999; KARPUSCHEWSKI; BLEICHER; BEUTNER, 2011).

Thermal damages caused by grinding change the properties of the workpiece, in terms of microstructure and / or residual stresses. Therefore, *Barkhausen* noise has become an important method to detect grinding burn. Some of its characteristics, such as being objective, fast, relatively flexible and non-destructive, make the method very suitable to an industrial environment, including for gear manufacturing (KARPUSCHEWSKI; KNOCHE; HIPKE, 2008; KARPUSCHEWSKI; BLEICHER; BEUTNER, 2011).

However, the method still faces some challenges. One of the most problematic properties of the method is the fact that it is not possible to define static common value, since the signal is very sensitive to all material properties like hardness, structure and residual stresses. Due to this fact, the analysis of the results must be done very carefully, in order to be correctly interpreted. In addition, steps of calibration and referencing can be very time consuming due to the same signal sensitivity (KARPUSCHEWSKI; KNOCHE; HIPKE, 2008; KARPUSCHEWSKI; BLEICHER; BEUTNER, 2011).

3.4 Conventional methods for grinding burn detection

3.4.1 Nital etching

As already established in this work, the thermal damage can be present in the surface of a component in different levels. In some of these levels, the damage is not directly visible, requiring an appropriate method to detect it. One of the few established testing methods to detect thermal damage and widely used in the gears manufacturing environment is the nital etching (WOJTAS; SUOMINEN; SHAW, 1998; ALBAN, 2002; MALKIN; GUO, 2008).

The method applies several chemical steps that interact differently with the different components of the material. As a result, damaged areas are highlighted by a different coloration. Tempered damages, which in most cases are not directly visible, turn dark after nital etching while hardened damages turn white (WOJTAS; SUOMINEN; SHAW, 1998; KARPUSCHEWSKI; BLEICHER; BEUTNER, 2011).

Nowadays, there are several nital etching processes being used by industry in their production line Figure 3.12 presents one possible example for the nital etching application, as well as its result when it is applied on a workpiece surface with different thermal damages (ALBAN, 2002).
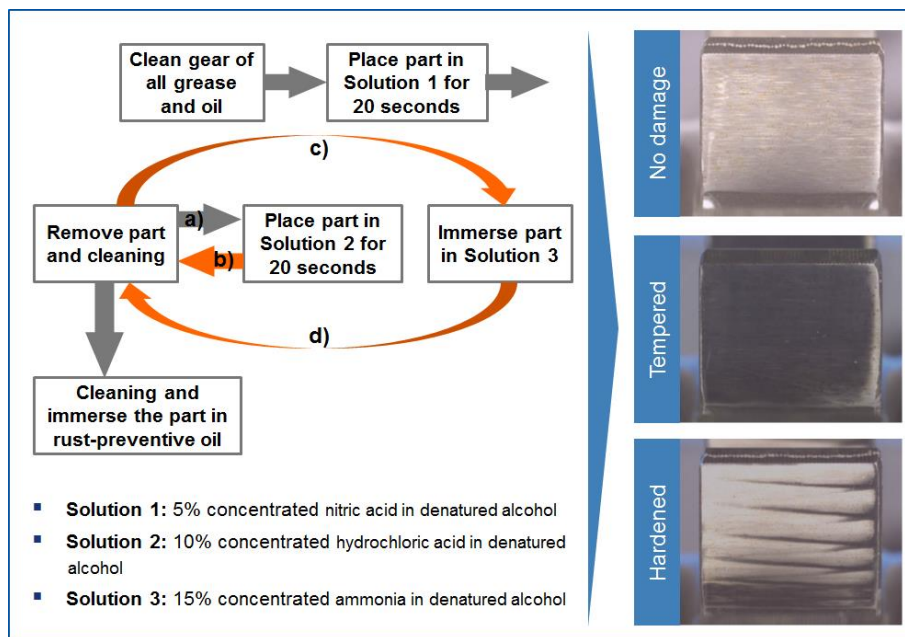
Figure 3.12 - Nital etching steps and example of the application into different degrees of grinding burn (ALBAN, 2002; SCHWIENBACHER, 2008).

The major disadvantage of the method is its subjective character. The result is obtained by visual inspection performed by an operator, which must be able to judge if the workpiece is to be rejected or not. Although the operator is specially trained to distinguish between a burnt and a regular area, sometimes they fail. Another limitation of the method is its restriction to analyse only the very top layer of the workpiece. Any sub surface grinding burn cannot be detected (ALBAN, 2002; DAVIS, 2005; KARPUSCHEWSKI; KNOCHE; HIPKE, 2008; KARPUSCHEWSKI; BLEICHER; BEUTNER, 2011).

3.4.2 X-Ray Diffractometry

The importance of residual stress is widely acknowledged and it was already described in earlier topics in this work. The X ray diffraction (XRD) appears as an important and most used method for measuring residual stresses (BHADESHIA; WITHERS, 2001; REGO, 2016). The method presents significative advantages such as spatial and volumetric resolution, quantitatively and being a relatively non-destructive method (HORNBACH; PREVÉY; MASON, 1995; ERRICHELLO, 2015). In some cases, due to the limited space available on the XRD machines, the workpiece needs to be cut down in order to be measured, which is a limitation for the use of the technique. XRD is able to measure the surface residual

stress non-destructively. However, if any sub surface residual stress profile is under analysis, the method becomes destructive due to the successive surface layers removal process (ERRICHELLO, 2015).

The XRD technique can be applied for a large range of functionalities, such as phase identification, crystalline structure identification, minerals identification and structural analysis, measurement of surface and depth residual stresses, and many other applications (SANTOS, 2012). For the measurements of residual stresses, which are a partial topic of this work, the technique is based on the fact that a metal, when under application of residual stress, suffers the influence of the final elastic strains, causing the atomic planes in the crystal structure to change their spacings (CULLITY, 1956).
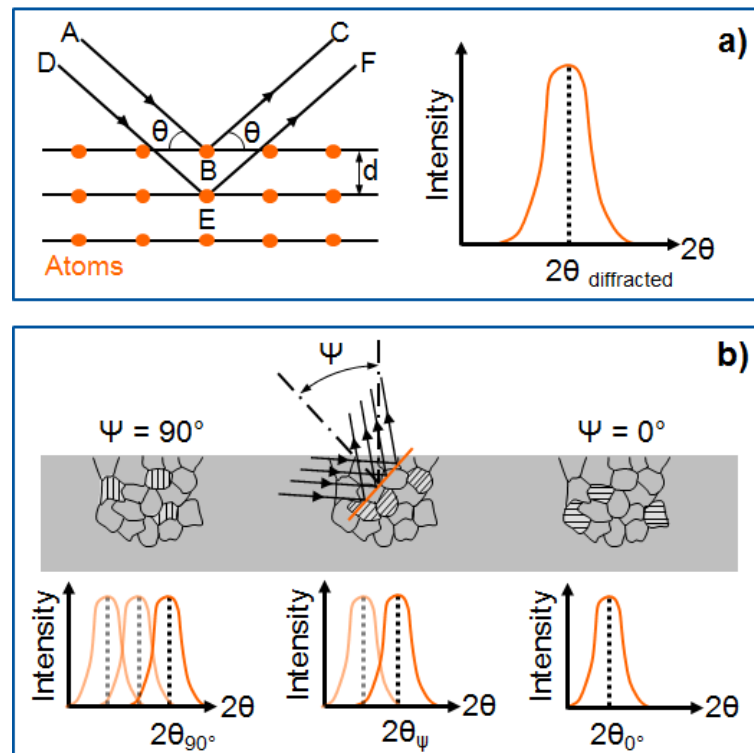
Figure 3.13 - Exemplification of residual stress measurement using x-ray diffractometry. A specific set of planes is scanned, locating the 2θ position along several tilt angles ψ. The alteration in peak position is then used in equations (CULLITY, 1956; MAIA, 2015).

Residual stress measurements by XRD are performed by the Bragg's law, which correlates the wavelength (λ) of a radiation beam with the incidence angle (θ) such that scattered rays manifest constructive interference. The angle between the diffracted and the transmitted beam is always 2θ, and is related to the distance between densely packed planes

(d) of the material under analysis, as shown in Figure 3.13 (CULLITY, 1956; BHADESHIA; WITHERS, 2001; MAIA, 2015).

When a specific polycrystalline material is elastically deformed, the lattice plane spacing changes and this is detected in the diffraction angle for a specific used wavelength (CULLITY, 1956; MAIA, 2015). The interplanar distance is obtained from the relation between the curve peak intensity versus scattering angle 2θ and the Braggs law. From the shift in the diffraction angle, the strain may be calculated and, therefore, the present stress is determined by means of calculation (CULLITY, 1956; MAIA, 2015). Nowadays, the most used method to determine the residual stresses by x-ray diffractometry is the $\sin^2\psi$ method. In this technique, a series of measurements are performed for different values of ψ (SANTOS, 2012; MAIA, 2015).

3.5   The *Hall* effect method

Magnetic methods have become a good alternative for the detection of grinding burn due to important characteristics such as: non-contact, non-destructive robust and the potential for direct microstructure characterization (YIN; PEYTON; STRANGWOOD, 2007). These characteristics increase the research on magnetic methods able to measure the presence of thermal damage in a component after the grinding process.

The technique presented in this study uses the advantages of a magnetic method for the assessment of griding burn, by the application of a *Hall* probe. In order to better understand how the technique works, it is first necessary to introduce the concept of the *Hall* effect.

The *Hall* effect is fundamentally based on a phenomenon called galvanomagnetic effects. This phenomenon describes physical effects arising in matter carrying electric current in the presence of a magnetic field. For the current study, the most important galvanomagnetic effect is the *Hall* effect, which will be used for the method measurement (POPOVIC, 2004).

Edwin H *Hall* was the first to detect the phenomenon, and therefore, had it named after him. In his first tests, he attempted to prove that a magnet directly affects the current instead of the wire bearing current, as it was believed at that time. The experiment contained a thin plate of a conductive material, which is carrying a current which can be the supply for a battery, for example. A pair of probes positioned in two nearly equipotential points in the

plate is connected to a galvanometer, in order to measure the voltage. (POPOVIC, 2004; RAMSDEN, 2006).
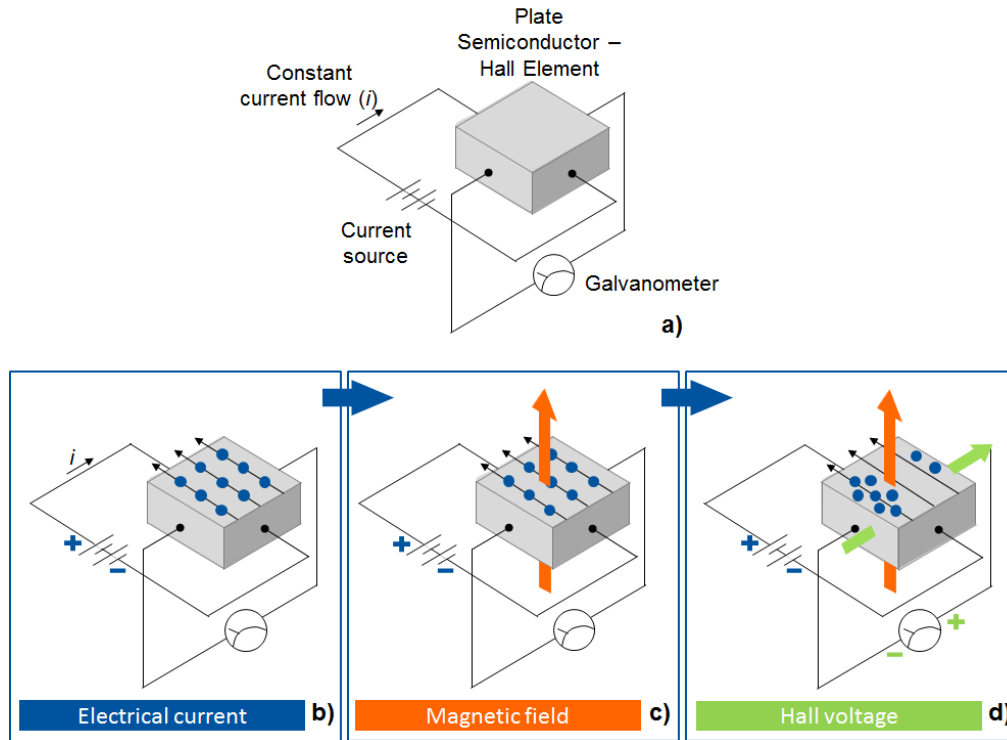
Figure 3.14 - *Hall* effect in a conductive plate (RAMSDEN, 2006).

When a magnetic field is applied perpendicularly to the plate, and therefore, perpendicularly to the current flow, a small voltage appears across the plate. This happens due to a known physical phenomenon that affects a moving charged particle when it interacts with a magnetic field.

By the presence of a magnetic field, a force is imposed to the particle, forcing it to change its original direction. In the case of the electrical current flowing in the plate of *Hall* experiment, the force induces most of the current electrons to one side of the plate. This generates a small voltage across the plate, which can be measured by the galvanometer. This voltage is called *Hall* voltage. The most surprisingly factor of *Hall*'s discovery was that it occurs under steady state conditions, which means that the voltage detected in the plate persists when the current and the magnetic field are constant. As a conclusion, *Hall* established that the new electromotive force was proportional to the product of the intensity of the magnetic field and the velocity of the electricity (POPOVIC, 1991; POPOVIC, 2004; RAMSDEN, 2006).

According to Popovic (1991), the *Hall* voltage that appears in the plate can be expressed in terms of the current I, as shown in the Equation 3.2

$$V_H = \frac{IB}{qnt}$$

(3.2)

In Equation 3.2, q denotes the magnitude of the electron charge, n is the carrier concentration in the plate, and t represents the plate thickness. Therefore, the *Hall* voltage is a linear function of (a) the applied magnetic field in the "sensitive" axis and (b) the spatial separation of the sense contacts. The main applications of the *Hall* plate are considerable from the equation. The *Hall* voltage may be regarded as a signal carrying information. When material properties, device geometry and biasing conditions are well known, the *Hall* voltage measured can provide the information about the magnetic induction field B. Consequently, the *Hall* device is used as a magnetic field sensor. In other words, the *Hall* plate converts a magnetic field into a *Hall* voltage. In turn, the *Hall* voltage is the electronic signal carrying information on the magnetic field, as shown in Figure 3.14 (POPOVIC, 1991; POPOVIC, 2004; RAMSDEN, 2006).

Nowadays, *Hall* devices consist of a thin, rectangular or squared sheet of certain materials, such as Si, GaAs, InSb or InAs. Often, the plate is fixed to a ceramic or carbon fiber substrate, in order to provide mechanical support and thermal stability to the probe (BOETTGER, 2014). The use of a *Hall* probe requires a measurement device known as gaussmeter. The gaussmeter is an instrument that conditions and amplifies a *Hall* sensor output, as well as provides to the user a calibrated flux-density information (BOETTGER, 2014). The use of a *Hall* probe requires specific cares that must be taken into account for the execution of the tests with the method proposed. Earlier researches described some factors that might influence the performance of the sensor, such as room temperature, distance between sensor and workpiece, and magnetic influence of surrounding equipments on the measurements (CHANG *et al*, 1992; SHIMIZU *et al*, 2004).

3.6   Summary and technological gap

The three most used techniques to detect grinding burns – Nital etching, *Barkhausen* noise and X-ray diffractometry – were presented. Although they are widely applied in the

field, there are restrains regarding some specific topics, which make each of them not suitable at some point. Based on literature of material and industrial experience, a table was gathered, with information about the behavior of each three measurement methods for specific points such as: destructive, automation, quantitative, reliability, time consuming and area., as shown in Figure 3.15.

	Nital Etching	Barkhausen noise	X-Ray Diffraction
Destructive	Medium	Low	Medium
Automation	Medium	Medium	Medium
Quantitative	Low	Medium	High
Reliability	Medium	Medium	High
Time Cons.	Medium	High	High
Area	High	High	Low
Cost	Medium	Medium	High

● High ◑ Medium ○ Low

Figure 3.15 - (COMLEY, 2005; KARPUSCHEWSKI; KNOCHE; HIPKE, 2008; MALKIN; GUO, 2008; ROWE, 2014).

The points were selected due their importance for an industrial environment. Each method is classified as "High", "Medium" and "Low" for each point of analysis. In the table, nital etching presents good qualities, such as measurement of great areas, but it also has its limitations, especially in the topics of quantitative and reliability. The table shows that the *Barkhausen* noise method also presents advantages like not time consuming, high area of measurement and relatively low destructivity. These are characteristics normally attributed to magnetic methods. However, the *Barkhausen* noise still presents disadvantages such as reliability, which is the main concern of the method. The X-ray diffraction method, although it presents great advantages such as high reliability and quantitatively, is not suitable for an industrial environment due to its occasional high costs and high time consuming.

In face of the disadvantages highlighted in the table of Figure 3.15, a new method for detection of thermal damage caused by grinding processes is required. Due to the potential of magnetic techniques, the new method suggested applies concepts of micro-magnetism by means of a *Hall* probe.

4   Experimental procedure

The main purpose of the actual study is to validate the *Hall* effect method for the detection of surface grinding burn. This means that an initial complete study of the technique is required. The main activities, experiments and methods applied are summarized in the Figure 4.1. The study was separated into three main phases, highlighted in the diagram by the colors grey and green. The *Phase 1*, in grey boxes, covers the first question of the specific objective of the work, which aims to investigate the influence of the measurement mechanism and environmental factors on the results, analyzing its robustness. The *Phase Pre-Tests* is an intermediate phase, where a first analysis of the method behavior in face of a known magnetic case is performed. The tests in this phase aim to verify if the method is capable of reproducing the expected results.
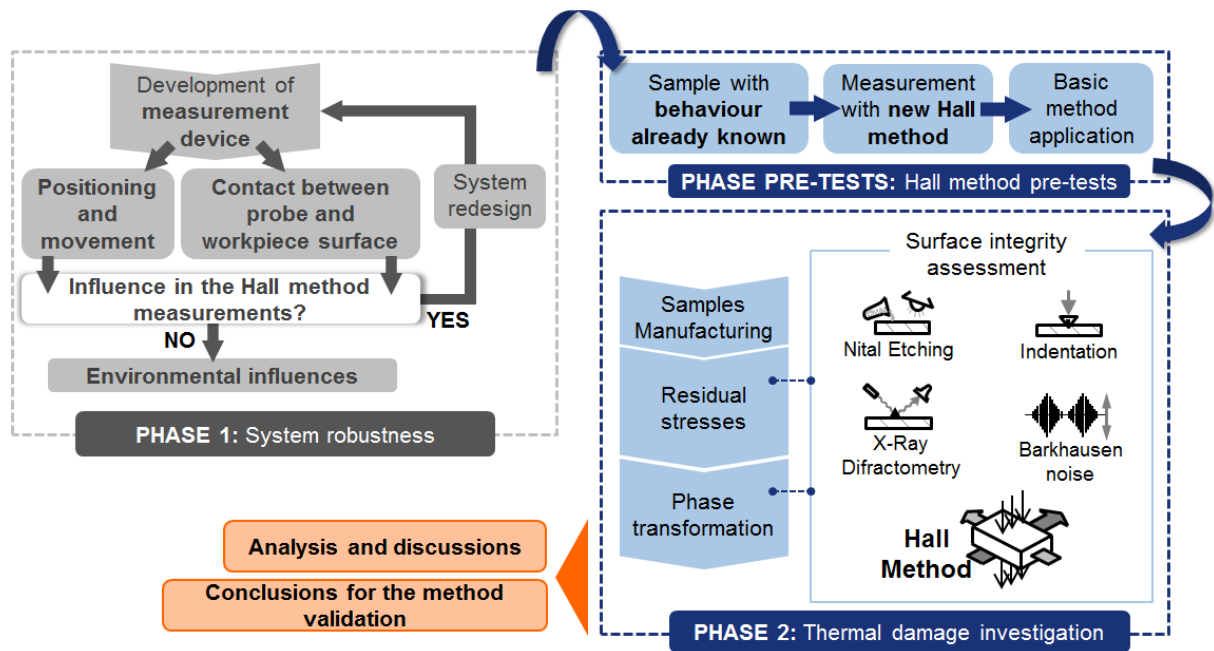
Figure 4.1 - Workflow of activities developed along the study.

The *Phase 2*, shows the activities performed in order to answer the second and third questions from the specific objectives. The tests of this phase analyse the thermal damages with and without phase transformation (residual stresses), by means of already established measurement methods. Next, the same thermal damages are investigated with the Hall

method, and the magnetic signals detect by are correlated with the material characteristics induced by the damage.

4.1 PHASE 1: System Robustness

In this topic, influences from the mechanical system as well as from the environment in the signal measured by the *Hall* probe are analyzed. The main purpose of this topic is to evaluate the equipment and optimize it by the investigation of its limitations. The relevant factors were raised and disposed in a diagram, shown in Figure 4.2. These factors were selected due to the influence they might cause in the measurements with a Hall probe, according to the literature.
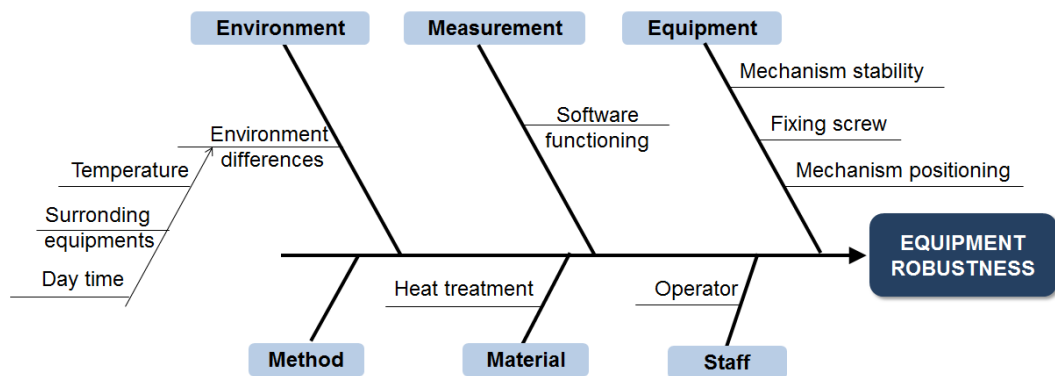
Figure 4.2 - Description of factors under investigation.

It is possible that other factors not listed in the diagram influence the signal measured. However, the current study does not investigate them.

4.1.1 System movement and positioning

The new *Hall* method proposes the scanning of a surface by a Hall probe, collecting its magnetic signal. An equipment was build for the probe movimentation during the scanning process. In order to verify if the positioning precision of the equipment is high enough to guarantee the precision for the scanning process, the movementation system is tested in this topic.

The scan routine created with *Labview* follows the steps: (1) Move *Hall* probe to the reference point. This point represents the first point of the scanning, and it is highlighted in Figure 4.3 as point 1; (2) In this position, *Hall* probe measures the local magnetic field 10 times; (3) The Gaussmeter sends the 10 measurements to the routine in the computer and then it calculates an average of the magnetic field for this point; (4) The average value is sent to a matrix which represents the discretization of the surface being measured; (5) Move *Hall* to the next point, in this case point 2, and repeats all the steps from step 3. The matrix with the surface measurements is represented in a colour scale, in the form of an image. Figure 4.3 shows a description of the steps followed for the scan routine.
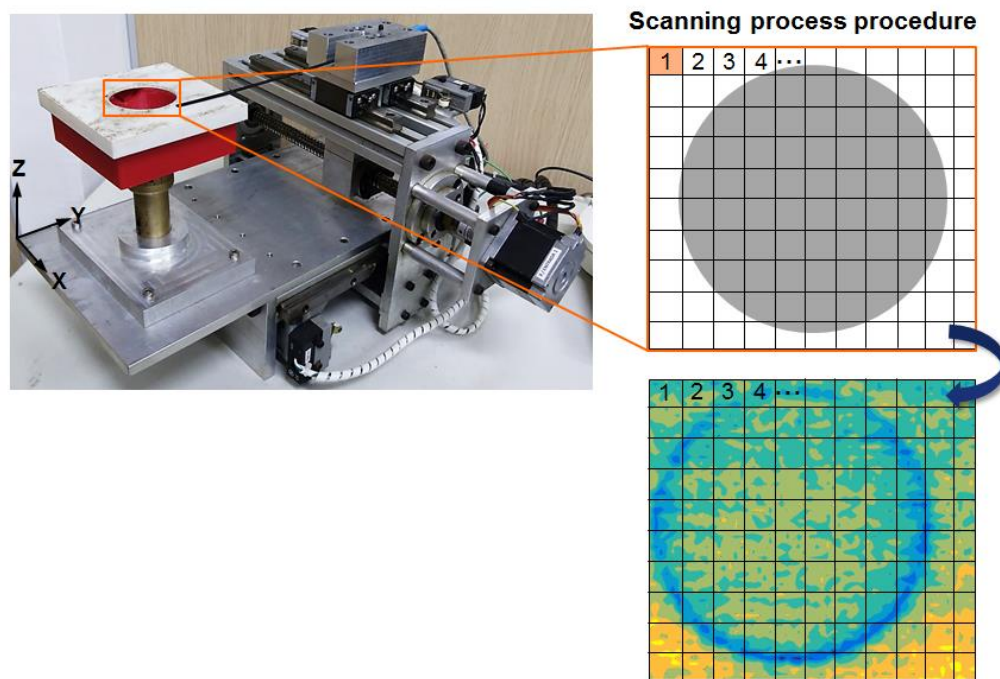
Figure 4.3 - Measurement equipment developed for the *Hall* method, and scanning process procedure.

The tests of movement precision verify the deviation between the nominal distance induced in the system and the actual distance measured. The actual distance is measured by a dial gauge, positioned in the equipment during its movemenation. The difference between the nominal and the actual distance measured is referred to as the position deviation.

The tests were performed in the directions X and Y, in both positive and negative direction, under three different velocities, 1000, 1200 and 1400 steps/s. Figure 4.3 shows the measurement equipment for a better understanding of its coordinate system. The distances

analyzed were 0.04, 5 and 10 mm. Table 4.1 describes part of the tests performed; the same table is used for the tests for the distances 5 and 10 mm. For statistical reasons, each condition is repeated 3 times. The outcome of this test is a range of the deviation expected by the system, in each analyzed condition.

Table 4.1 **-** Descriptions of movement tests of the equipment.

Distance [mm]	Speed [steps/s]	Movement direction and sense
0.04	1000	Axis X – Positive
0.04	1200	Axis X - Positive
0.04	1400	Axis X - Positive
0.04	1000	Axis X – Negative
0.04	1200	Axis X – Negative
0.04	1400	Axis X - Negative
0.04	1000	Axis Y – Positive
0.04	1200	Axis Y - Positive
0.04	1400	Axis Y - Positive
0.04	1000	Axis Y – Negative
0.04	1200	Axis Y – Negative
0.04	1400	Axis Y - Negative

4.1.2   Influence of system mechanism in the *Hall* probe signal

The measurement system, regarding its mechanical construction, was analyzed in order to verify its influence on the measurements. The main concern during measurements is to assure the contact between the *Hall* probe and the workpiece surface. Otherwise, the probe might be only partially in contact to the surface, leading to false results. The *Hall* device consists of a carbon fiber bar of 200 mm length, with the *Hall* probe itself localized 2 mm from its tip. Therefore, when the system guarantees the contact between the bar's tip and the workpiece surface, it also guarantees that the *Hall* probe is in contact to the material.

Based on this premise, two models of support for the *Hall* probe were suggested and tested: (1) applying a small weight of 2g at the bar's tip; (2) inducing an angle of 7° between

the *Hall* probe and the workpiece surface. The use of the weight or the angle aims to push the bar's tip against the workpiece, increasing the possibility of contact. The value of 2g for the weight was chosen because it was a value big enough to force the bar down, but not too big to damage the equipment, breaking it. The same thought was used to define the angle of 7° for the other model proposed. Both models were taken into consideration due to the easy application and for not damaging the equipment. The evaluation of both models is made by the measurement of contact length between the bar tip and the workpiece surface. A *matlab* routine was developed for this measurement. During the tests, the distance between the workpiece and the *Hall* bar was varied, as shown in Figure 4.4.

1. Hall probe bar
2. Workpiece support
3. Workpiece
4. Distance between workpiece surface and Hall probe
5. Scale
6. Contact length
7. Small weight
8. Hall probe with angle to the workpiece surface
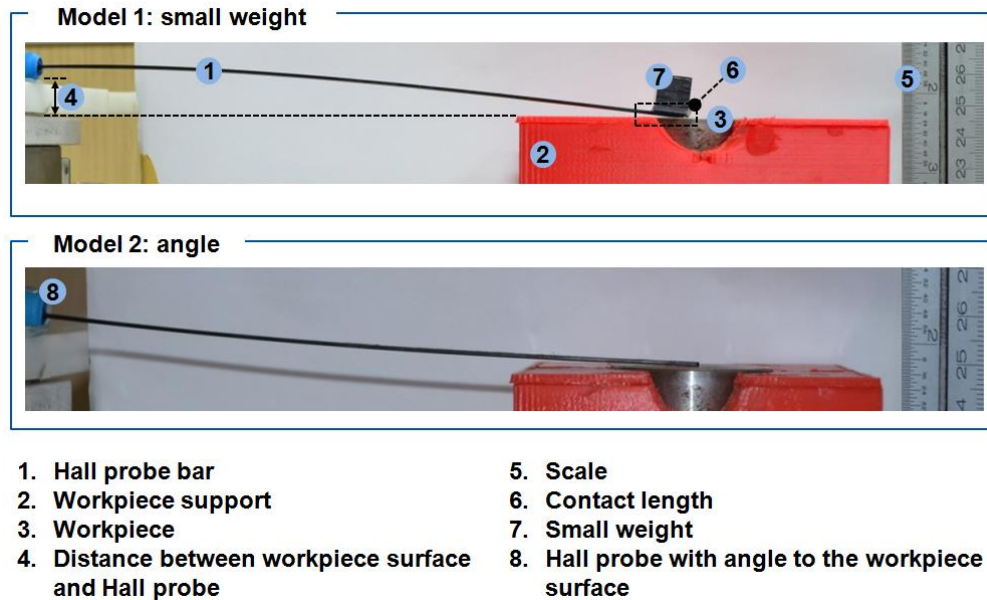
Figure 4.4 - Tests for most suitable mechanism to ensure the contact between the *Hall* probe and the workpiece surface.

In the end, the objective of this test is to define which support is more suitable to the measurement requirements, as well as to establish the distance between the workpiece surface and the *Hall* probe for an optimal length contact.

The tests for both models were performed under the same circumstances, following the steps: (1) Positioning the scale; (2) Positioning the weight at the bar's tip – 2g / Positioning the *Hall* probe with an angle of approx. 7ºC to the workpiece surface; (3) Positioning the workpiece at the required height; (4) Photographing the lateral of the system; (5) Uploading the picture in a *Matlab* routine to analyze the area of contact. For each model

tested, different highs of the workpiece are tested, 1, 3, 5, 7, 9, 11, 13 and 15 mm, being the 15 mm the value where the workpiece is the closest to the *Hall* probe.

4.1.3 Repeatability and reproducibility

Repeatability of measurements is defined as the variation in repeat measurements, which are made under the same conditions and on the same subject (MONTGOMERY, 2001). Since the current work aims to understand the advantages and limitations of the new method for detection of grinding burn, it is important to study the repeatability of the process in the current conditions, in order to avoid false results. For these tests, all the other factors that will be further investigated in the reproducibility tests are kept constant. The room temperature is kept on 19°C (normal temperature of the room), all the other equipment of the room are turned off during the measurements, and all the tests are done in a specific period of the day – from 12h to 16h. The same workpiece is scanned for all the tests, with the following characteristics: ground surface, without presence of thermal damage and non-magnetized. Seven repetitions of measurements are used. For the analysis, repeatability may be expressed quantitatively in terms of dispersion of the results, by means of the standard deviation analysis. To evaluate, in % , the influence of this dispersion on the results, the Equation 4.1 is used.

$$R = (\sigma/\mu)*100 \tag{4.1}$$

Where σ is the standard deviation of the measurements and μ is the average.

Another key factor to be considered is the method's reproducibility, which is defined as the variation of measurements made on a piece under changing conditions (MONTGOMERY, 2001). The factors under alteration are defined according to their relevance in the environment where the measurement system is currently placed and, therefore, possible relevance in the measurements results. The factors analyzed in the reproducibility tests are described in Figure 4.2, such as day time, temperature, other equipments in the room and operator. The experimentation strategy used is the *one-factor-at-a-time* approach. The method establishes the selection of a starting point for each factor, then the successive variation of each factor over a certain range, while the other factors are held constant (MONTGOMERY, 2001).

The tests about mechanism stability and positioning were already described in the earlier topics. This topic investigates the following factors: day time, surrounding equipments,

temperature, operator and stepper motor influence. The results were analyzed and it was verified if any factor has influence on the measurements. When an influence is detected, a solution is introduced in the system and/or in the measurement routine in order to avoid false results. This is an important analysis and its outputs will help to determine the measurement procedures for the further tests.

The tests consist of the following steps: (1) establishing the factor under analysis; (2) preparation of workpiece in the measurement system and the environment; (3) scanning of the surface with the measurement system; (4) generation of an image from the data measured with the *Hall* probe; (5) selection of the circular area representing the workpiece surface. This step aims to remove the measurement points that do not belong to the workpiece, facilitating further calculation; (6) calculation of average value of the signal; (7) variance analysis, One-Way Anova. Figure 4.5 shows the steps followed for the image analysis of repeatability and reproducibility.
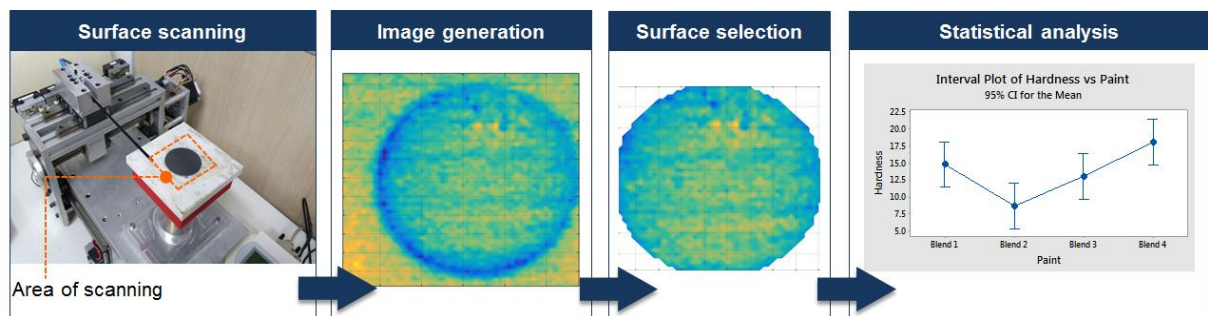
Figure 4.5 - Description of the steps followed for the repeatability and reproducibility analysis.

4.2 Workpiece preparation

4.2.1 Workpiece description

The scope of this work is the surface measurement of gears. However, for the measurements in the actual equipment, it was chosen a workpiece that represents the gear flank surface, instead of the gear itself. This choice was made in order to facilitate the measurements, avoiding the scanning of a complex geometry, such as the gear flank, and replacing it for a simpler geometry. The gear represented by the workpiece has the following characteristics:

- Material: steel AISI 4320

- Hardness: 60 – 62 HRC

- Carbon surface layer: 0,8mm

- Surface finishing on the teeth flank:
    - Ra: 0.30µm
    - Rz: 2.30µm

These are values normally used for a regular cylindrical gear, used as example. The workpiece shape and dimensions used in this work are presented in Figure 4.6. It is a cylinder with 48.5mm of diameter and 25mm thickness, made of steel AISI 4320.
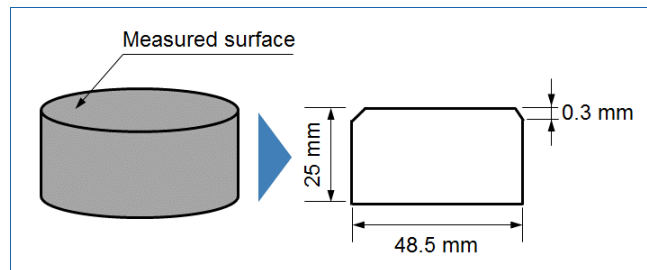
Figure 4.6 - Shape and dimensions of the workpiece used for the tests.

In order to represent the gear flank surface, the workpiece was prepared using manufacturing processes usually used for automotive gears. This was done in respect to the research scope. Figure 4.7 shows the all the usual processes performed through the gear manufacturing chain: forging, hobbing, heat treatment and grinding.
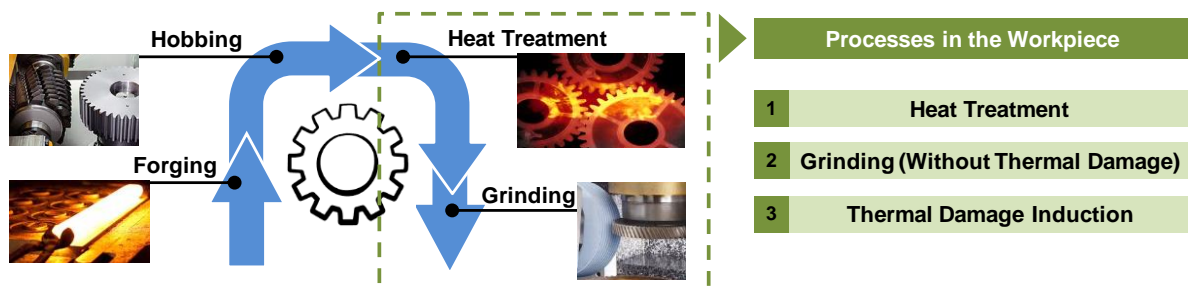
Figure 4.7 - Processes in the gear manufacturing chain and highlight of processes steps performed in the workpiece.

For the workpieces used in the work, only the two final processes, heat treatment and grinding, were performed. These two processes were performed in three steps, as shown on

the right of Figure 4.7: Heat treatment, Grinding (Without Thermal Damage) and Thermal Damage Induction. These three processes are more detailed explained in the next topics.

The parameters for the heat treatment and grinding were defined according to the surface characteristics required.

4.2.2   Heat treatment

Carburizing, or case hardening, is a usual heat treatment in gears industry, aiming to secure a hard case and a relatively soft but tough core (RAKHIT, 2000). After the treatment, the workpiece will have high carbon content at the surface graduating into the low-carbon core.
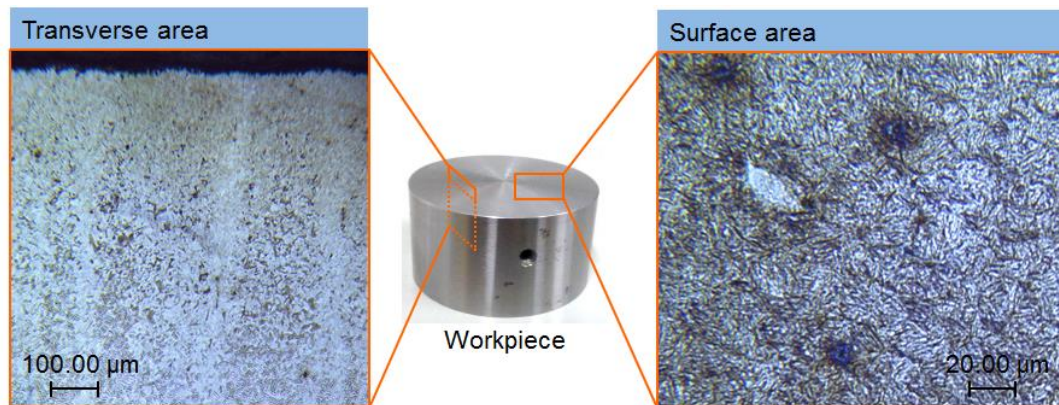
Figure 4.8 – Workpiece metallography after heat treatment.

Carburizing was performed, followed by quenching and tempering. The surface hardness after the treatment is 60 HRC, with a case depth of 0.8 mm, while the core is 33 HRC, measured at 10mm from the surface. The surface contains a maximum of 5% of retained austenite. This is an acceptable value, considering the production of gears. The Figure 4.8 shows a metallography of the surface, on the right, as well as transverse area of the workpiece, on the left. The image of the surface shows small black areas characterized as cementite that appears during the temper process, through the martensite structure. The bigger black areas are the retained austenite.

4.2.3 Grinding Process

The main objective of the grinding process is to reproduce the flank surface integrity of the gear to the surface of the cylindrical workpieces. As described before, no thermal damage should be induced at this moment, but the process is important in order to obtain the surface mechanical properties required. Therefore, the process must be carefully conducted so the surface is not damaged. Another concern is regarding the workpiece clamping during the process. Usually, clamping systems of grinding machines use magnetic tables. Since magnetism significantly influences the *Hall* method measurements, the magnetic table must be avoided. To replace the table, a mechanical vise was used, and an accessory was manufactured to fix the workpiece to the vise. The fixation system is explained in Figure 4.9.

Figure 4.9 - Description of the grinding process used for the cylindrical workpieces.

The grinding was performed in the facilities of the SENAI "Santos Dumont" São José dos Campos, Brazil. Pre-tests were performed in order to set the correct parameters to achieve the surface roughness required, Ra = 0.3 µm and Rz = 2.3 µm. The machine used was a plane grinding from the company Ferdimat, model TA63 and the grinding wheel was AA46M5V. As for the machining parameters, after the pre-tests they were defined as: total removed material of 0.1 mm, wheel rotation speed of 1900 rpm, wheel feed speed of 1.1 mm. Lubricant was utilized during the tests, so the temperature does not excessively increase, avoiding

damage the surface integrity of the workpieces. The lubricant was Tamaru 2730, from the manufacturer Quaker Cool.

4.2.4 Thermal damage induced by laser

One of the goals of the study is to analyze the capacity of the new method in measuring different levels of thermal damage, such as oxidation, thermal softening and re-hardening. In order to guarantee that this goal will be fulfilled, the workpieces must contain the specific thermal damage level required. Therefore, the generation of the damage must be performed by a controlled and reproducible process, which can assure the type of thermal damage induced. The generation of the burn is mainly influenced by two factors: temperature and time. Since temperature control during the grinding process is not trivial, another process was used to generate the burns: laser. The laser process presents the advantages of being a method with high control of the induced temperature and heat induction time. Therefore, the process presents high reproducibility, which makes it more suitable to the study purposes.

Each level of thermal damage is achieved at a certain temperature, depending on the material, as described on the upper side of Figure 4.10 a). Pre-tests were performed, to achieve the correct laser parameters: laser power percentage, interaction time, heat curve time.

Figure 4.10 b) presents the two laser set ups used. The set up for thermal softening and re-hardening contains an optic pyrometer which is responsible to measure the temperature surface during the process. The laser power is connected to the pyrometer, so the temperature measured is responsible for the laser power control. This system allows the increasing or decreasing of the laser power automatically, according to the temperature measured at the surface by the pyrometer. However, the pyrometer is precise only for temperatures above 400°C. Due to this, this system is used only for the damages of re-hardening and thermal softening, 900 and 500°C, respectively.

For the damages of oxidation, between 100 and 250ºC, a manual pyrometer was used. Unlike the set up before, the manual pyrometer is not connected to the laser, and parameters such as power percentage, must be set manually. The control of the process was done by the time of laser exposure and the temperature of the workpiece surface registered by the manual pyrometer. The temperature must be kept lower than 300°C, and a constant value of power was set.
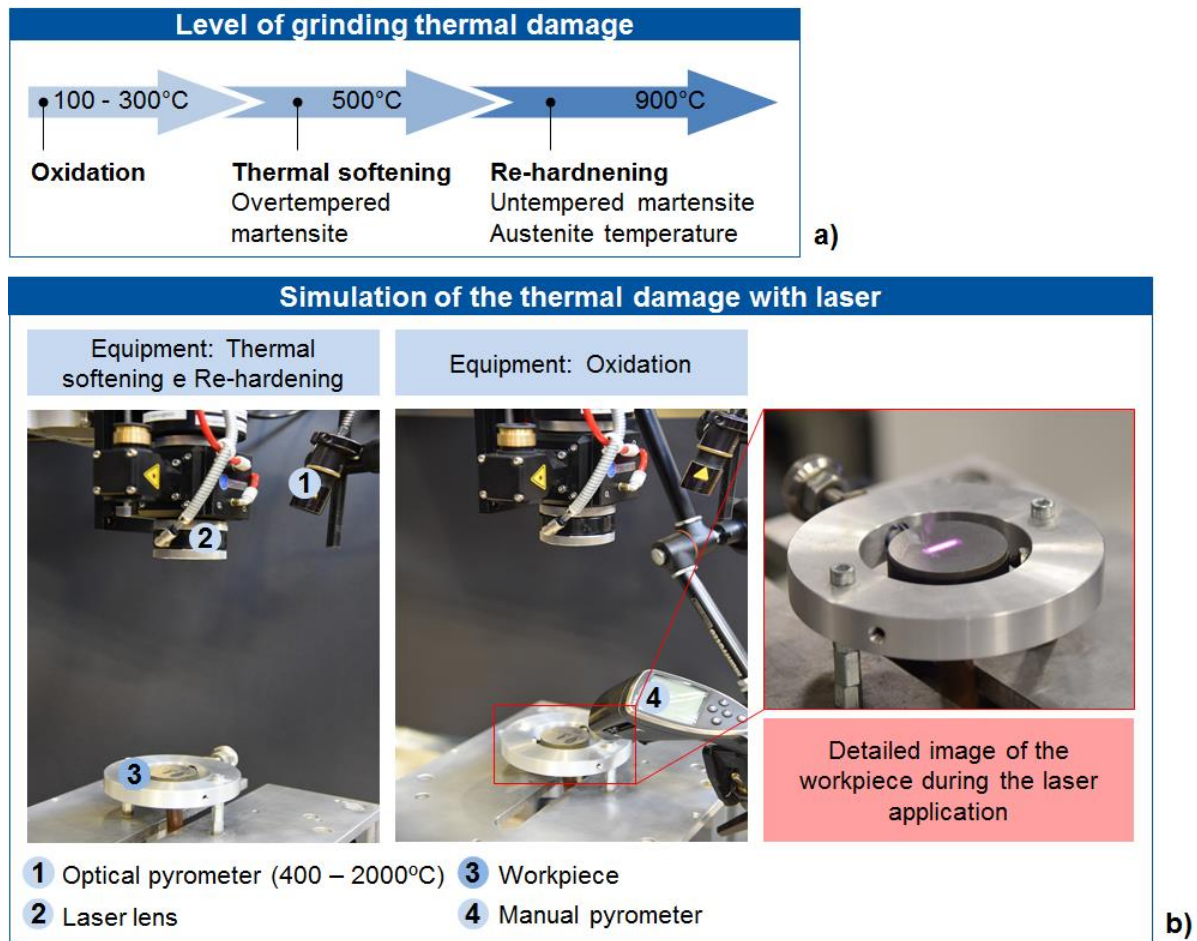
Figure 4.10 - Laser system for simulation of thermal damage: a) Description of the degrees of grinding burn and its respective temperatures; b) Set up of the laser tests, with optical pyrometer for thermal softening and re-hardening degrees and manual pyrometer for the oxidation degree.

The laser used is a diode laser of continuous wave, from the company Laserline GmbH, model Laserline LDF 5000-40. Its maximum power is of 5000W.

The objective of the pre-tests with laser is to determine the correct laser parameters which can reproduce the material characteristics of each thermal damage level required. Based on the laser system described before, the variables analyzed in the pre-tests were defined: temperature [°C] and interaction time [s]. Table 4.2 describes the tests performed. The values of temperature and interaction time were defined according to information obtained in literature, in the works of SANTA-AHO, 2012 and SANTA-AHO, 2012

Table 4.2 – Parameter for the pre-tests with laser process.

Level of Thermal Damage	Temperature [ºC]	Interaction Time [s]
Oxidation	< 300	7
Oxidation	< 300	10
Thermal softening	500	2
Thermal softening	500	3
Thermal softening	500	4
Re-hardening	900	2
Re-hardening	900	3
Re-hardening	900	4

The curves of temperature and laser power variation during the laser interaction time are shown in the Attachements. The curves as shown only for the damages of thermal softening and re-hardening.

After the pre-tests, the workpieces were analyzed by metallography and micro-hardness tests, to verify the influence of the laser on the material surface.

4.3 PHASE PRE-TESTS: Hall method pre-tests

This phase is a first investigation about the performance of the method regarding the measurement of a magnetic situation already known. The main objective of the test is to verify if the method is able to give the expected result, when facing this known situation.

Figure 4.11 describes the steps for this test: *(1)* a non-magnetized workpiece is chosen and measured with the *Hall* method, in order to verify the initial magnetic state of the workpiece. The resolution of the scan is 1 x 1 mm;
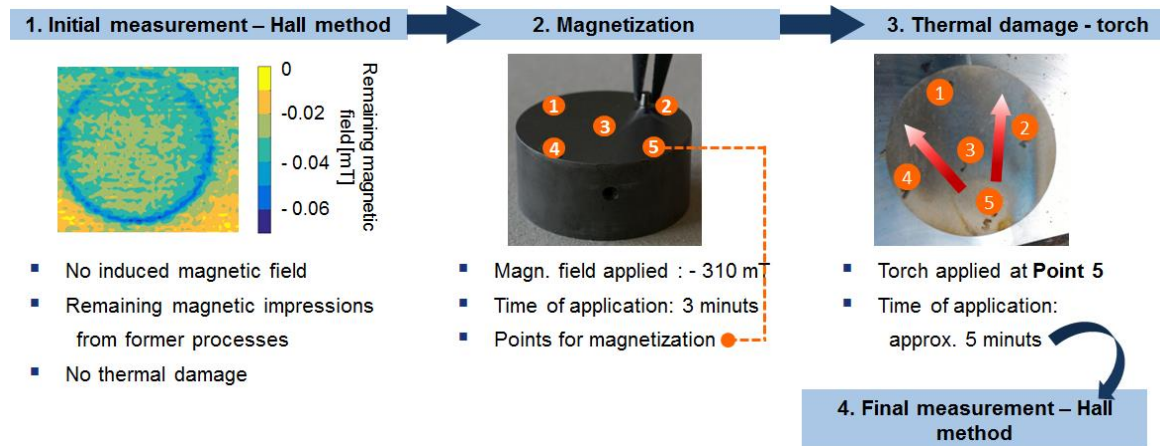
Figure 4.11 - Description of steps for the pre-tests using the new *Hall* method.

(2) the second step is to magnetize the workpiece. A cylindrical magnet with a signal of -310 mT is applied in five different points over the workpiece surface, for three minutes; *(3)* the following step is to induce a thermal damage by the application of a torch to the workpiece surface. The torch is applied to the point 5, shown in Figure 4.11, while the rest of the surface is protected with an asbestos fabric. Although the asbestos fabric does not avoid the heat transference inside the material, it prevents the torch flame from getting directly in touch with the surface. With this set-up, it is expected that, since the heat flux is different in each magnetized point, a difference in the magnetization signal should be detected, according to the heat induced to this point.

The workpiece is analyzed before and after the torch application, regarding four characteristics: Signal magnitude average, Minimum signal, Magnetized area size, Standard deviation of the signal magnitude. These analyses are performed in a squared area with dimensions of 15 x 15 mm around each magnetized point. The same area is measured before and after torch application.

The workpiece magnetic signal after the torch application is measured with the Hall method and compared with the established literature. It is expected that the Hall method is able to detect the alteration in the magnetic signal induced by the torch. Once the result is confirmed, the next phase starts.

4.4 PHASE 2: Thermal damage investigation

To answer two questions proposed by this study, the next steps are performed. Regarding the evaluation if the method can detect the different alteration in the material

phase, two degrees of thermal damage were inducted in the workpiece by laser process, thermal softening and re-hardening. For the evaluation if a damage with the same material microstructure will also be detected by the *Hall* method. a different state of residual stresses was induced in the workpiece, represented by the phase of oxidation, shown in Figure 4.12.
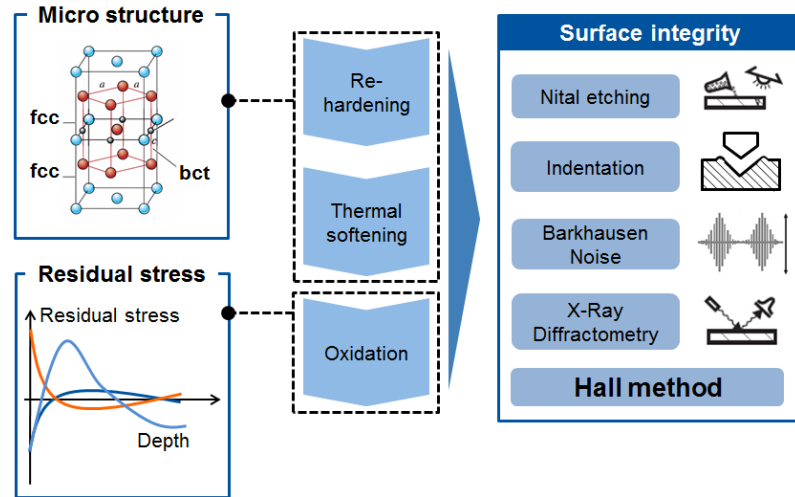
Figure 4.12 - Presentation of the degrees of grinding burn investigated in this work, as well as the measurement methods used for the evaluation of the workpiece surface.

After inducing the damage in the workpiece surface, each condition is measured by different methods of burn detection as well as the new *Hall* method. This step aims to compare the performance of the *Hall* method on different material structure detection, as well as different states of residual stress with already consolidated methods such as nital etching, *Barkhausen* noise, indentation and x-ray diffractometry

For the main tests, the results were submitted to a saturated factorial test of two factors, measurement method and degree of thermal damage, with four and three levels, respectively. In total, twelve tests were performed, as shown in Table 4.3.

Table 4.3 - Definition of tests.

Condition	Measurement method	Thermal damage degree
1		Oxidation
2	*Barkhausen* noise	Thermal softening
3		Re-hardening
4		Oxidation
5	X-Ray Diffractometry	Thermal softening
6		Re-hardening
7		Oxidation
8	Nital Etching and Indentation	Thermal softening
9		Re-hardening
10		Oxidation
11	*Hall* method	Thermal softening
12		Re-hardening

4.4.1 Nital etching and indentation

The tests for nital etching and indentation were performed at the Laboratory for Machine Tools and Production Engineering (Werkzeugmachinenlabor − WZL), from the RWTH Aachen University, in Germany.

The surface of the thermal damage induced by laser presents an intense color, highlighting the damaged area from the rest of the workpiece. The intense color is present for each of the three thermal damages induced. Due to this, the tests for nital etching at the surface could bring misleading results, since their analysis is based on the color modification of the material when reacting to special chemicals. In order to avoid this problem, the nital etching tests were performed through the depth of the thermal damage, as shown in Figure 4.13 a). One workpiece of each thermal damage was tested.

The indentation was performed on a Hardness Test Machine from the company *LECO*, model M-400-H. A load of 1kg was used, for 10 seconds. For the measurements, a line of 12 points crossing the thermal damage was designed, according to Figure 4.13 b). For statistical reasons, the measurement is performed three times, in three different lines near one another.
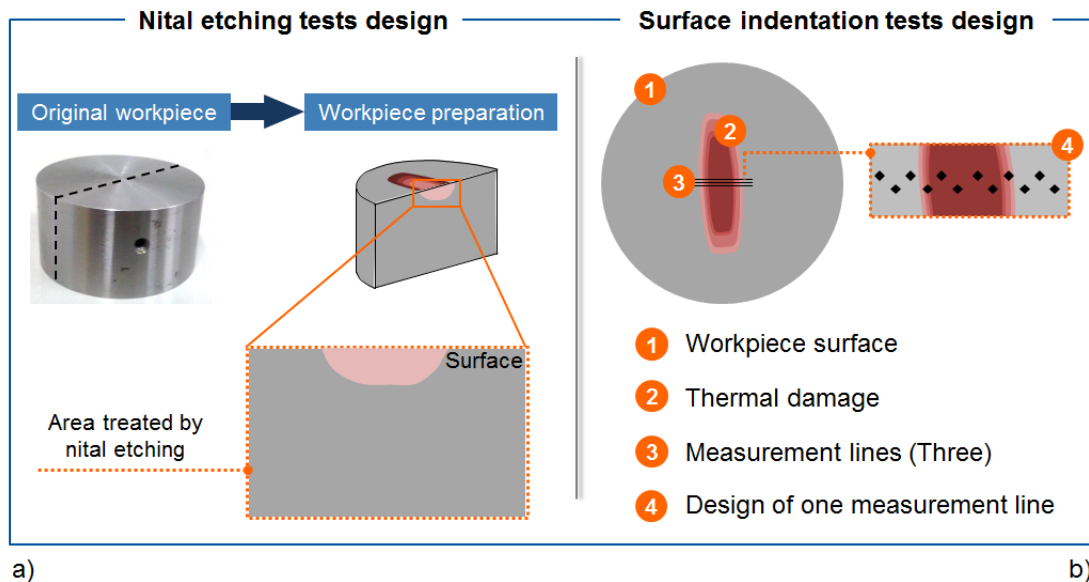
Figure 4.13 - Visualization of the test design of two usual methods for detection of grinding burn regarding phase transformation, a) nital etching on the workpiece section; b) indentation at the workpiece surface.

4.4.2 *Barkhausen* noise

The tests were performed at the Laboratory for Machine Tools and Production Engineering (Werkzeugmachinenlabor – WZL), from the RWTH Aachen University, in Germany. The equipment used was the Microscan 600 from the company Stresstech.

It is well known that the method is highly sensitive to the positioning of the sensor. Due to this, the first step for the *Barkhausen* noise measurements was to design and construct a device to guarantee that the contact between the workpiece surface and the sensor is always the same. The device, shown in Figure 4.14 a), enables the sensor to be positioned always parallel to the workpiece surface, and to be moved in the X and Y axis. The workpiece is moved in the Z axis, putting it in contact with the *Barkhausen* sensor.
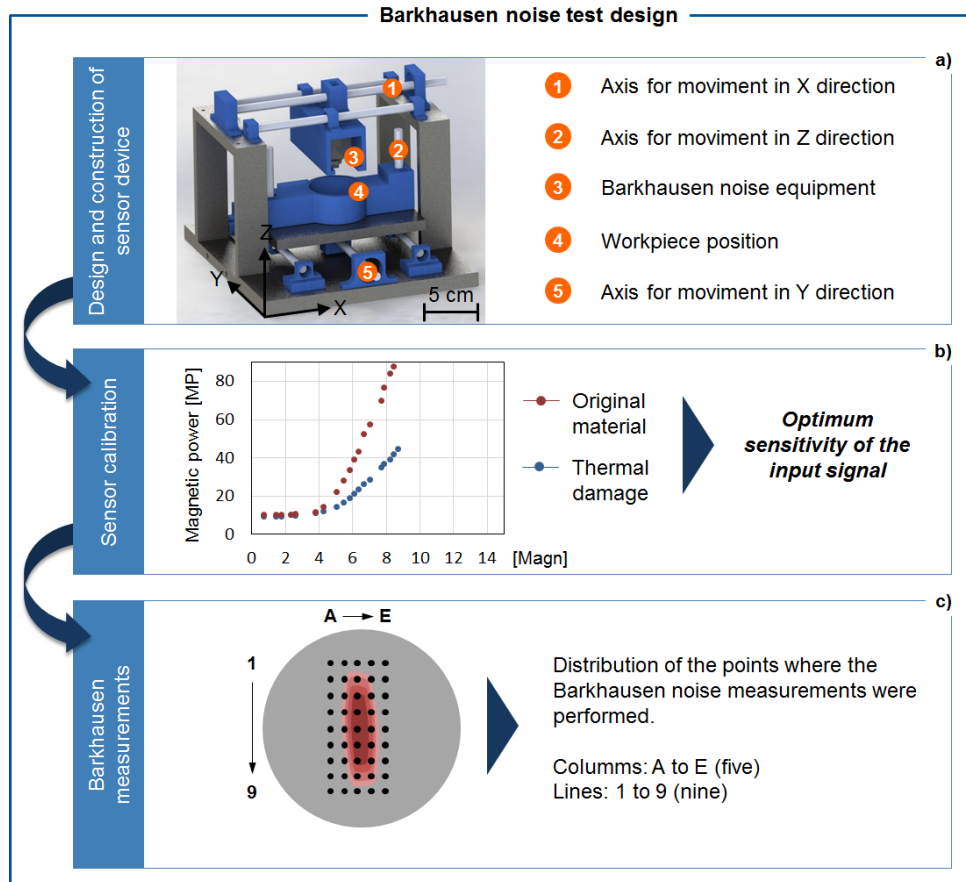
Figure 4.14 - Description of the steps performed for the *Barkhausen Noise* measurements. a) System build in order to apply the *Barkhausen* probe equally in the workpiece surface; b) calibration of the system; c) distribution of the measurement points on the workpiece surface.

The second step is the instrument calibration, which was carried out using a thermally damaged and a non-thermally damaged area of the same workpiece. This step is shown in Figure 4.14 b). Each of the areas was subjected to a series of measurements with the sensor statically held against the workpiece surface. The procedure involved increasing the level of input signal (Magn) and at the same time monitoring the sensor output in magnetic power (MP). The objective is to obtain the optimum sensitivity of the input level for the measurements, which is done by the input level relative to the maximum difference in output for the two measured areas. In this instance, a value of 8V was selected, according to the diagram shown in Figure 4.14 b). For the surface assessment, a matrix of 9 lines and 5 columns was defined, giving a total of 45 points of measurement on the surface, as shown in Figure 4.14 c). The matrix covers the entire area of the thermal damage, as well as a region where, supposedly, no damage was infringed.

The *Barkhausen* noise measurements were performed in one workpiece of each thermal damage level. For statistical means, each workpiece was measured three times.

4.4.3   X-Ray Diffractometry

The tests for residual stress measurements were performed on the machine *Stresstech X3000* diffractometer, localized at the Laboratory for Machine Tools and Production Engineering (Werkzeugmachinenlabor – WZL), from the RWTH Aachen University, in Germany. Cr Kα radiation with Vanadium filter was used with a voltage of 30 kV. The diffraction plane for the steel alloy of the workpiece is {211}, at a 2θ diffraction angle of 156.2°. Both positive and negative values of tilt angles were considered, from $\psi = 0°$ to $\psi = \pm45°$. The measuring point has a diameter of 3 mm. The measurements were performed in the directions $\varphi = 0°$, 45° and 90°, according to the Figure 4.15. The three degrees of grinding burn were analyzed. For each degree, the surface is investigated in 5 points, crossing the region thermally affected. The distance M, covered by the measurement is defined according to the size of each thermal damage analyzed.
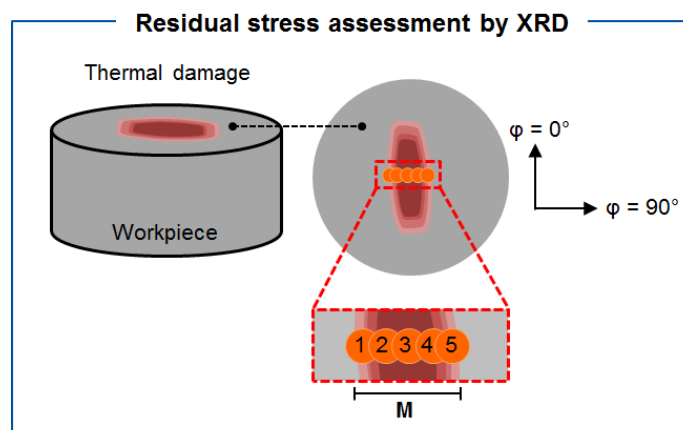
Figure 4.15 - Description of the tests for assessment of residual stresses by means of x-ray diffractometry.

4.4.4   New *Hall* method

The tests were performed at the Competence Center in Manufacturing (CCM), a research laboratory from the mechanical department of the Aeronautics Institute of Technology (Instituto Tecnológico de Aeronáutica – ITA), in Brazil.

The *Hall* probe is from the transverse type, model HS-TGB5-104020, from the company Magnet-Physik. The *Hall* probe is placed in a carbon fiber bar, with dimensions of 1.0 x 4.0 x 200 mm, for thickness, width and length, respectively. The *Hall* probe is placed at the bar's tip, and has an active area with a diameter of 0.4 mm. The range of measurement is from 3 mT to 3 T. It has a resolution of 1μm, basic accuracy of 0.5% up to 1.5T and 1% up to 3T, and temperature correction. Further information regarding the probe can be found in the attachments. The Gaussmeter connected to the probe is the model FH 54, from the company Magnet-Physik. The equipment provides a display with a precision of $3^{3/4}$ digits, measurement ranges between 3mT – 3T, basic accuracy of ±0.3%. Further technical informations are found in the attachments.

The scanning of the workpiece surface is controlled by a routine developed in *Labview*. The basic functioning of the scanning process involving the probe movement and data acquisition was already explained in the topic 1.1.1. For the measurements of the workpieces with thermal damages, the scanning with the *Hall* method has the following parameters:

- Scanning area: 57 x 57 mm^2
- Steps of resolution: 1 mm (X and Y)
- Speed: 1300 steps/s

The area of scanning is defined in order to be greater than the dimension of the workpiece surface. The method presents the advantage of spatial resolution control, providing a more or less refined measurement, according to the user requirements. However, the more refined the measurement, the longer it will last. For the thermal damage measurement, steps of 1mm are chosen because it presented a good combination between spatial resolution and measurement speed.

The general procedure followed for the measurement of the thermal damage with the new *Hall* method is described in Figure 4.16.
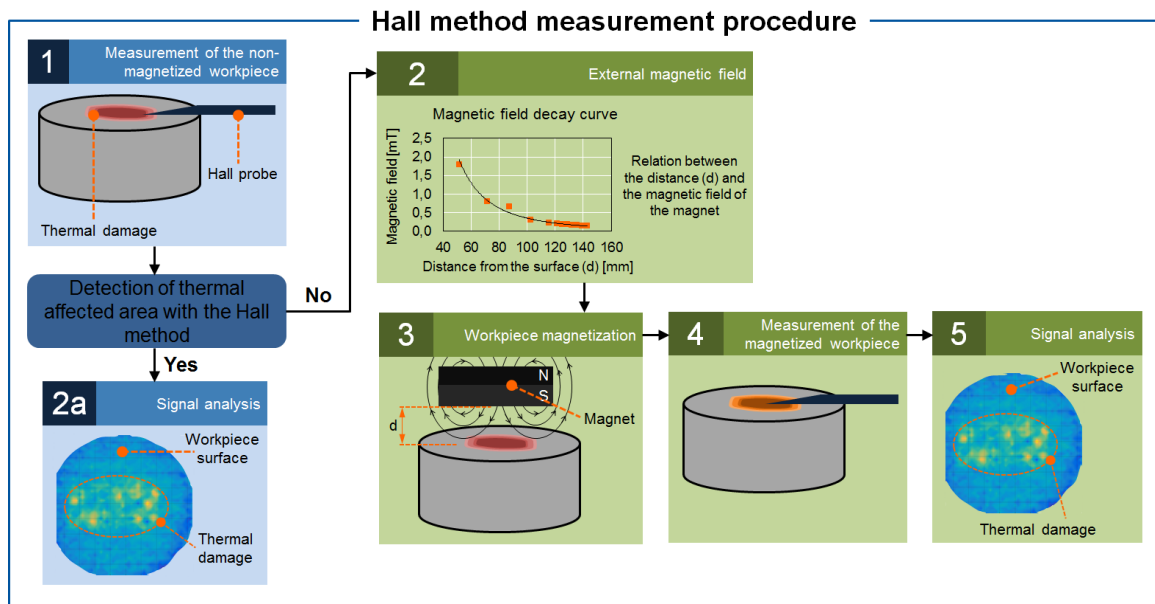
Figure 4.16 - Workflow for the measurements of the workpieces thermally affected using the new *Hall* method.

In this first step, called Measurement of the non-magnetized workpiece, the workpiece is scanned with the *Hall* method, without being magnetized. In this phase, the natural signal of the workpiece is measured and an initial magnetic state of the material is established. The resolution of the scan is 1 x 1 mm. The measurement is analyzed in order to verify if the affected thermal area is highlighted. If the thermal damage is detected, the signal of the measurement is further analyzed, as explained in the step 2a. If not, the magnitude signal of the workpiece must be slightly increased by means of magnetization., shown in in the step 2b. Further informations regarding the application of the magnet are described in the next topic. Following, in the step 3b, called Workpiece magnetization, a constant magnetic field is applied to the region of the thermal affected area. In the next step 4b, named Measurement of the magnetized workpiece, the workpiece already magnetized is scanned with the *Hall* method. The resolution of the scanning is the same used in the first step, 1 x 1 mm. In the last step 5b, Signal analysis, the measurement matrix is analyzed with the aid of visual assessment, and the magnetic signal is further investigated.

(2.1) *Application of magnet on the workpiece surface:*

This step is an alternative in case the natural remanence magnetic field in the workpiece is too low to overcome the influence of the environment. In this situation, the signal must be slightly increased, in order to evidence the presence of the thermal damage. A

ferrite magnet is used, with dimensions of 36 x 23.3 x 16 mm and a nominal magnetic field of 0.11 T. Because the external magnetic field to be applied must be low, the magnet needs to be positioned at a certain distance from the surface. Therefore, the determination of the decay curve of the magnet signal is required. This curve correlates the magnetic field of the magnet over a certain distance. For the curve determination, the *Hall* probe is positioned in different distances, d, from the surface: 51, 71, 87, 102, 115, 121, 125, 128, 132, 135, 139, and 143 mm, and the magnetic field of the magnet is measured. Figure 4.17 a) describes the test, where d_1 is the first distance analyzed, 51 mm, and d_n is the last one, 143 mm.
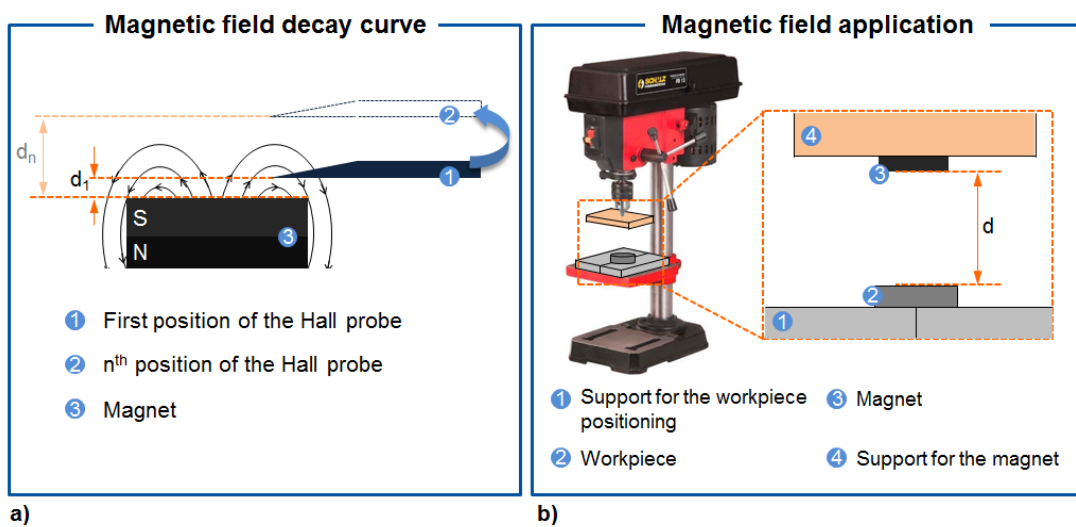
Figure 4.17 - Description of the set up for the magnetization of the workpieces. a) investigation of the magnet to be applied, regarding its magnetic field decay over distance; b) set up for the application of the magnet at the workpiece surface.

The main objective is to determine at which distance the magnet must be from the surface of the workpiece in order to give the field magnitude required.

For the application of the magnet at the workpiece surface, a support was developed for a reproductive way of applying the magnet, as shown in Figure 4.17 b). The support is fixed on a bench drill machine, in order to facilitate the movimentation in Z direction, which is important for a controllable approximation and move away from the magnet to the workpiece. The repeatability of the setup is tested by the magnetization of two workpieces with the same characteristics, under the same magnetization conditions. This is an important test to verify if the setup is able to induce the same magnetic field under the same conditions.

5   Results and discussions

In this topic, the results obtained by the experimental procedure described in Chapter 4 will be analyzed. The topic 5.1 will discuss the results for the investigation regarding the system robustness and the influence of distinct factors on the measurements, answering the first question established in the Objective. Topic 5.2 describes the results for the workpiece preparation, regarding the laser process for grinding burn simulation and the magnetization process applied on the workpieces. In addition, the topic also presents the results of a pre-test using the *Hall* method, in order to verify its measurement ability facing a known condition. This topic is a preparation for the next ones. Topic 5.3 investigates the results for characterization and measurements with the new *Hall* method of the thermal damages within phase alteration, described as thermal softening and re-hardening. The results of this topic will answer the second question established in the Objective. The topic 5.4 analyzes the results for characterization and measurement with the new *Hall* method of the thermal damage without any phase alteration, described as Oxidation. This topic will answer the third and last question established in the Objective.

5.1 Analysis of system robustness and its influence on measurements

In this topic, each sub-topic investigates the factors described in the Figure 4.2 and the potential of each of them to interfere in the measurements of the *Hall* method. The factors under investigation in this topic are: positioning precision, mechanism for *Hall* probe contact to the workpiece surface, and influence of environmental factor, such as temperature, day hour, other equipment and operator.

5.1.1   Positioning precision of the measurement mechanism

This topic presents the results regarding the range of position deviation for the mechanical system built. The analysis for the X axis are shown in Figure 5.1. As established by Table 4.1, the tests were performed in plus (+) and minus (-) direction of the axis, in three different speeds, 1000, 1200 and 1400 steps/sec., along three different distances, 0.04, 5 and

10 mm. the deviation analyzed in the graphics represents the difference between the nominal and the measured distance values. Each bar represents the average deviation obtained in each condition.
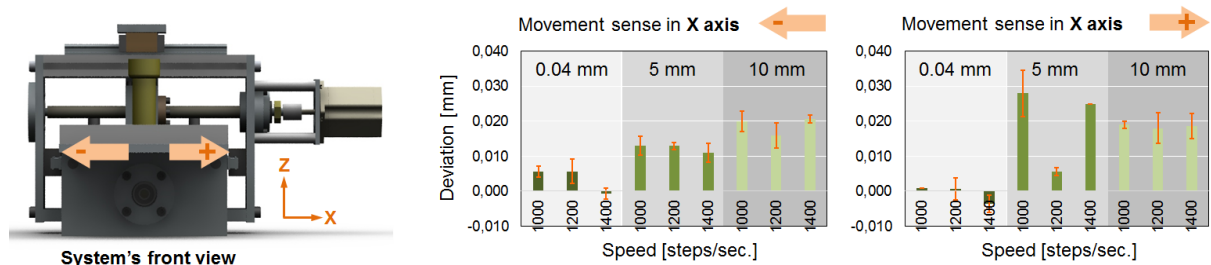
Figure 5.1 - Analysis of the positioning precision for X axis, for both positive and negative direction.

The graphic in the center of Figure 5.1 shows the deviation, in mm, induced by the system in the axis negative direction. As the distance increases from 0.04 to 10 mm, the deviation also increases, reaching a maximum of +20 µm. In this axis, the speed does not influence the deviation. The results in the axis positive direction follow partially the same tendency detect in the negative direction. The exception is found in the distance of 5 mm, where the error increases to a maximum of approximately 25µm.

Figure 5.2 shows the results for the tests performed in the Y axis, in both positive and negative direction. In general, the deviation induced in the Y axis is smaller than the deviation detected in X axis. In the negative direction, shown in the center of Figure 5.2, it is difficult to find a tendency according to the distance applied in the system. In general, the maximum deviation measured is approximately. 10µm.
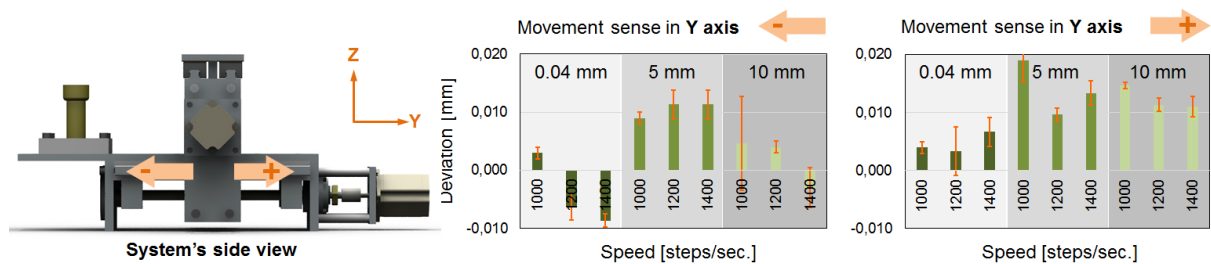
Figure 5.2 - Analysis of the positioning precision for Y axis, for both positive and negative direction.

As an outcome of the analysis, a table is generated, with the positioning deviation estimated for each axis, in both positive and negative directions, for the different distances tested. Table 5.1 gives the average values measured.

Table 5.1 – Error of positioning induced by the mechanical system.

Distance [mm]	X Axis		Y Axis	
	Positive	Negative	Positive	Negative
0.04	-0,67 µm	+ 4 µm	+ 5 µm	-4 µm
5	+20 µm	+12 µm	+ 14 µm	+11 µm
10	+19 µm	+19 µm	+ 12 µm	+ 2 µm

The values of deviation are relative small in comparison to the nominal distances investigated. This result shows that the system build does not negatively influence the scanning process.

5.1.2 Mechanism stability during measurements

This topic investigates the contact between the *Hall* probe and the surface under investigation, for two different *Hall* probe support models proposed, as shown before in Figure 4.4. Each of the models is evaluated according to the contact length induced in the bar tip, as Figure 5.3 demonstrates. Since the *Hall* probe is localized 2 mm from the bar tip and has a diameter of 0.4 mm, the contact length must be bigger than 4.4 mm, in order to guarantee the contact between the probe itself and extra 2 mm around it, for safety.

The first model, shown in Figure 5.3 a), proposes the use of a small weight at the bar tip. By the progressive increase in the workpiece high, it is expected a variation in the contact length. However, the graphic in Figure 5.3 a) shows that the contact length is not much altered by the variation in the workpiece high, and a value bigger than 4mm is only achieved in the last point. The application of the weight in the tip of the bar also presents a practical problem for the function of scanning. The presence of the weight might disturbe the movimentation of the probe, influencing the scanning and the measurements of the surface.
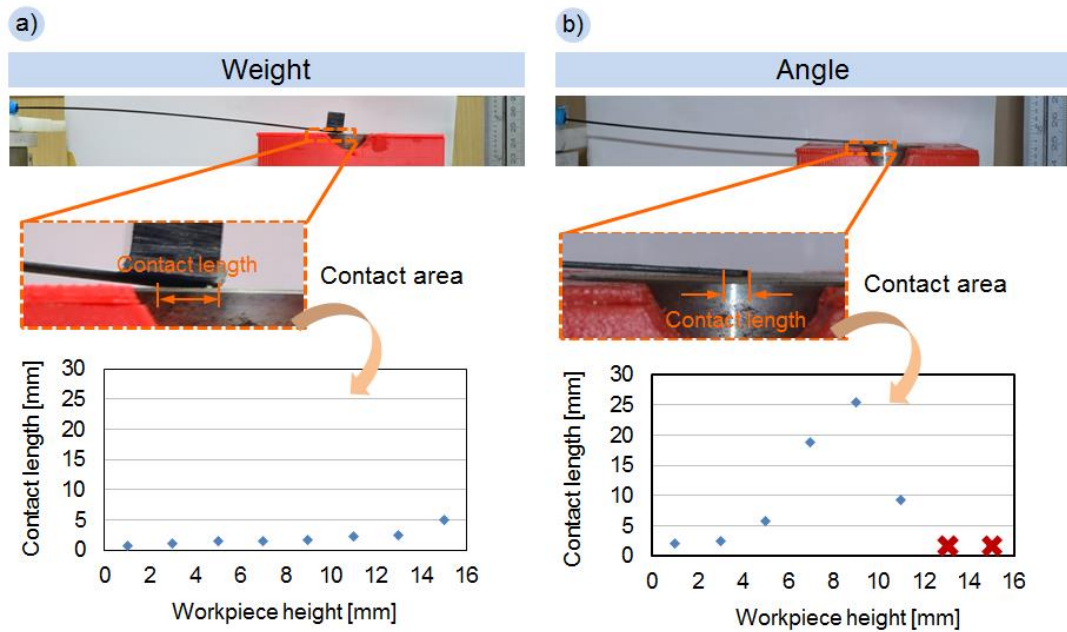
Figure 5.3 - Description of models tested for supporting the *Hall* probe during the scanning process. a) model using a weight to increase the contact length; b) model using an angle to increase the contact length.

The second model investigated, shown in Figure 5.3 b), uses an angle of 7° between the probe and the surface, instead of the weight, to improve contact. In this case, the increase of the workpiece high influences the contact length, raising it significantly. The contact length increases until a point where the bar tip loses contact with the surface, for workpiece high of approximately 10 mm. Until this point, the contact length reaches values greater than the size of the *Hall* probe, which is ideal for the measurements with the new method. In addition, the use of the support with the angle gives the advantage of not adding any obstruction to the movement of the probe during scanning.

After the tests, the support for the *Hall* probe is manufactured, applying an angle of 7°, and the high of the workpiece for further tests is defined as 5mm.

5.1.3   Repeatability and reproducibility

The results of the tests for repeatability of the new *Hall* method are described in this topic. As already described in Chapter 4, all factors further investigated in the reproducibility tests are kept constant. For the repeatability tests, the sample size is 7 repetitions. The analysis is made by the average signal calculated from the measurements in the surface of the

workpiece. The same tests are performed by two different operators. The results of the tests are shown in the table of Figure 5.4, and they are calculated according to the equation 4.1, established in the topic 4.1.3 of the Chapter of Materials and Methods.

	Repetition	Signal [mT]	Average (μ) [mT]	Standard deviation (σ) [mT]
Operator 1	R1	-0,02509	-0,02580	0,00235
	R2	-0,02965	R =	9,12753
	R3	-0,02420		
	R4	-0,02299		
	R5	-0,02428		
	R6	-0,02800		
	R7	-0,02637		
Operator 2	R1	-0,02525	-0,02335	0,00253
	R2	-0,02516	R =	10,83521
	R3	-0,02079		
	R4	-0,02243		
	R5	-0,01926		
	R6	-0,02525		
	R7	-0,02530		

Figure 5.4 - Repeatability results of the *Hall* method.

The standard deviation of the measurements shows a value of approximately 10% of variation, for both operators. This variation expresses quantitatively the repeatability of the method in terms of dispersion in the measurements.

The next step was to analyze the role of different factors on the measurements with the *Hall* method. For this investigation, the strategy of experimentation used is the *one-factor-at-a-time* approach, as already described in Chapter 4. Following, the results are analyzed according to the *Analysis of Variance (ANOVA)*. The *ANOVA* establishes that, for a confidence interval of 95%, the *P-value* < 0.05 confirms that the variation of the parameter under analysis generates distinct results. On the other hand, if the *P-value* > 0.05, the results under analysis are not statistically different. Complementing the analysis, the value of R^2 indicates the strength of the correlation between the results measured and the factor under analysis. A low value of R^2, $R^2 < 75\%$, denotes that the influence of the factor on the results is low (MONTGOMERY, 2001).
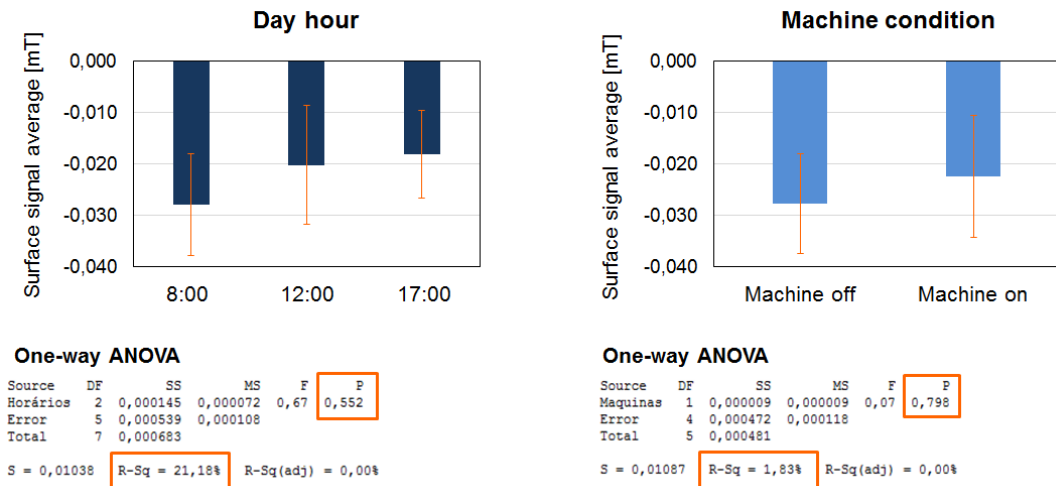
Figure 5.5 - *ANOVA* results regarding the day hour and machine condition on the *Hall* method measurements.

The influence of the day hour and the other equipment present in the room on the *Hall* method measurements are analyzed in Figure 5.5. Measurements on different hours of the day are performed, 8h, 12h and 17h. For statistical reasons, 3 repetitions are made for each level. In the case of the day hour, the *P-value* is 0.552, and the R^2 is 21%, which indicates that the results are not statistically different and that the influence of the day hour on the measurements is low. Regarding the influence of the equipment of the room, the equipment analyzed was a measurement coordinated machine. According to Figure 5.5, the *P-value* for the analysis regarding the machine is 0.798, and the R^2 is 2%. In this case, the results are also not statistically different and the influence of the machine on the measurements is very low.

Next, the temperature in the room is analyzed. The tests varied between three levels of temperature, 20°, 22°, 25°, with 3 repetitions. The temperature in the room must be constantly under control, and can be varied only in a specific range, which determined the values for the evaluation. Since the Gaussmeter contains a temperature compensator device, it is expected no alteration in the measurements inside this range varied. The *Analysis of Variance* performed showed a *P-value* of 0,609 and a R^2 of 15%, indicating that the influence of temperature on the measurement is very low, as shown in Figure 5.6.

The right side of Figure 5.6 shows the analysis of reproducibility regarding the operator conducing the experiments. Two operators conducted the tests and each of them repeated the tests 3 times. The same *ANOVA* performed in the tests before was used here, showing a value of *P-value* of 0.085 and a R^2 of 22%. These values indicate that the results of

each operator analyzed are not ecstatically different from each other, and the influence of the operator on the measurements is very low.
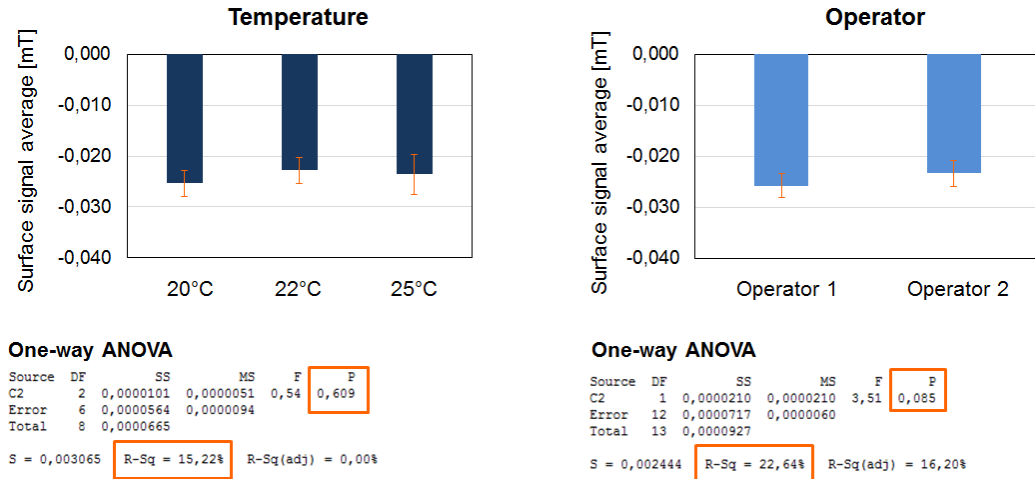
Figure 5.6 - *ANOVA* results regarding the temperature and operator on the *Hall* method measurements.

The tests performed by the tests *one-factor-at-a-time* show that the influence of the four factors tested: temperature, day time, operator and machine condition, on the *Hall* methods measurements is very low, and it does not cause damage to the results.

5.2 Workpiece preparation and *Hall* method pre-tests

5.2.1 Thermal damage induced by laser

The objective of the tests is to determine the correct laser parameter which can reproduce the material characteristic of three different thermal damage degrees: oxidation, thermal softening and re-hardening. The workpieces were analyzed by metallography and micro hardness tests. Figure 5.7 shows the results for the oxidation level, regarding the micro-hardness and metallography.

At this point, the main concern during the pre-tests was to keep the temperature below 300ºC, which was done by the control of the interaction time. Two interaction times were used: 7 and 10 seconds, and the temperatures measured at the surface were, 240 and 277ºC, respectively.

Figure 5.7 - Investigation of the laser process simulation for the oxidation degree of grinding burn, by means of metallography and hardness tests in the workpiece section.

The Oxidation level is the first step for thermal damage during grinding, and it is characterized by no phase alteration in the material and for a slight change of color in the surface (ROWE, 2014). The detection of phase alteration for grinding burn is mainly made by the tests of nital etching and indentation. The analysis of the hardness over the depth is shown in the graphic of Figure 5.7. In the graphic, the curve of both conditions tested are very similar to the curve of the original material. This result suggests that no phase transformation happened on the workpiece. The hardness curve of the original workpiece decreases along the depth. This is an expected phenomenon of the cemented layer, according to Callister (2013). In his book, Callister explains that during carburizing, the carbon diffusion decreases into the core direction, due to the difficulty of the carbon to reach certain depth.

The affirmation of no phase transformation in the oxidation damage is further confirmed by the nital etching tests, shown in the picture of Figure 5.7. The different phases of material will react differently to the chemicals of the test, and a different coloration is detected (MAYER *et al*, 1999; DAVIS, 2005). However, no alteration in the color is visualized in the test, which confirms that no phase alteration occurs due the thermal input by the laser for the oxidation tests. For oxidation, interaction time of 10 seconds was selected.

Figure 5.8 shows the results of the tests for Thermal Softening level, regarding micro-hardness and metallography. At this point, the temperature at the surface is kept at 500°C, during three different interaction times, 2, 3 and 4 seconds. When the hardened steel is heated above the tempering temperature, it results in the thermal damage called Thermal softening, or temper burn (WOJTAS; SUOMINEN; SHAW, 1998, SUNDERRAJAN, 2012).
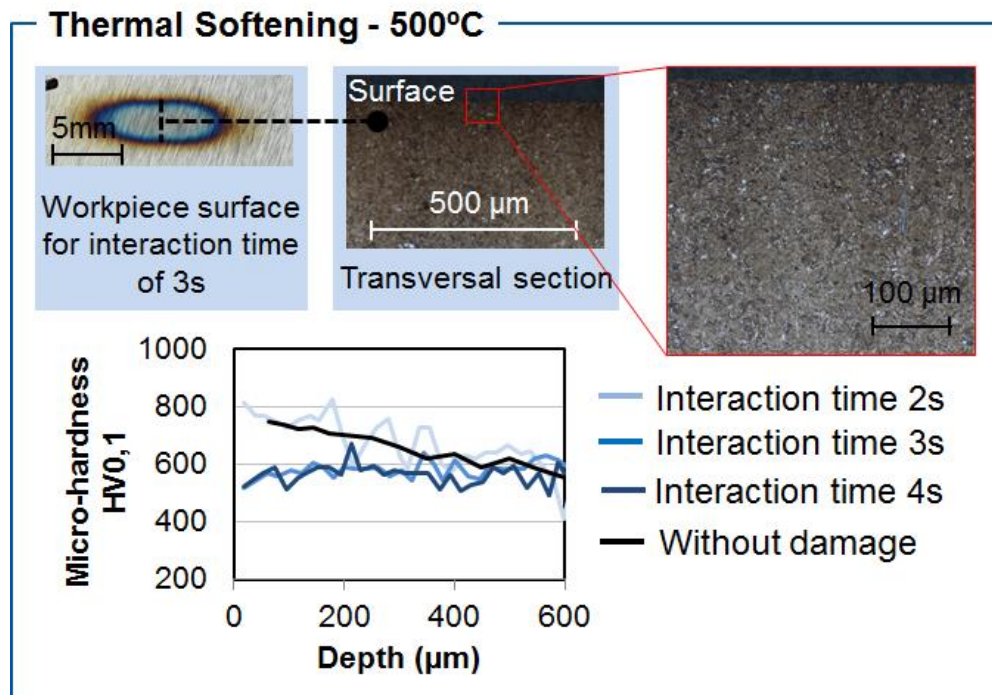
Figure 5.8 - Investigation of the laser process simulation for the thermal softening degree of grinding burn, by means of metallography and hardness tests in the workpiece section. Three different interaction times are investigated.

As a result, the material presents a microstructure of overtempering martensite, causing a tangible decrease in the surface hardness as well as development of tensile residual stresses (WOJTAS; SUOMINEN; SHAW, 1998; SUNDERRAJAN, 2012). The graphic of the hardness over the depth in Figure 5.8 shows that for interaction time 3 and 4, the hardness is reduced at the surface. The reduction of the hardness is a good indicator of the presence of overtempered martensite. To confirm this affirmation, the nital etching test shows a dark layer of material at the surface of the workpiece. According to literature, the overtempered martensite reacts with the chemicals of the nital etching generating a dark coloration (MALKIN; GUO, 2007, SCHWIENBACHER, 2007). The both tests confirm the presence of overtempered martensite, which characterizes the thermal softening degree of damage. For the

manufacturing of workpiece of further tests, the interaction time of thermal softening chosen was 3 seconds.

Increasing the temperature to the austenitizing point, 720°C, and rapidly cooling it by the stop of laser input, will cause the most severe thermal damage, also called a re-hardening burn (WOJTAS; SUOMINEN; SHAW, 1998). Figure 5.9 shows the results from the tests performed for Re-hardening level, regarding micro-hardness and metallography. For the laser tests, the surface temperature was kept at 900°C, above the material austenizing temperature, for three different interaction times, 2, 3 and 4 seconds. The characteristic of this thermal damage is a surface layer of hard and brittle untampered martensite, which is an unacceptable defect for gear functional requirements (MAYER *et al*, 1999; MALKIN; GUO, 2007).
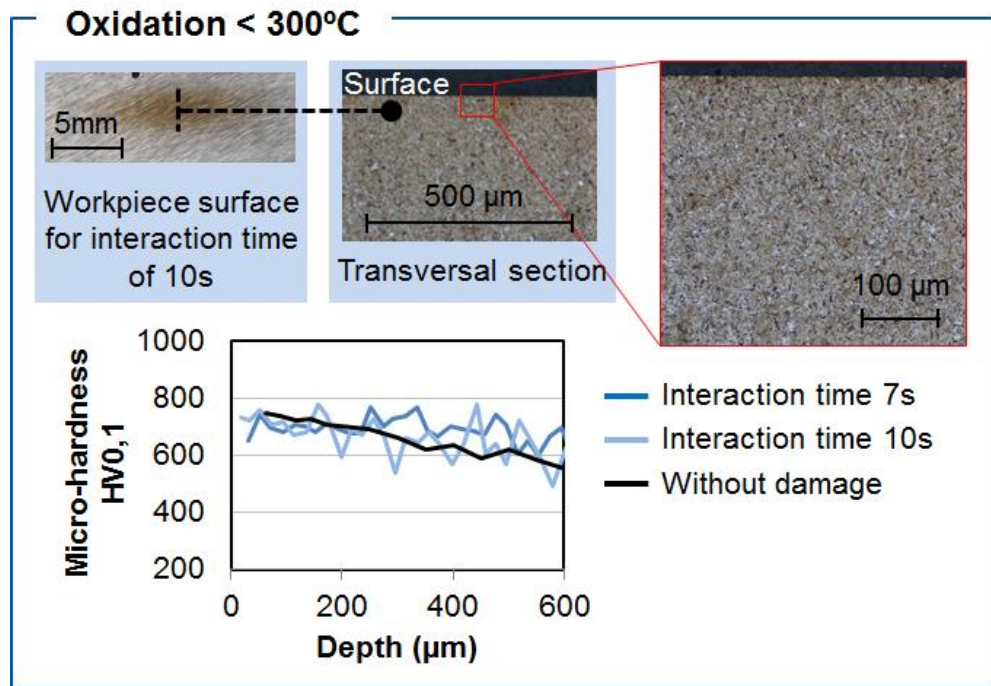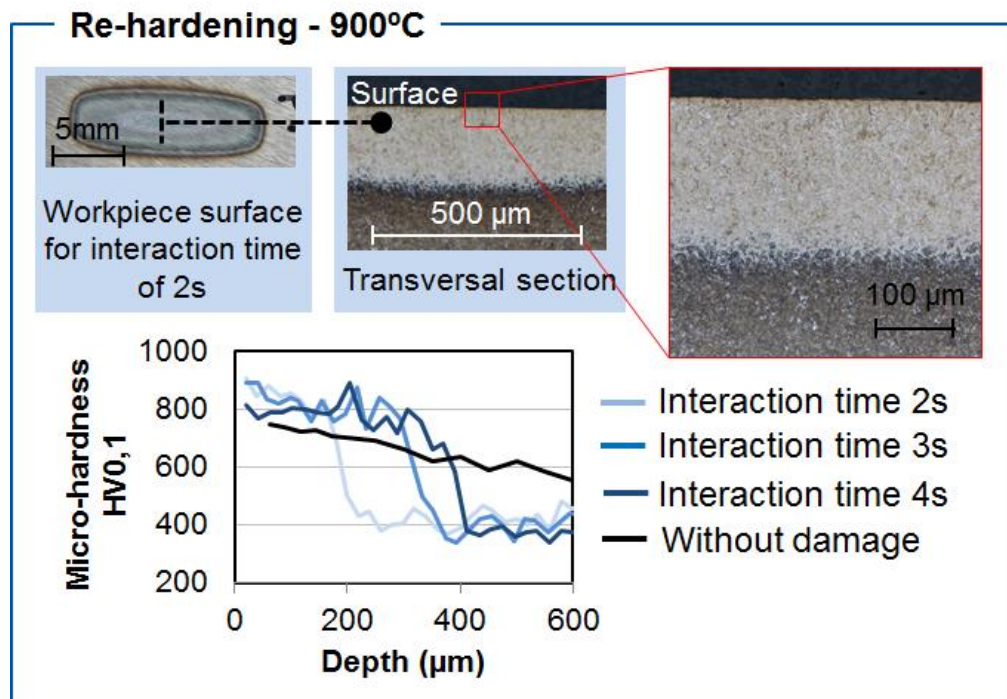

Figure 5.9 - Investigation of the laser process simulation for the thermal re-hardening degree of grinding burn, by means of metallography and hardness tests in the workpiece section. Three different interaction times are investigated.

The micro-hardness tests shown in the graphic of Figure 5.9 demonstrate that for all the interaction time tested, a region of high hardness is obtained. The images of the nital etching complement this analysis by showing a white layer of material in the region of the thermal damage. According to literature, untempered martensite reacts to the chemicals applied by the nital etching tests, changing the coloration to white (DAVIS, 2005;

SCHWIENBACHER, 2007). This is a confirmation of the presence of untampered martensite, formed by the laser heat input.

One important characteristic of re-hardening grinding burn is that the damage areas are always surrounded by area characterized as thermal softening (WOJTAS, 1998) According to the section image shown in the middle of Figure 5.9, the white layer of material is surrounded by the darker layer, which can imply the presence of overtempered martensite. For the generation of this thermal damage level, an interaction time of 2 seconds was used, due to its smaller affected layer.

5.2.2 *Hall* method pre-test

The first results obtained with the *Hall* method are explained in this topic. As stated in Figure 4.11, the main objective of this test is to verify the ability of the current *Hall* method to measure a ferromagnetic material and to present results correspondent to the micro-magnetic theory. The left side of Figure 5.10 shows the *Hall* method measurement of the workpiece surface after its magnetization in five different points, under the application of the same magnet. The difference in the area affected by the magnet in each of the points is due the difficulty in applying the magnet. However, the maximum signal magnitude is the same for all the points, as shown in the image of Figure 5.10.
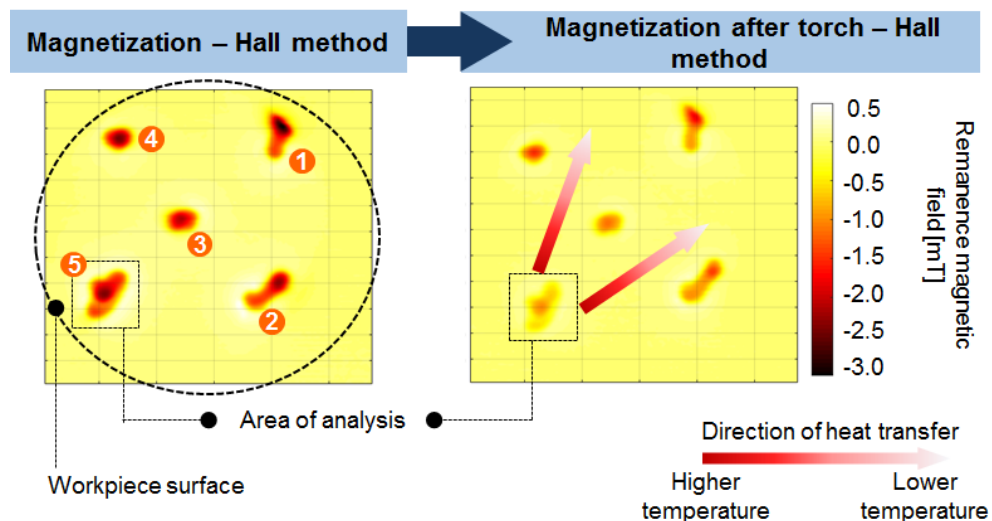
Figure 5.10 - Scanning of the surface with the *Hall* method, characterizing the remanence magnetic field at the surface, before and after the application of a heat source.

After the application of the torch, the surface is once again measured with the *Hall* method and the result is shown in the right side of Figure 5.10. A first visual analysis of the image shows that the signal is altered in all five points. This alteration is greater in the Point 5, where the torch was directly applied. On the other hand, in the point directly opposite, Point 1, the signal magnitude presents a smaller alteration in comparison to the other points. In order to better verify this behavior, analysis regarding the Signal magnitude average, Minimum signal, Magnetized area size and Standard deviation are performed. The area utilized for these analysis is highlighted in Figure 5.10, in the dashed square.

Figure 5.11 gathers the results of the four characteristics analyzed. The first graphic on the left of Figure 5.11 shows that the signal magnitude average decreases for all the points, after the torch is applied. The decrease of the signal is in accordance with the micro-magnetic theory. It establishes that increasing the temperature of a material with a remanence magnetic field, will cause the re-orientation of the magnetic grains, leading to a demagnetization of the material. The degree of demagnetization of the material is highly influenced by the temperature reached. As high as the temperature induced, greater is the material demagnetization degree (BOZORTH *et al*, 1959; NISHIZAWA, 2008). The decrease of the signal magnitude is greater in the point 5, according to the graphic of Δ of the signal. This is an expected result, because the point 5 is the region most affect by the heat input. As the points are further away from point 5, the heat input is smaller, and, therefore, the influence in the magnetic signal is smaller as well.

This phenomenon is observed in the other three factors analyzed. Regarding the size of the magnetized area, the signals with smaller magnitude surrounding it are easily re-orientated, turning the signal closer to zero. This phenomenon occurs more strongly in Point 5, due the temperature increase, and progressively decreases as the points move away from the region where the torch was applied.
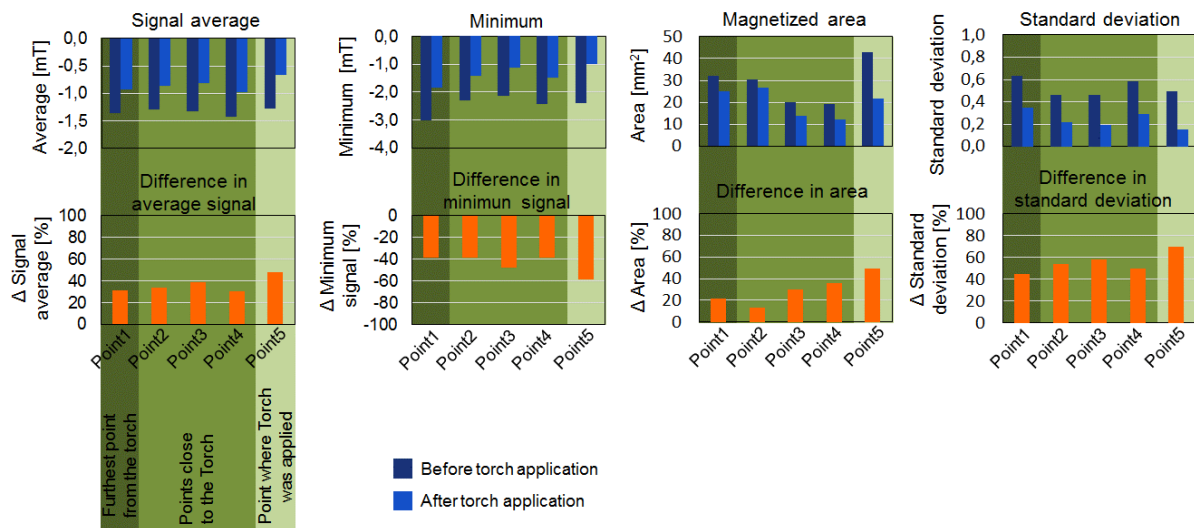
Figure 5.11 - Analysis of the signal before and after the application of the heat source, by means of the new *Hall* method. Five regions over the surface are compared, regarding the signal average, minimum signal, magnetized area and standard deviation.

The results of these tests are a first evidence that the equipment built with the *Hall* probe is able to measure alterations in the magnetic remanence field under the influence of temperature increase. Further than this, the method also presented the ability to distinguish the regions differently affected by the temperature. These results are a great motivation for further analysis of the method.

5.2.3   Workpiece magnetization

In the case the magnetization in the workpiece is required for the tests with the new *Hall* method, the process must be done carefully and always in the same way. The magnetization is performed by the use of a ferrite magnet placed on the on top of the workpiece, at a certain distance from the surface. Figure 5.12 shows the first investigation regarding the magnet.
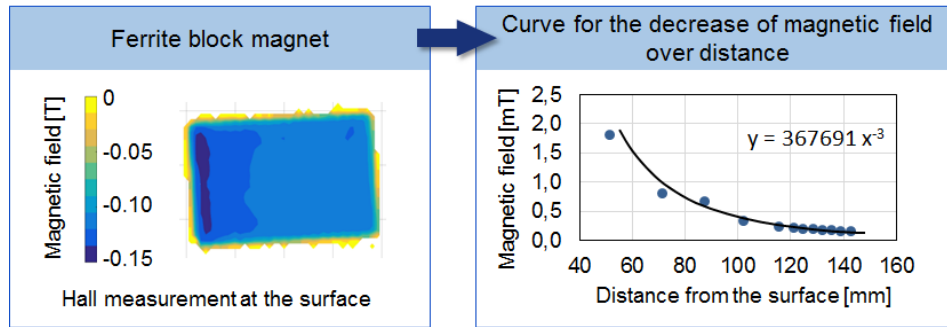
Figure 5.12 - Analysis of the magnet magnetic field and decay curve over distance.

In the left of Figure 5.12, the magnet surface is scanned by the *Hall* method, in order to verify the characteristics of the external magnetic field given by the magnet. Next step is to generate the magnetic decay curve, to correlate the magnetic field applied over the distance. For this test, the *Hall* probe is placed above the magnet over different distances. With these measurements, a curve is generated to represent the magnetic decay. The curve generated by the measured points has the equation 367691 x^{-3}, which is in accordance to the established equation of the magnetic field, B, of an ideal dipole measured along its axis, given by the Equation 5.1.

$$B_{axis} = \frac{\mu_0}{4\pi} + \frac{2\mu}{d^3}$$

(5.1)

For the magnetization of the workpieces, a test of reproducibility for the application of the magnet was performed. For this test, a setup is used, where the magnet is applied at a distance of 13 mm from the workpiece surface. At this distance, according to the curve found, the magnetic field applied is -167 mT.

Two identical workpieces, non-previously magnetized, are placed in the set-up for the application of the magnet. The final objective is to generate the same result in both workpieces for the application of the magnet. This will assure the reproducibility of the set up for the magnetization of other workpieces. Figure 5.13 presents the measurements of both workpieces performed by the *Hall* method, showing the remanence magnetic field.
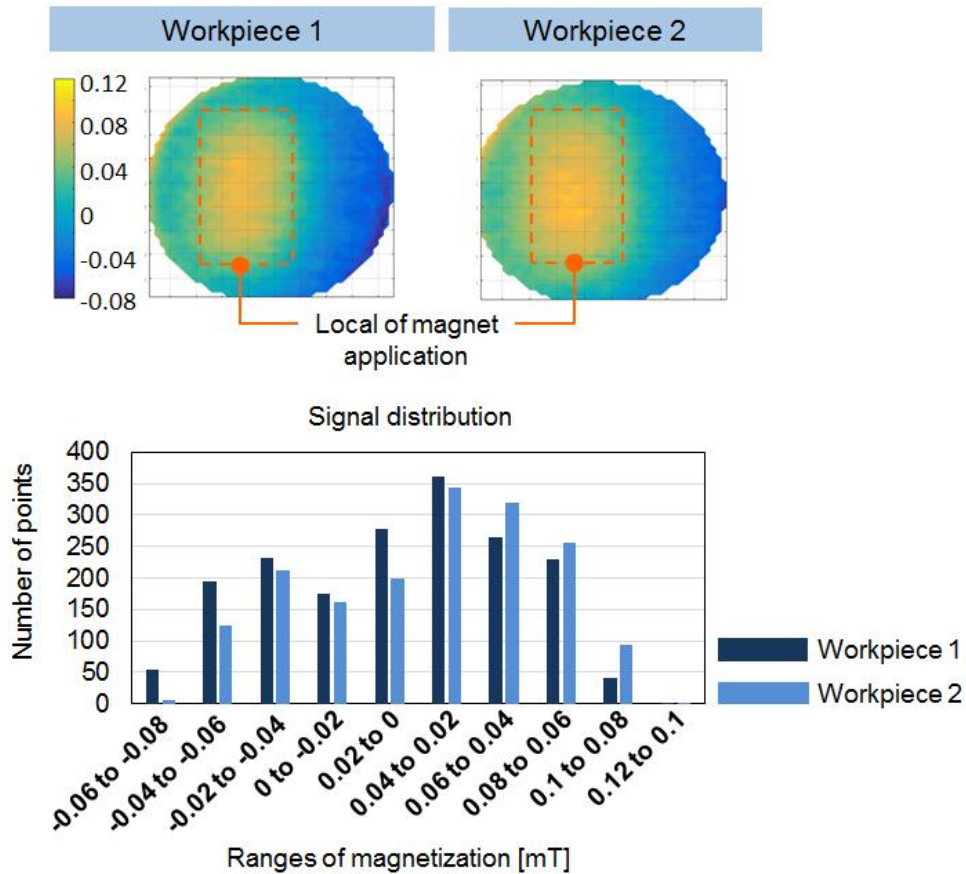
Figure 5.13 - Analysis of the reproducibility tests for the magnet application.

A first visual analysis indicates that the effect of the application of the magnet was the same in both workpieces. An analysis of the signal distribution over the workpieces, shown in the graphic of Figure 5.13, shows a very similar tendency in both cases. This indicates that the set up for the magnet application in the workpiece is capable of reproducing the same magnetization conditions in the workpieces under investigation. This result assures that the magnetization influence is constant in all the workpieces, and if it is required during the *Hall* measurements, the results of different scannings are comparable.

5.3 Integrity assessment of the surface for thermal damages with phase transformation

5.3.1 Investigation and characterization of the thermal damages: Thermal Softening and Re-hardening

This part of the study aims at answering the second question established in the objective, regarding the influence of different material phases on the electro-magnetic properties of the workpiece surface, and its potential to be detect by a *Hall* probe. For this topic, two levels of thermal damage were investigated, thermal softening and re-hardening. However, before the measurements with the new *Hall* method are performed, an investigation of the workpiece surface, for both thermal damages, is required. This investigation is carried out using methods widely known for the detection of grinding burn, such as nital etching, indentation, magnetic *Barkhausen* noise and x-ray diffractometry. This step is very important not only for the surface characterization, as well as for the comparison between these already established measurement methods and the new *Hall* method.

The first damage to be investigated is the thermal softening. The upper part of Figure 5.14 describes the results of the indentation performed at the workpiece surface, through the damage. The graph shows that the hardness profile constantly decreases, as the measurement points get near the damage center. This is an expected result for thermal softening, since the temperature induced in this case is high enough to cause phase transformation of the material from a tempered martensite to a overtempered martensite structure (WOJTAS; SUOMINEN; SHAW, 1998; MALKIN; GUO, 2008). In this phase, due to the increase of temperature, the carbon, trapped before into the tempered martensite structure, is diffused into the material in the form of cementite, reducing the material hardness (BRAMFITT; BENSCOTER, 2002). The hardness reduction is greater in the center of the damage, because it is the region that receives the greater thermal input of the laser.
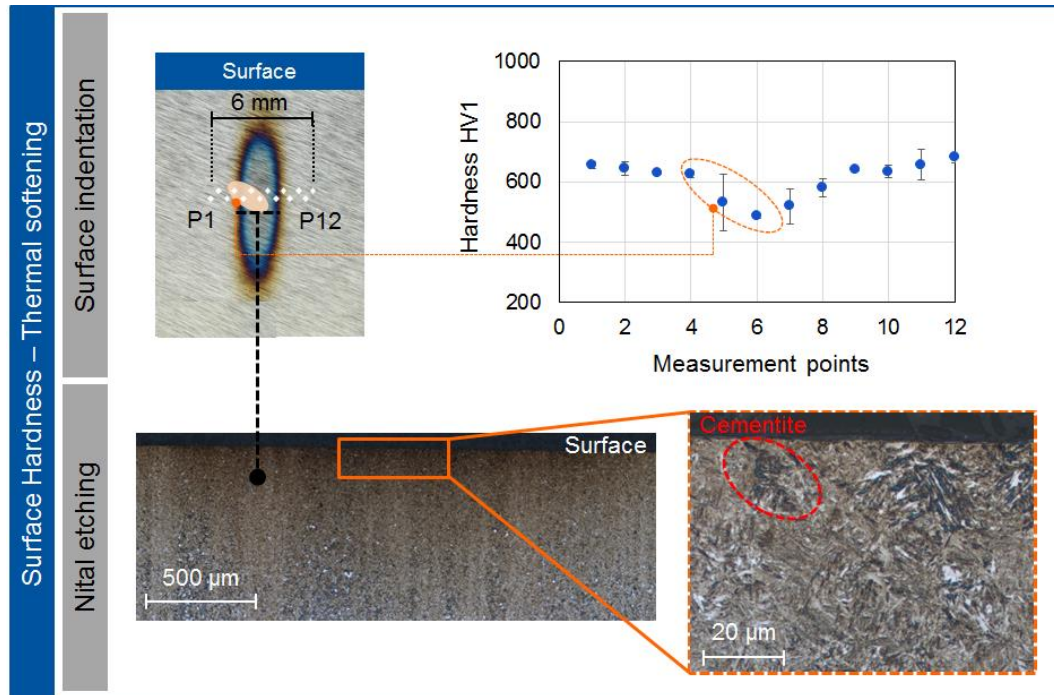
Figure 5.14 - Analysis of the thermal softening degree of damage by means of surface indentation and nital etching over a workpiece section.

The bottom of Figure 5.14 presents the results of the nital etching performed at the profile of thermal softening damage. The images show a dark region at the surface of the workpiece under the effect of the chemicals applied. The modification in coloration brought from the nital etching evidences the presence of a different material phase in that region. In the case of a dark coloration, it means the presence of overtempered martensite, or, in terms of grinding burn, thermal softening phase. The zoomed image of the material structure, at the bottom right of Figure 5.14, highlights darker regions, which can be characterized as cementite that was formed by the increase of temperature. The cementite is highlighted by the dashed red circle in the image of the bottom right of Figure 5.14.

This level of grinding burn is not only characterized by the phase modification, but also by the alteration in the residual stress state. This is already expected, since the thermal input invariably affects the stresses inside the material structure (CHEN; ROWE; McCORMACK, 2000; MALKIN; GUO, 2008). The upper part of Figure 5.15 displays the results for the MBN, as well as the points distribution for the measurements. The results show a high increase of the MBN signal in the center of the thermal affected area. This increase of the signal is a combination between two important factors: microstructure and residual stresses.

Figure 5.15 - Characterization of the thermal softening degree of damage by means of Magnetic *Barkhausen* noise and X-ray diffractometry.

Regarding microstructure, materials with different hardness will have a different behavior towards magnetization (BLAOW; EVANS; SHAW, 2005; GAUNKAR, 2014). A soft phase reaches the magnetic saturation at a low applied field, and it is easily magnetized and demagnetized. In opposite to this, a hard phase is more resistant to magnetization and demagnetization, and a higher magnetic field must be applied (BLAOW, 2005; GAUNKAR, 2014). Due to these characteristics, the *Barkhausen* signal for soft materials is more pronounced in comparison to a hard material. This behavior is verified in the results of the *Barkhausen* measurements for the thermal softening damage. In the central region of the thermal affected area, the signals are higher in comparison to the external region. As already established in the indentation tests, the region in the center is softer than other regions of the

thermal affected area, which explains the high *Barkhausen* signals detected. The second factor affecting the *Barkhausen* signal is the presence of residual stresses in the structure. The results of the XRD measurements, shown in bottom of Figure 5.15, demonstrate a tensile profile of the residual stress. The tensile stress has its peak at the center of the thermal affected area, decaying gradually as the measurement is moved away from the center. Because the center of the damage is the region with bigger thermal input, it is expected that the tensile residual stress is higher in this point. The presence of tensile residual stress also influences the *Barkhausen* noise measurements, increasing the signal magnitude (GAUNKAR, 2014). The interaction between the soft overtempered microstructure and the tensile residual stress state in the center region are responsible for the high values of amplitude detected by the MBN.

The second condition to be investigated is known as the most severe thermal damage that can be induced during the grinding: Re-hardening. The analysis of surface indentation is shown in the upper part of Figure 5.16.
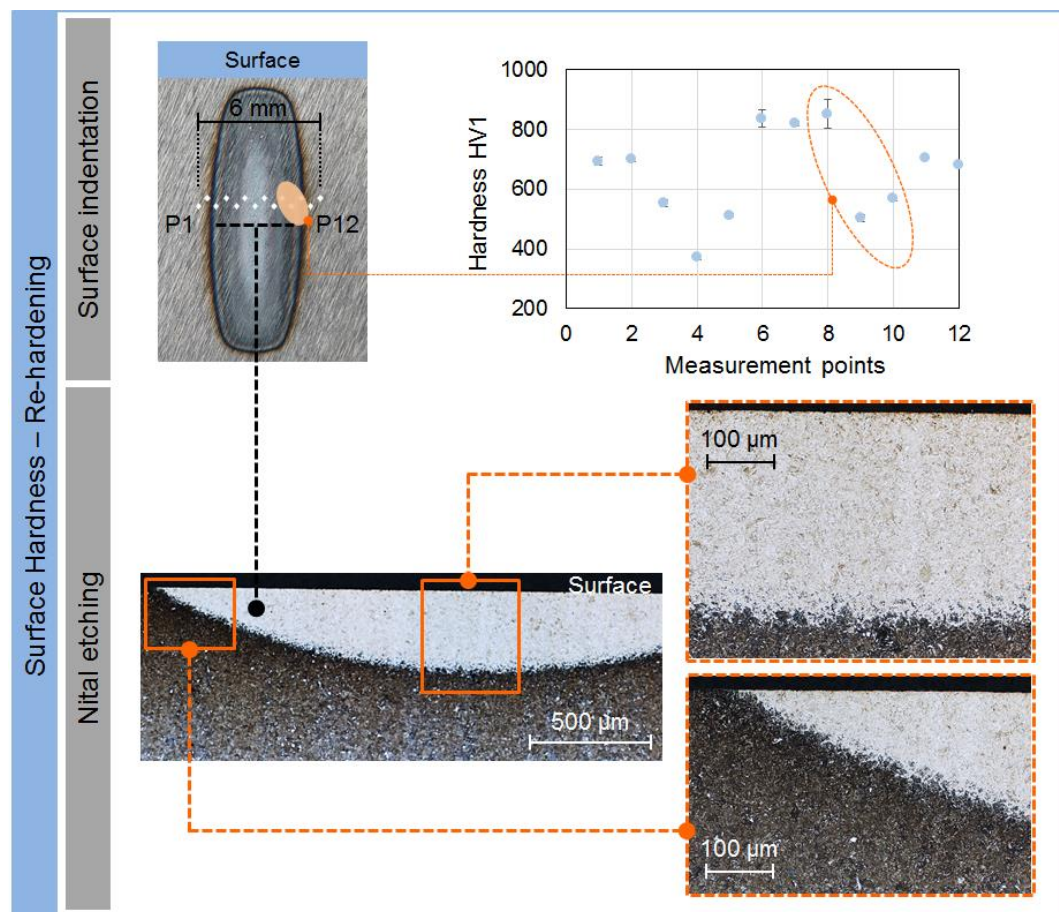
Figure 5.16 - Characterization of the re-hardening degree of damage by means of surface indentation and nital etching.

In the graphic, the hardness increases in the central area of the damage, described in the points 6, 7 and 8. The high hardness detected in the region is due the formation of untempered martensite during the laser process at high temperature (MALKIN; GUO, 2008; ROWE, 2014). This affirmation is further confirmed with the nital etching analysis, shown in the images at the bottom of Figure 5.16. The white layer highlighted in the surface is a specific result of this test, caused by the reaction of untempered martensite under the application of the chemicals applied for the tests. A more careful look in the images of the nital etching points out the presence of a dark layer surrounding the white untempered martensite. This dark layer represents a region thermally affected by the laser and that was under phase transformation. The laser input, however, was not high enough in this region to cause the re-hardening, but it was enough to cause the transformation of the material to overtempered martensite. This is an usual effect on the re-hardening type of grinding burn, already detected in the works of (WOJTAS, 1998). This affirmation is confirmed with the results of the tests of indentation, in the points 3, 4, 9 and 10 of the graphic in Figure 5.16. The hardness is significantly lower at these points, representing the position where the overtempered martensite is localized, around the untempered martensite.

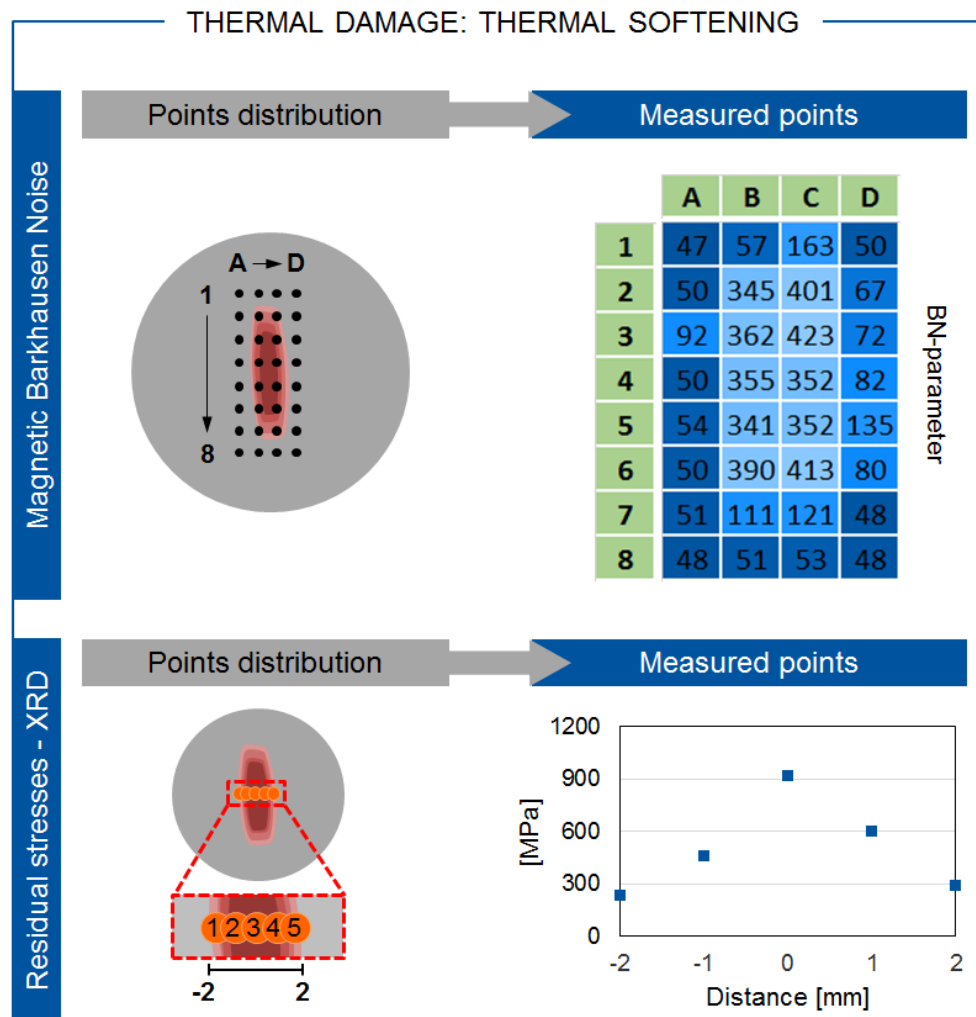The characterization of the thermal damage is further conducted by the measurements of Magnetic *Barkhausen* noise, shown in Figure 5.17.
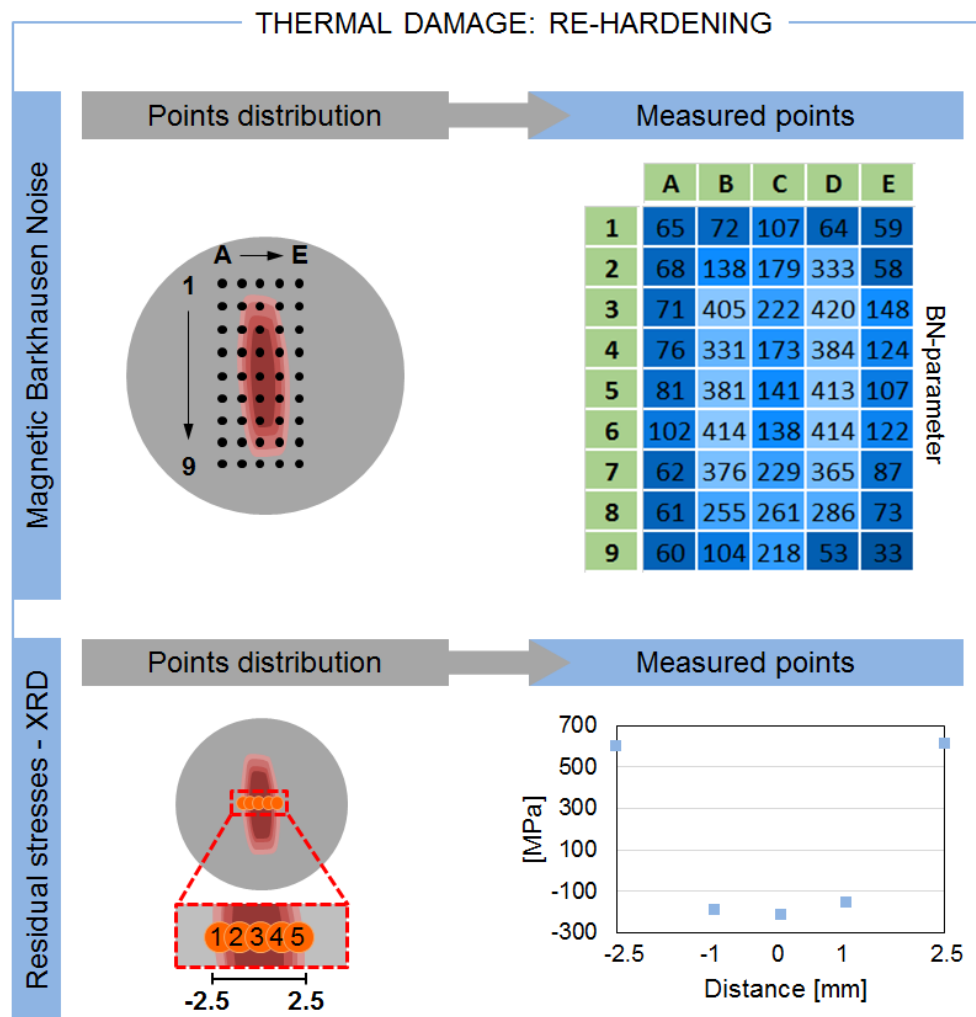
Figure 5.17 - Characterization of the re-hardening degree of damage by means Magnetic
Barkhausen noise and X-ray diffractometry.

The MBN method characterizes the surface not only regarding its phase, but also regarding the presence and the profile of residual stress state. The upper part of Figure 5.17 shows the results obtained from the measurements with MBN. The colored table with the results presents a region, represented by columns B and D, with high magnitude signals. Firstly, the high magnitude can be explained by the presence of the soft layer of overtempered martensite around the untempered martensite, already detected in the indentation and nital etching tests. Concurrently, the decrease of the signal magnitude in the center of the table, in column C, is partially explained by the presence of the hard phase of untempered martensite. The bottom of Figure 5.17 shows the results for the XRD measurements, regarding the residual stress state at the surface. Through the damage, the RS has first a very high tensile character. Next, in the center of the damage, the state becomes compressive, and then, back to

tensile state. The margin of random error in these measurements with this equipment is ± 15 MPa (REGO *et al*, 2016).

This stress profile curve has its main influence in the two phase transformations that occur during the laser process of this damage. Phase transformations very often induce abrupt changes in the volume, which contribute significantly for alteration in residual stresses (BALART *et al*, 2004). In the case of re-hardening damage presented in this study, the center region of the damage is transformed into untempered martensite, which represents a transformation with increase of volume. At the same time, the region around the center goes through a different transformation, and it compresses the material in the center. As a result, the profile of the curve of residual stress is first tensile, then compressive and back to tensile. Both RS and the microstructure alteration influence the measurement seen in the *Barkhausen* noise measurements.

After the characterization of both damages, thermal softening and re-hardening, the workpieces are measured with the new *Hall* method.

5.3.2 Surface integrity assessment with the *Hall* method: Thermal Softening and Re-hardening

This topic presents the analysis of the measurement performed by the *Hall* method of the two types of thermal damages with material phase alteration: thermal softening and re-hardening. The measurements follow the procedure described in Figure 4.16 in the chapter of Materials and Methods. Figure 5.18 shows the image of the measurement of a surface having a thermal softening damage. Investigations regarding the surface, shown in earlier topics, established that phase alteration occurs, transforming tempered martensite into overtempered martensite, a softer phase.
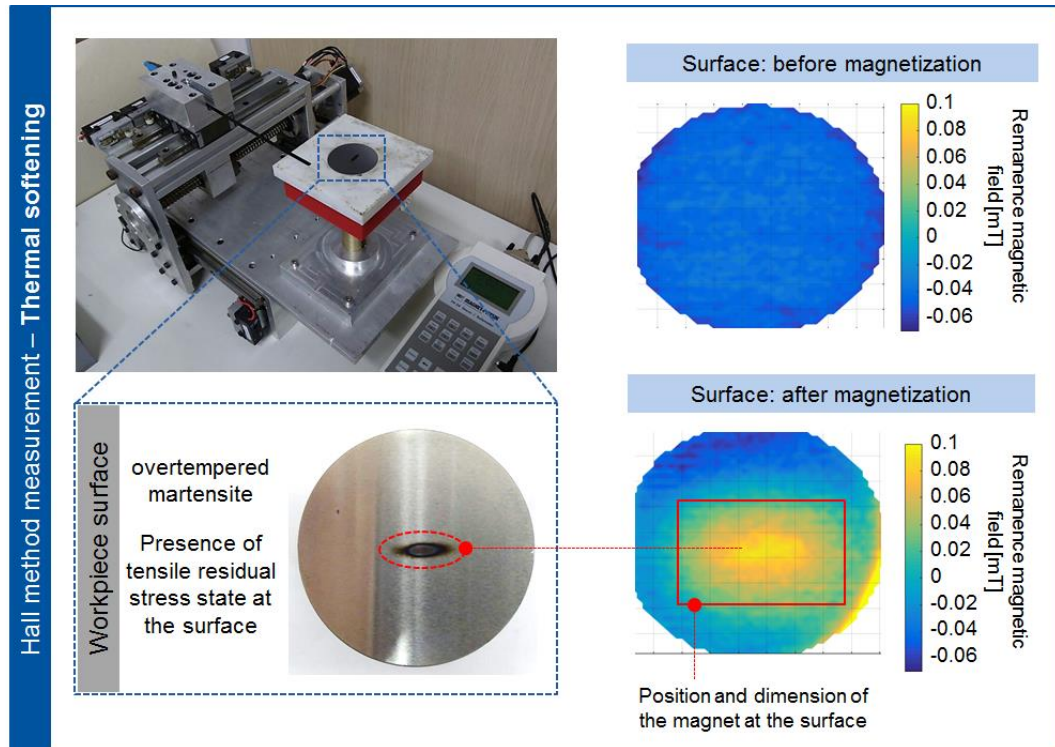
Figure 5.18 - Scanning of a surface with thermal softening using the new *Hall* method. The measurements of the workpiece non-and magnetized are shown.

The right side of Figure 5.18 shows the *Hall* method results of the workpiece, before and after magnetization. The scanning of the workpiece before magnetization shows a relative constant signal through the whole surface, and no signal alteration in the region thermally affected is detected. This result can be explained due to the very low natural remanence field signal of the workpiece, that is easily influenced by the natural noise of the environment. Consequently, a possible alteration in the remanence magnetic field due the presence of thermal softening is covered up, making harder to distinguish the area thermally affected. Therefore, the magnetization of the workpiece is performed, according to the set up described in the topic 5.2.3. This step aims to increase, at a minimum extend, the magnetic signal at the surface. This increase brings the signal above the influence of the environmental noise, and, ultimately, highlights the thermal damage signal.

The image of the workpiece after magnetization generated by the *Hall* method, bottom right of Figure 5.18, shows an alteration in the signal magnitude, localized in the area where the damage is expected. This is an expected result, according to the micro-magnetic theory. It determines that a microstructural variation in the material leads to a change in its magnetic

properties, and can be reflected in the behavior of the remanence field of the material (YIN; PEYTON; STRANGWOOD, 2007; KARIMIAN *et al*, 2014).

Figure 5.19 presents a more detailed analysis regarding the signal magnitude investigation in the workpiece. In the upper left of Figure 5.19 a), the *Hall* measurement of a workpiece without thermal damage is presented. In the upper right side of Figure 5.19 a) the measurement of a workpiece with thermal softening is displayed, under the same magnetized process.
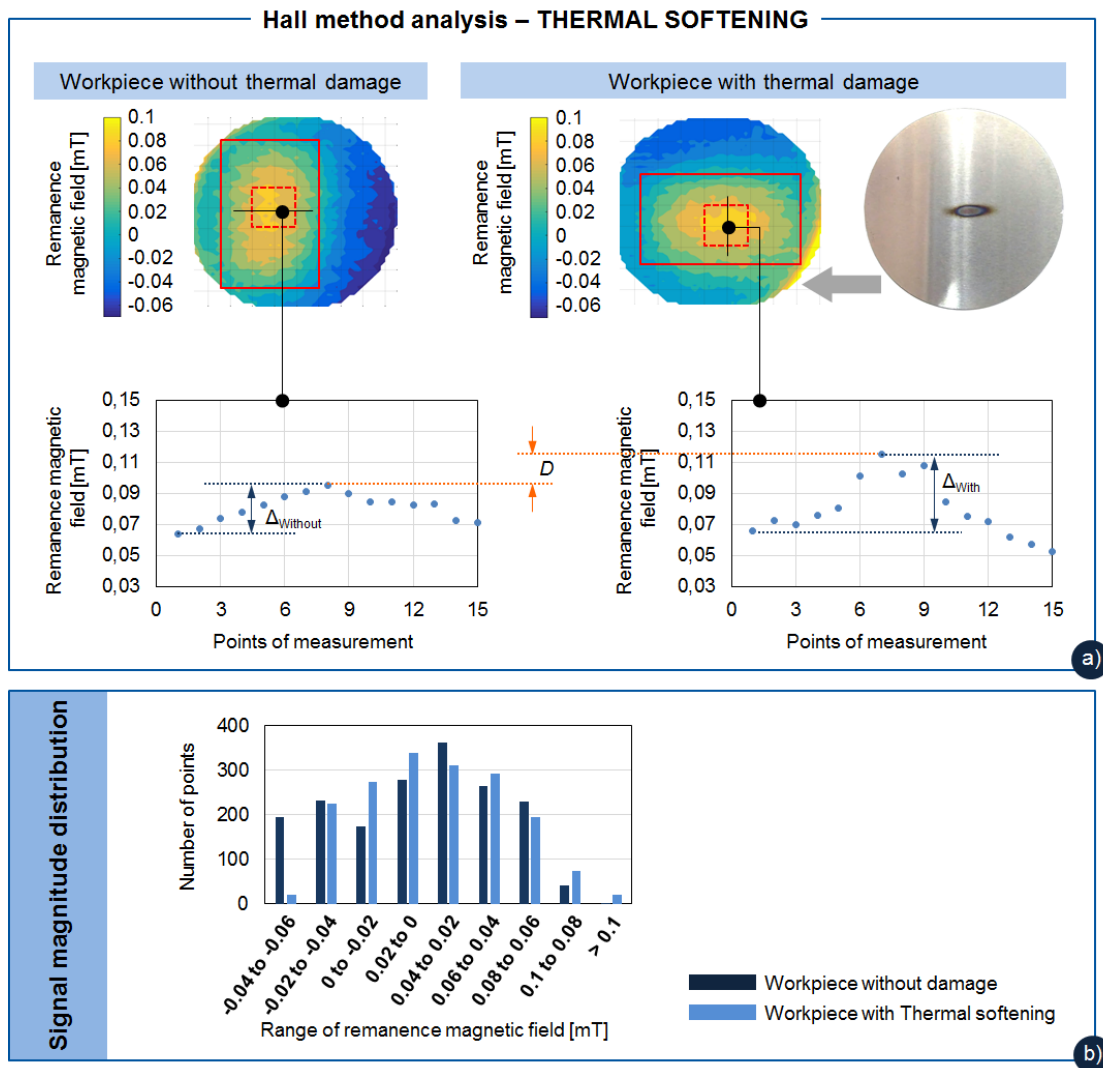
Figure 5.19 - Analysis of the remanence magnetic field signal measured by the scanning with new *Hall* method. a) Comparison between the workpieces with and without thermal softening at the surface, regarding the peak of the signal and gradient in the region of the thermal damage; b) analysis of the general signal distribution for the workpieces with and without thermal softening.

The first analysis performed is the signal magnitude distribution, shown in the graphic in the Figure 5.19 b). This analysis aims to show any general alteration in the signal magnitude due the presence of the thermal softening. The area considered for the analysis is determined by the red rectangle drawn in the images, and it represents the position and size where the magnet was applied. According to the graphic, the tendency of both distributions, with and without thermal damage, is very similar, indicating no general signal attenuation caused by the thermally affected area. A more localized analysis is performed in an area defined by the dashed red square, shown in the workpieces surface in Figure 5.19 a), representing the region most affected by the thermal damage. The average of the remanence signal magnitude in this area is calculated for both with and without damage conditions. The workpiece without damage has an average of 0.076 mT, similar to the 0.078 mT average of the workpiece with damage. On the other hand, the standard deviation calculated in the same area is increased by the presence of thermal softening, from 0.006 to 0.009. This increase in standard deviation shows that the gradient of the signal in this area is bigger with the presence of a different material phase. This confirmation is further analyzed with the remanence magnetism profile shown in the graphics in the bottom of Figure 5.19 a). In this graphic, the peak of the signal increases with the presence of overtempered martensite. In the left side of Figure 5.20, the comparison of the peak signal for the workpiece without damage and with thermal softening is compared in the graphic. The difference is represented by the letter *D*, and the signal increases approximately 35% due the presence of the overtempered martensite.
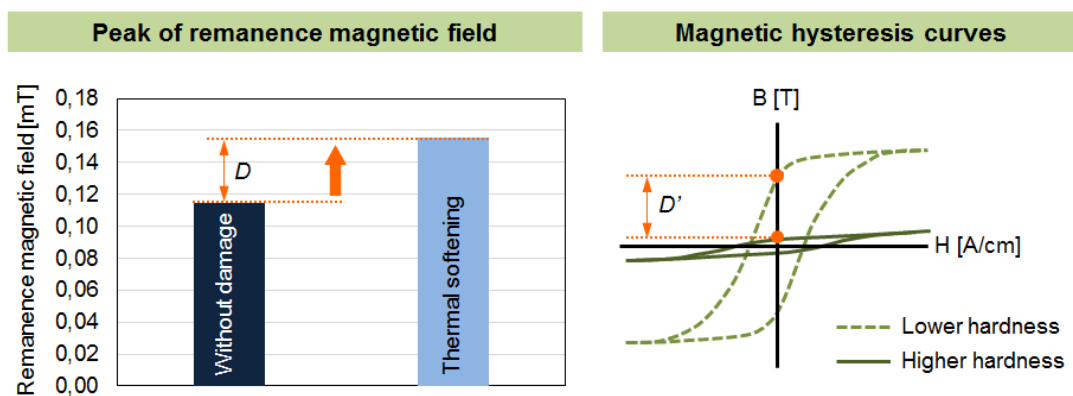
Figure 5.20 - Analysis of the signal measured by the *Hall* method for the workpieces with and without thermal softening, comparing it with the hysteresis curve of a ferromagnetic material (IKHMAYIES *et al*, 2017).

This behavior is explained by the influence of the microstructure on the magnetic hysteresis curve, which will affect the remanence magnetic field in the material (DESVAUX *et al*, 2004). The profile of the hysteresis curve of a microstructure with low hardness, like the overtempered martensite, is narrower than for a material with high hardness, as shown in the example of a curve of magnetic hysteresis on the right of Figure 5.20. Consequently, the remanence magnetic field in a low hardness microstructure is higher, in comparison to a harder material, under the same external magnetic field influence, as described by the *D'*. (THEINER, 1997; IKHMAYIES *et al*, 2017). This fact makes the remanence magnetic signal greater in the region where there is overtempered martensite, a soft layer, highlighting the presence of this phase. This alteration of the magnetic signal due the presence of a different microstructure is detected by the *Hall* method and it is used to indicate the presence of a thermal damage with phase transformation. The gradient between the peak and the area surrounding it for the workpiece with thermal damage is also higher, described in the graphics of Figure 5.20 a) by the factor Δ (with and without damage).

The next thermal damage analyzed is considered the most severe degree of grinding burn: re-hardening. Figure 5.21 shows the image of the scanning with the *Hall* method of the workpiece before and after magnetization.
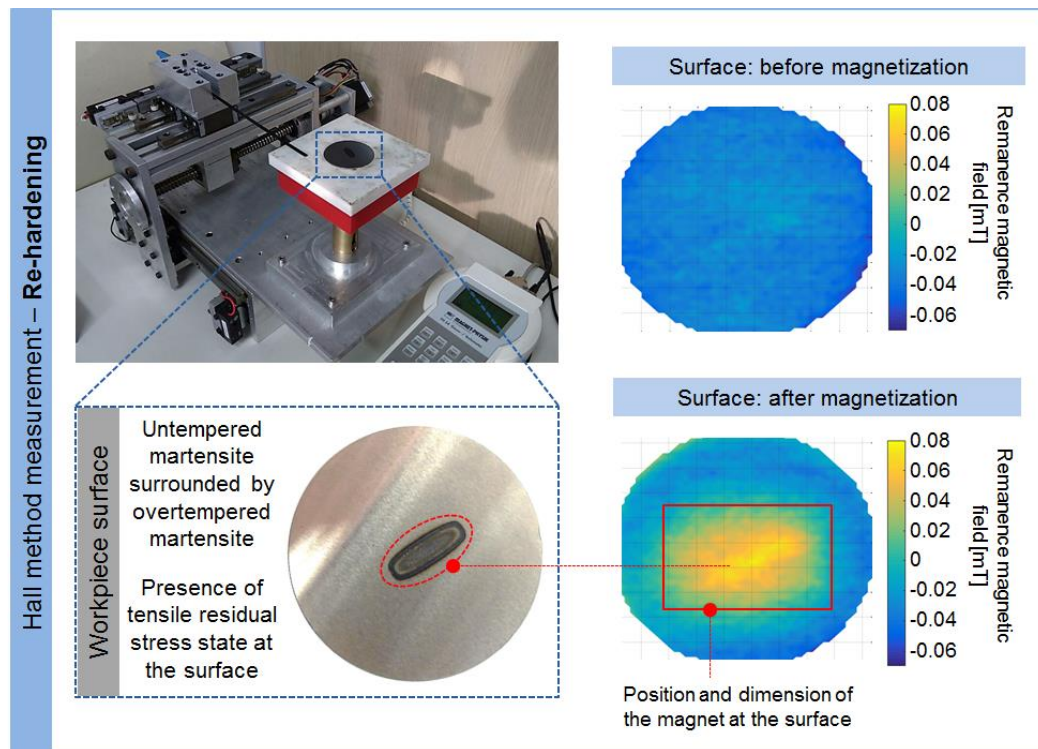
Figure 5.21 - Scanning of a surface with re-hardening using the new *Hall* method. The measurements of the workpiece non-and magnetized are shown.

For this degree of damage, the natural remanence magnetic signal of the workpiece was not high enough to highlight the damage, and the surface magnetization was required. The image at the right bottom of Figure 5.21 shows the measurement with the *Hall* method of the surface after magnetization. In this image, the region where the thermal damage is localized presents a higher remanence magnetic field signal, contrasting with the surrounding area.

Further analysis regarding the signal magnitude in the thermal damage are presented in Figure 5.22.
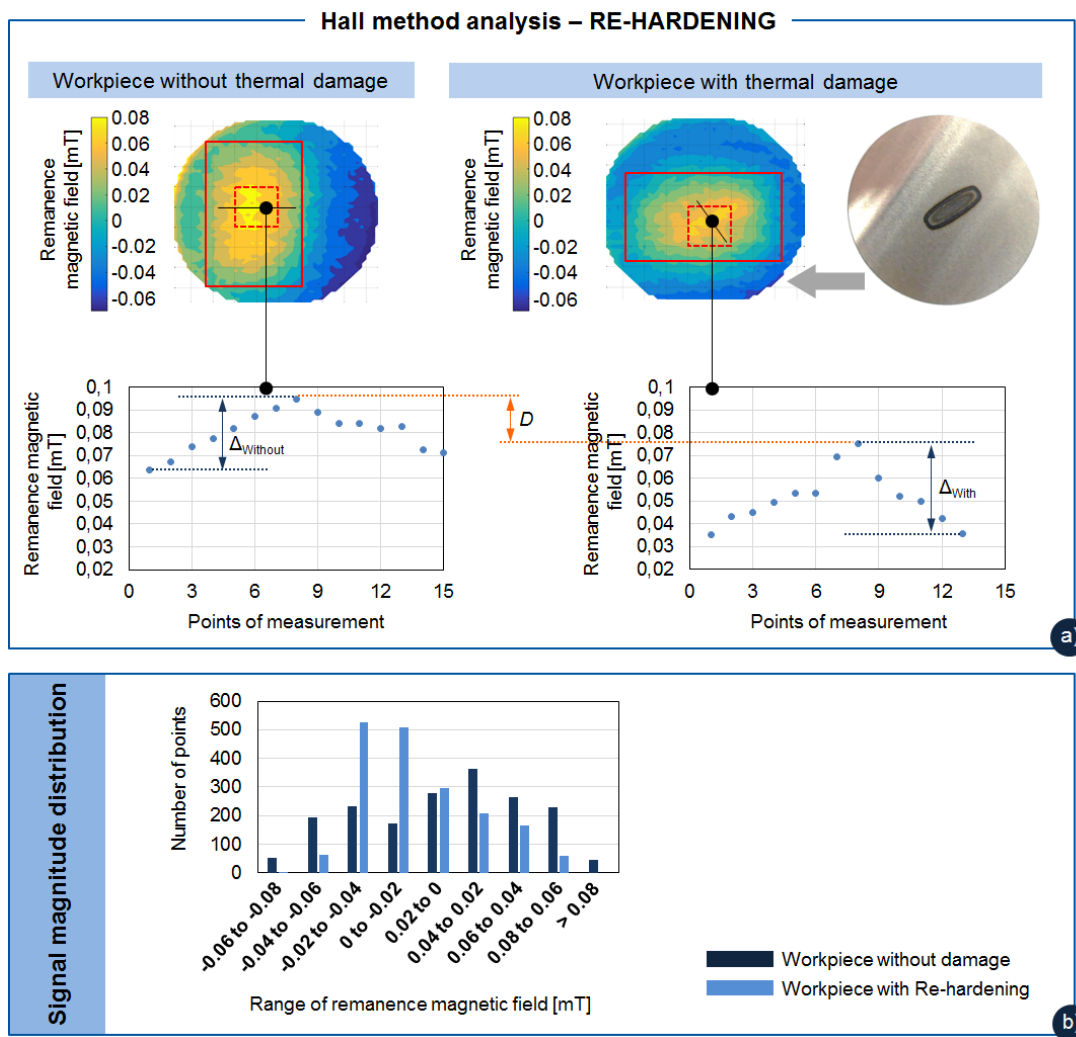
Figure 5.22 - Analysis of the remanence magnetic field signal measured by the scanning with new *Hall* method. a) Comparison between the workpieces with and without re-hardening at the surface, regarding the peak of the signal and gradient in the region of the thermal damage; b) analysis of the general signal distribution for the workpieces with and without re-hardening.

Figure 5.22 b) presents the graphic for the signal distribution analysis performed in the area limited by the red rectangle, in workpieces with and without damage. The distribution shows a decrease of the general signal inside the area, that might be attributed to the presence of the re-hardening.

A more localized investigation is performed in the region of the damage, delimited by the dashed red square shown in the images of Figure 5.22 a). The average signal inside this region decreases from 0.07 mT of the workpiece without damage, to 0.05 mT, of the workpiece with re-hardening. The standard deviation in the same area is also altered from 0.006 mT of the workpiece without damage to 0.01 mT for the workpiece with re-hardening. This alteration in the standard deviation is a strong indication of the presence of a different phase in the region, influencing the remanence magnetic field.

The graphics in the bottom of Figure 5.22 a) shows the profile of the remanence magnetism in the both workpieces. Comparison of the highest peak signal in both workpieces shows the decrease in the magnitude of approximately 20% (*D*) in the wokpiece with presence of thermal damage, which in this case means the presence of untempered martensite. These results are in accordance with the micro-magnetic theory, which establishes that the presence of a microstructure with higher hardness profile alters the hysteresis curve, making it flatter, as shown in the right of Figure 5.23 (GOLDMAN, 1999; ZHOU *et al*, 2014).
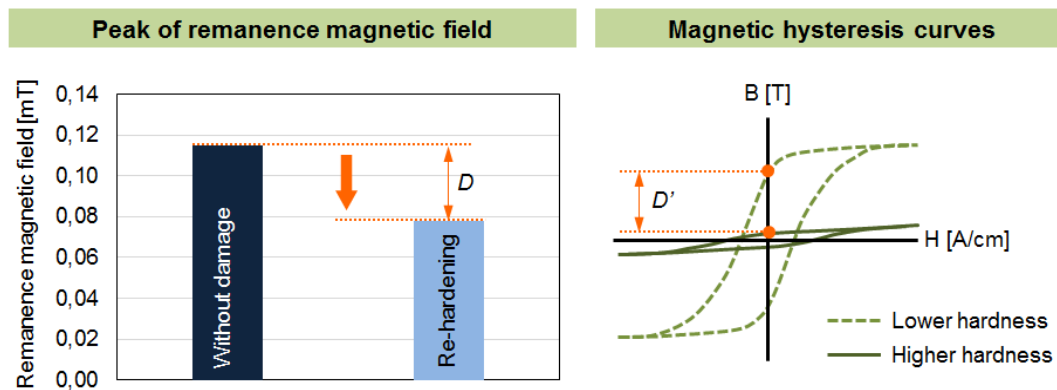
Figure 5.23 - Analysis of the signal measured by the *Hall* method for the workpieces with and without re-hardening, comparing it with the hysteresis curve of a ferromagnetic material (IKHMAYIES *et al*, 2017).

The effect of this alteration on the remanence magnetic field of the material is to reduce the potential of the material to retain the magnetic influence of an external field applied, showing a decrease described as D' in the curve of Figure 5.23. The alteration in the

magnetic signal is detected by the *Hall* method in the workpieces with the presence of re-hardening. This indicates the ability of the method to detect the presence of a phase transformation in the material, in this case from tempered to untampered martensite.

5.4 Integrity assessment of the surface for a thermal damage without phase transformation

5.4.1 Investigation and characterization of the thermal damage: Oxidation

The less severe degree of grinding burn, Oxidation, is investigated in this topic. This burn is characterized for not inducing phase transformation in the material. The only indication of damage is the soft change of color at the surface (MALKIN; GUO, 2008). The upper part of Figure 5.24 shows the indentation performed at the surface, through the thermal damage. As expected, no alteration is detected in the surface indentation tests. The hardness value is constant in all the points measured. This non-alteration in the results leads to the conclusion that no phase change occurs in the surface of the material.
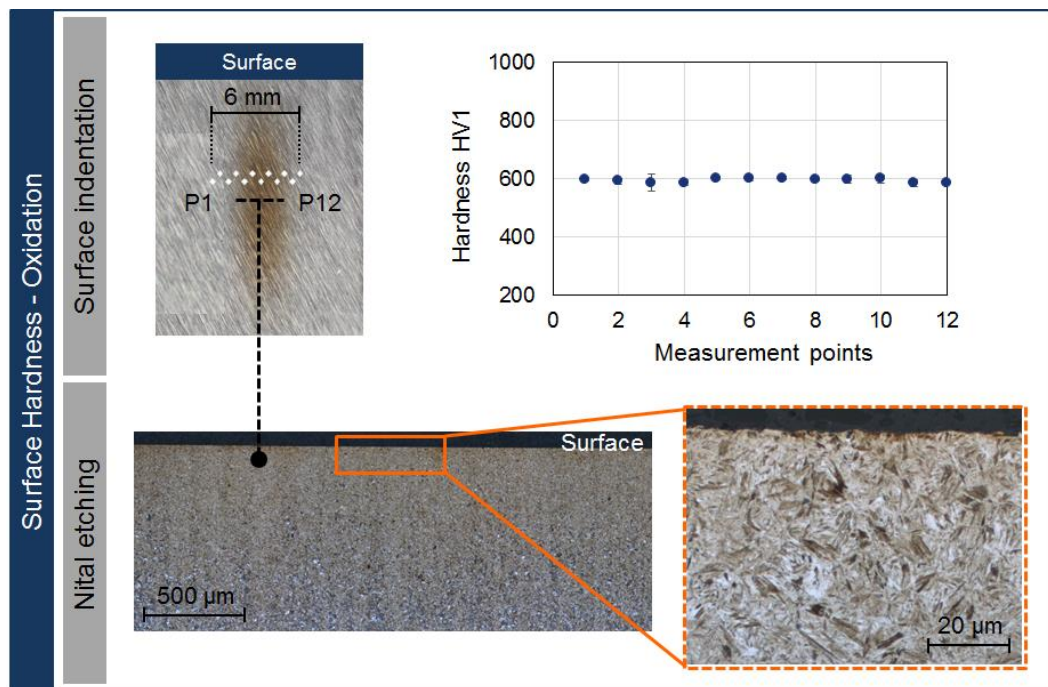
Figure 5.24 - Analysis of the oxidation degree of damage by means of surface indentation and nital etching over a workpiece section.

This conclusion is further confirmed with the analysis with nital etching shown in the bottom of Figure 5.24. The images of the nital etching show no color alteration in the area of the thermal damage, indicating no phase alteration in the material.

Although the laser input did not cause phase alteration in the material, as established by the indentation and nital etching analysis, the heat induced at the workpiece surface might cause alteration in the residual stresses state. Due to the thermal input given by the laser process, the presence of tensile residual stresses at the surface of the workpiece is expected, as also seen the work of Santa-aho (2012). The effect of the material expansion and contraction at the surface will contribute to the tensile profile of the final residual stresses detected. Due to the laser input, the middle area of the damage goes through a high increase of temperature, expanding, as shown in the arrows at the workpiece surface for the heating step, at the bottom of Figure 5.25. The surrounding material is also heated, but at a lower degree, and it will not expand in the same magnitude as the material in the center. As the workpiece cools down, the temperature on the material surrounding the center will decrease faster than the center itself. At the end of the cooling process, while the center is still cooling down, the surrounding is already at room temperature. This makes the center still contracts while the surrounding is already at the final shape. Therefore, the material surrounding the center region will hold the contraction movement of the center, inducing a load in the center in the opposite direction of contraction. At the end, this condition will lead to a tensile profile of residual stresses, as demonstrated in the bottom of Figure 5.25. This is an important factor, since the residual stress state also influences the electro-magnetic properties of the material, affecting the way domains align during magnetization (GAUNKAR, 2014). This influence can be detected in the measurements of MBN, shown in the upper part of Figure 5.25. According to Gaunkar (2014), the presence of compressive stresses tends to decrease the signal amplitude of MBN, whereas tensile residual stresses generate signals with high amplitude.

Figure 5.25 - Characterization of the oxidation degree of damage by means Magnetic *Barkhausen* noise and X-ray diffractometry. At the bottom, the description of the final tensile residual stresses development at the surface.
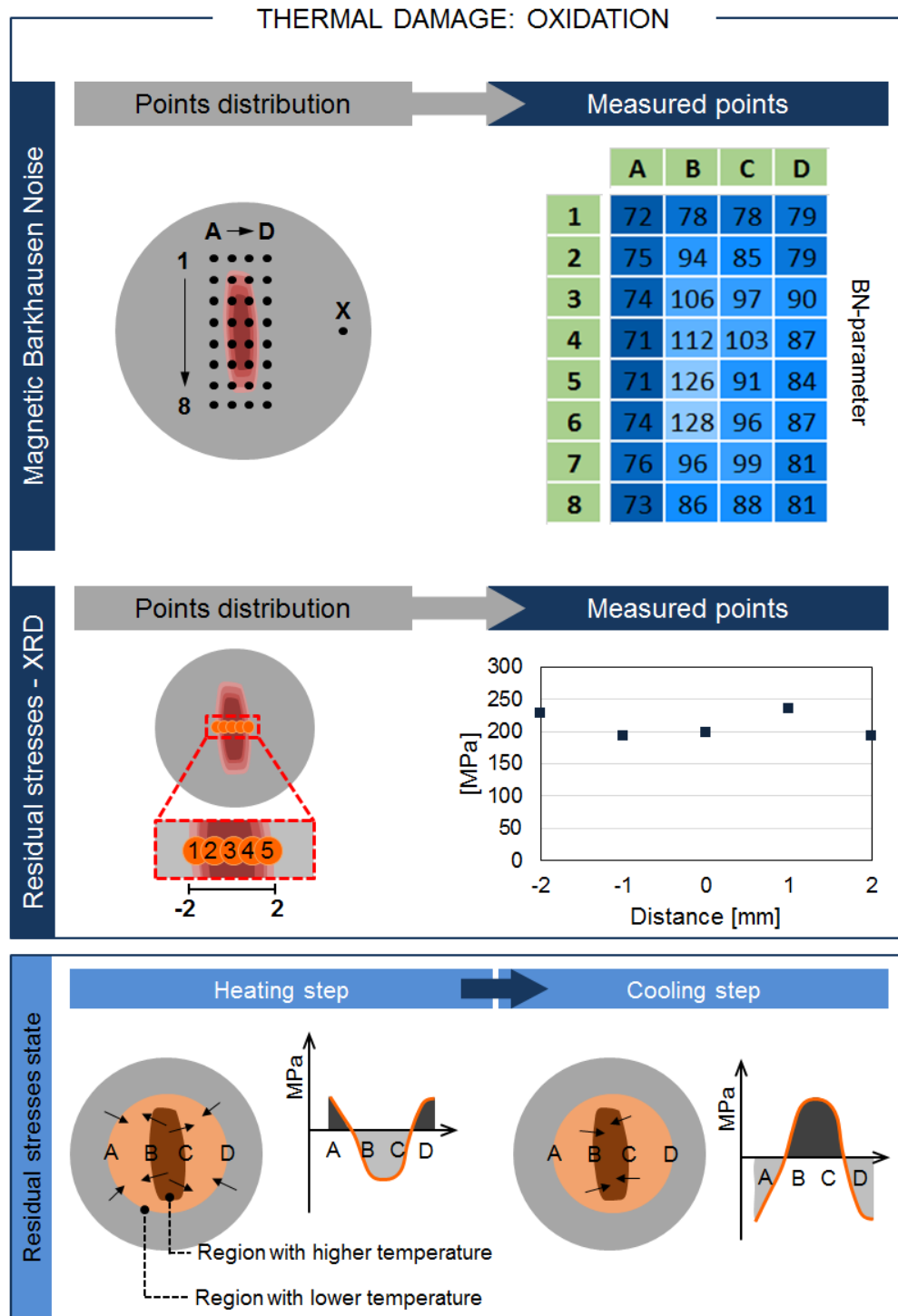
The upper part of Figure 5.25 shows the measurement results of one workpiece as well as the position of each measured point. One point at the surface, away from the thermal

damage, is chosen for a measurement with the MBN. In this point, shown in Figure 5.25 as the point X, the influence of the heat should be minimum, and the MBN signal is, in average, 50. The MBN signal amplitude obtained in the region thermally affected by the laser are higher than the signal measured in a region non-thermally affected. In this measured region, defined by four columns and eight lines, the external points present a lower signal amplitude in comparison to the points in the center. Nevertheless, the external points have lower values than the points in the center, the values are still higher than the measurements of a region non-thermally affected. This result shows that the heat input induced by the laser affects the entire region under analysis, modifying the residual stress state to a tensile profile.

The region in the center presents the highest values, which is expected since it is the area most affected by the laser, and, consequently, by the temperature. The measurements performed by the *Barkhausen* method are further confirmed with the results obtained with the XRD method, shown in the bottom part of Figure 5.25. The residual stresses measured in the region highlight a tensile state along the thermal damage. This result shows that this level of thermal damage achieved temperatures too low for phase alteration, but high enough to change the residual stress state at the workpiece surface.

5.4.2 Surface integrity assessment with the *Hall* method: Oxidation

This topic presents the analysis of the measurements with the *Hall* method of the workpiece with oxidation. Figure 5.26 introduces the results of the scanning for the workpiece before and after magnetization. According to Theiner (1997), when the material is under residual stresses, the hysteresis curve of the material undergoes alteration, depending on the stress profile. This phenomenon alters the signal magnitude of the remanence magnetic field of the material, and this alteration can be detected by the *Hall* probe. However, the measurement without magnetization of the workpiece does not show the expected signal alteration.
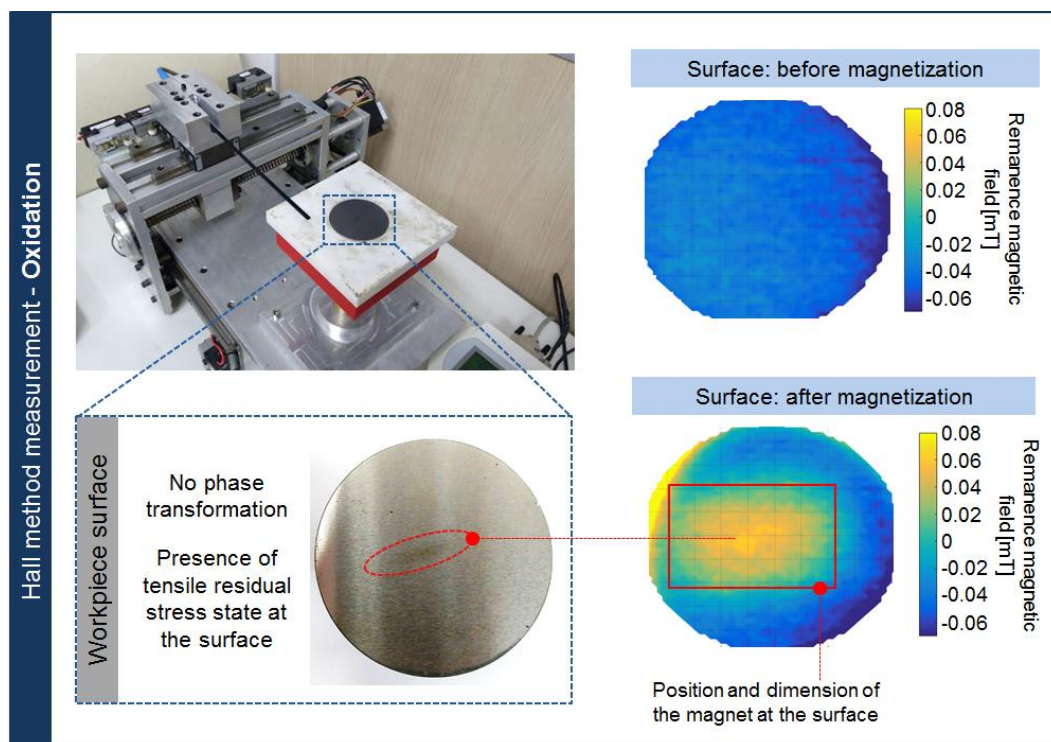
Figure 5.26 - Scanning of a surface with oxidation using the new *Hall* method. The measurements of the workpiece non-and magnetized are shown.

The natural remanence signal of the workpiece is not high enough to be out of the environmental noise influence. Therefore, the alteration in signal due the presence of oxidation thermal damage is covered up, making harder to distinguish the thermally affected area. For this reason, the workpiece is magnetized, with the same magnet, same magnetic field and same setup application used for the workpieces before. The magnetization increases the remanence signal of the workpiece, highlighting the region thermally affected. Even though the workpiece has been magnetized, the signal magnitude is still low. The result of the magnetization in the workpiece is shown in the bottom right of Figure 5.26.

Figure 5.27 shows a more detailed analysis of the signal magnitude detected in the thermal damage region. In the upper left of Figure 5.27, an image of a magnetized workpiece without thermal damage is shown, for comparison with the magnetized workpiece with thermal damage, shown in the upper right. The first analysis performed was the signal magnitude distribution, shown in the Figure 5.27 b). This analysis considered the signal inside the area determined by the red rectangle, which represents the area where the magnet was applied. The comparison between the distributions without and with thermal damage shows that the presence of oxidation generally decreases the remanence magnetic field. This

behavior can be attributed to the alteration in the residual stress state, already detected by the measurements of characterization. The region closer to the thermal damage, delimited by the red dashed square, is analyzed. The average of the signal in the region decreases from 0.076 mT of the workpiece without damage to 0.051 mT for the workpiece with oxidation. The standard deviation of the same region is very similar, indicating that the gradient in the signal caused by the damage is not very strong.
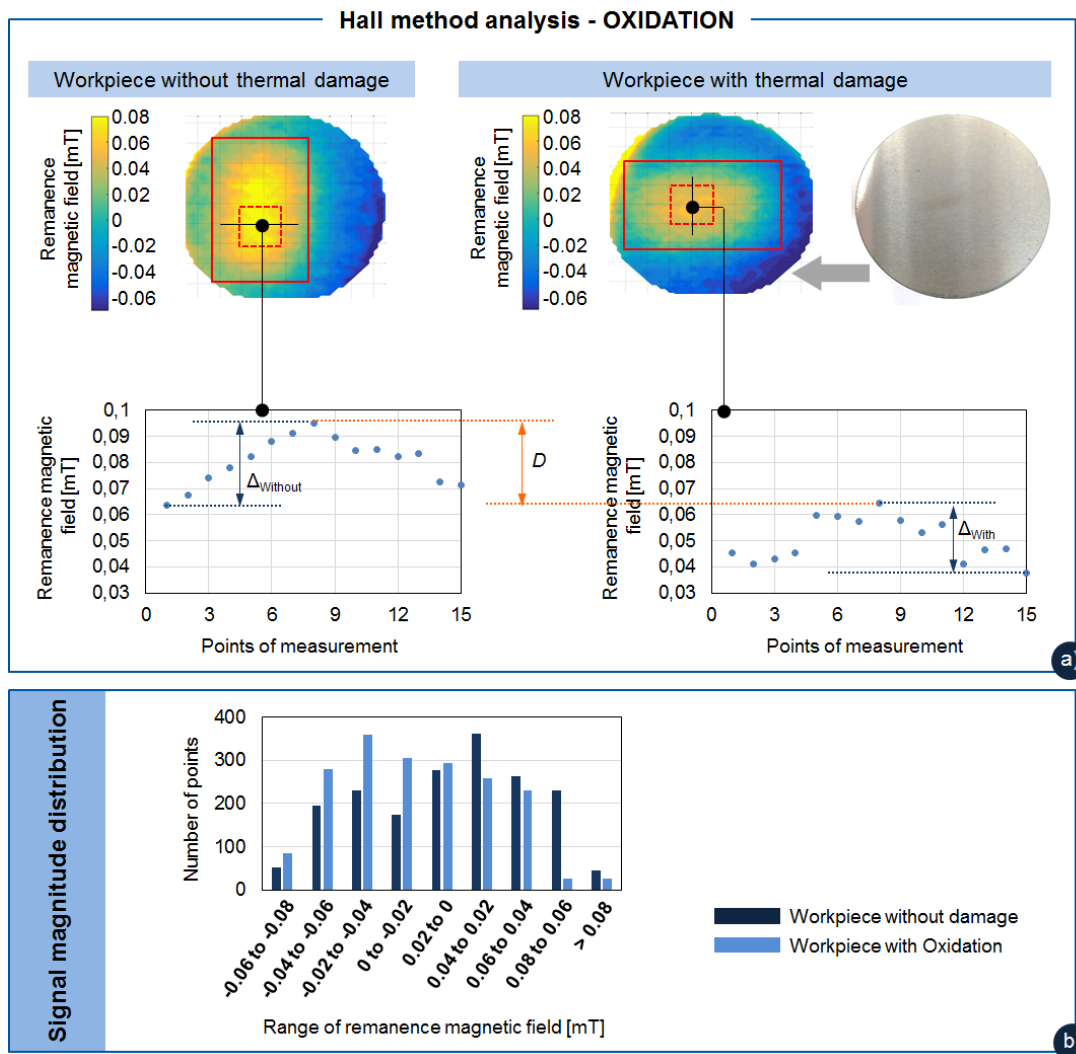
Figure 5.27 - Analysis of the remanence magnetic field signal measured by the scanning with new *Hall* method. a) Comparison between the workpieces with and without oxidation at the surface, regarding the peak of the signal and gradient in the region of the thermal damage; b) analysis of the general signal distribution for the workpieces with and without oxidation.

Further analyses are performed in the profile of magnetization through the damage, shown in the graphics of Figure 5.27 a). In the graphic, the peak magnitude of the signal in the

workpiece with thermal damage decreased, approximately 30% (*D*), in comparison to the workpiece without damage.

As already established in earlier analysis, the oxidation damage does not undergo any phase transformation. On the other hand, the damage generates a tensile residual stress state at the surface, which also can influence the magnetic profile induced in the workpiece. The presence of residual stress can influence the magnetic behavior of a material, especially regarding remanence magnetic field. Literature establishes that tensile residual stress alters the hysteresis curve of a material, narrowing it, as it is shown in the right side of Figure 5.28. Consequently, the remanence magnetic field in the surface is higher in comparison to a material under compressive residual stress, presenting a more flattened curve (THEINER, 1997; DEUSVAUX *et al*, 2014). This behavior, however, is not reproduced in the workpiece with oxidation damage. Instead of having its signal increased by the tensile residual stress profile induced by the oxidation, as expected, the signal decreases in comparison to the workpiece without damage. This shows the influence of residual stresses on the remanence magnetic field of a material.
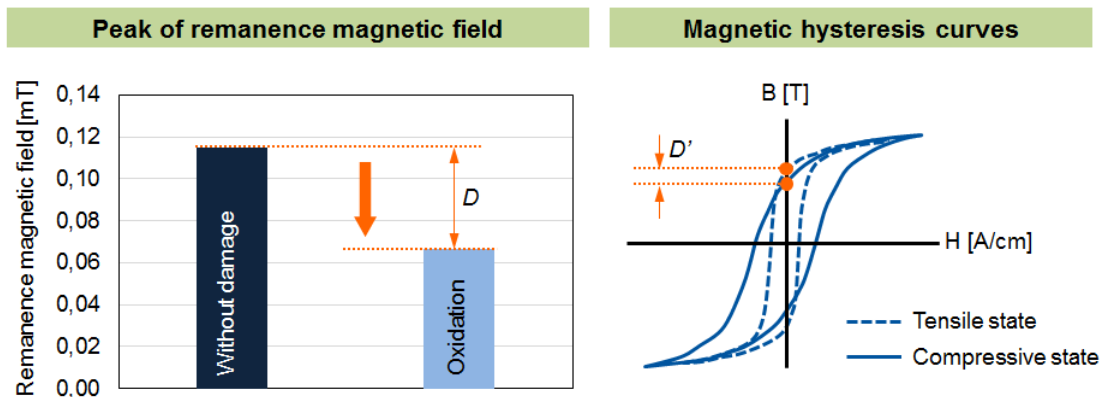
Figure 5.28 - Analysis of the signal measured by the *Hall* method for the workpieces with and without re-hardening, comparing it with the hysteresis curve of a ferromagnetic material (THEINER, 1997; IKHMAYIES *et al*, 2017).

This behavior of the magnitude signal can be explained by the interaction between the magnetization direction and the direction of atuation of compressive and tensile residual stresses characteristics. This phenomenon is better explained in the topic 3.3.2, in Chapter 3. In the case of the experiments with oxidation, a possible explanation for the behavior detected by the *Hall* method is that the direction of the magnetization applied was not in favor of the

direction of tensile residual stresses. Due to this, the remanecent magnetic field for this situation is smaller.

In Chapter of Objective, two research questions regarding the capability of the new method on detecting the presence of different degrees of grinding burn. One question focused on the response of the new method regarding a grinding burn with phase transformation. The second question investigates the same method for a grinding burn without the phase transformation, but with an alteration of the residual stress state.

The results from the investigation performed along this study show that the *Hall* method was able to detect the alteration in the magnetic flux of the workpiece. This alteration was induced by the presence of a new phase and/or a new state of residual. Due to this, the method was able to highlight the region affected by the thermal damage, correlating the magnetic signal detected by the sensor and the material properties induced by the damage.

6 Conclusions and suggestions for future developments

The current study proposed the investigation of the potential of a new method for thermal damage detection, generated in the grinding process of gears, by means of *Hall* effect. The method was evaluated regarding its robustness and ability to measure two types of thermal damages: with and without phase transformation (residual stress state alteration). The damages were first carefully examined by already established techniques, in order to characterize the material under investigation. The material characterization was vital for the understanding and, ultimately, correlation between thermal damage material features and the magnetic behavior detected by the *Hall* method proposed. From the results observed during the research, conclusions are established in this chapter. For a better organization of all the topics addressed in the study, the conclusions are grouped by the questions established in the Objective.

Thermal damage with phase transformation

The *Hall* method scanning of a surface with the thermal softening damage shows a region with higher magnetic signal than a workpiece without any thermal damage. The increase of signal is localized in the area where thermal damage was detected. This increase is coherent with the micro-magnetic theory: the presence of the soft layer of overtempered martensite induces a higher remanence magnetic field, which was detected by the *Hall* method. This result confirms the ability of the method to detect a phase alteration from tempered to overtempered martensite at the surface.

The *Hall* method scanning of a surface with the re-hardening damage reveals a region with a lower remanence magnetic signal than a workpiece without any thermal damage. The increase in the signal happens in the area where the damage was localized. The decrease of the signal is coherent with the micro-magnetic theory: it establishes that the presence of a hard layer of untempered martensite induces a lower remanence magnetic field, which was detected by the *Hall* method. This result also confirms the ability of the method to detect the phase alteration from tempered to untempered martensite at the surface.

The phase transformation is followed by the change in the residual stress state, mostly from a compressive to a tensile profile. However, the effect of the residual stress alteration on the remanence magnetic field is generally overcasted by the influence of the phase transformation, much more intense.

Thermal damage without phase transformation (residual stresses)

The workpiece with the oxidation damage presented no phase alteration but a tensile residual stress profile. MBN and XRD measurements showed the presence of tensile residual stress in an area greater than the visual thermal damage. A peak of tensile is detected in the center of the thermal damage, due the greater thermal input induced by laser in this region.

The scanning with *Hall* method shows a general decrease in the remanence magnetic field, not only in the region where visually the thermal damage is localized, but also in the surroundings. The relative constant profile of tensile residual stress in the thermally affected area makes the entire area respond similarly to the magnetic field applied, reducing the remanence magnetic signal.

The peak of the tensile residual stress in the center of the damage is not that high, and its effect on the magnetic remanence field is limited. Therefore, the damage is highlighted much subtler in this case. The result shows, however, the ability of the new method to detect the presence of an alteration in the residual stress state.

System Robustness

The analysis of positioning provided the degree of precision given by the equipment movimentation. The positioning deviation induced by the system is relative small in comparison to the nominal distance applied. Therefore, the movimentation does not jeopardize the scanning process, assuring its reliability during the measurements.

The repeatability of the system showed a variation of approximately 10% on the measurements. The value is considered low and ultimately does not affect the measurement quality, since the magnetic signal variation due thermal damage is expected to be higher than this. The reproducibility showed that, statistically, neither of the environmental factors analyzed contributed changing the signal

measured with the *Hall* method. Thus, their influence on the measurements is either irrelevant or constant through all measurements.

The natural magnetic signal of the workpieces is too low and the constant environment noise, present in all *Hall* measurements, covers the signal alteration possibly induced by the thermal damage. The magnetization increased the signal in the damaged region above the measurement noise, highlighting the effect of the thermal damage on the remanence magnetic field of the workpiece.

Thermal damage induction

The simulation of the three degrees of thermal damage: oxidation, thermal softening and re-hardening, was performed by means of laser process. The surfaces were analyzed by usual methods of grinding burn detection, and the results were in accordance to the literature. The laser process was able to consistently simulate the final surface state generated by a grinding burn, in its three degrees.

Further challenges and developments suggested

- Investigation of the method in terms of quantification of the signal measurement for the correlation between the material properties examined and magnetic remanence field in the material.
- Investigation of the thermal damage depth influence on the magnetic remanence signal measured by the *Hall* method at the surface. This is an important factor for the characterization of the thermal damage in gears.
- Further investigation regarding the *Hall* method behavior for other ferromagnetic materials and alloys.
- Study of the filtering of the signal measured by the Hall method, in order to eliminate noises and making the natural remanence magnetic field of the workpiece more evident.
- Study of an efficient protection chamber, isolating the workpiece from the environment. In addition, optimization of the scanning mechanism, in order to improve the scanning process in terms of speed and *Hall* probe movimentation.

The research showed, based on the results of a first stage of experiments, that the method prototype is robust enough for the performance of measurements with the *Hall* probe. It was shown that the system did not interfere in the measurements by changing its results. This conclusion answers the first question established in the Objective, regarding the system robustness. Further experiments regarding the method applicability showed that the technique was able to clearly evidence the presence of the three thermal damages degrees analyzed, due to the signal alteration induced either by phase transformation or by alteration in residual stress state. The magnitude of the signal detected was also different for each damage degree, showing the method capability of, not only detecting but also, distinguishing each of the damages. Based on these results, questions two and three, established in the Objective, are answered as well.

This study was a first investigation on the potential of the magnetic method for detection of grinding burn, using the *Hall* effect. The method proposed has unique characteristics not yet addressed in other studies, making this research a first step for the development of a technique that correlates the remanence magnetic field and material characteristics of thermal damages. However, direct comparasions between the new *Hall* method and other already established techniques are still too soon to be made. This is mainly due the prototype character of the device today, which presents a limitation in terms of time and measurement area. Other topics such as reliability, quantitative and destructive must be further investigate in future researches, as already suggested. Based on the results obtained, the main contribution of this research is the confirmation of the fundamental theories supporting the method functioning proposed. This confirmation is a great motivation for further developments of the technique, especially in the field of grinding burn detection in the gear segment. The new method appears as a good future alternative to the current methods used in this field, especially due to its possible quantitative and non-destructive character, very important characteristics for the gear industrial application.

References

AHMAD, M. Noise and Excitation Behavior of Gears. In Lecture for Gear and Transmission Technology, 2017, Aachen. 54p.

ALBAN, L.E. Failure of Gears. In ASM handbook Vol. 11. **Failure Analysis and Prevention.** United States of America: ASM International, 2002. 2909 p.

BALART, M.J.; BOUZINA, A.; EDWARDS, L.; FITZPATRICK, M.E. The Onset of Tensile Residual Stresses in Grinding of Hardened Steels. **Materials Science and Engineering A**, n. 367, p. 132-142, 2004.

BHADESHIA, H.K.D.H.; WITHERS, P.J. Overview Residual Stress Part 1 – Measurement Techniques. **Material Science and Technology**, n. 17, p. 355-365, 2001.

BLAOW, M.; EVANS, J.T.; SHAW, B.A. Magnetic Barkhausen Noise: The Influence of Microstructure and Deformation in Bending. **Acta Materialia**, n. 53, p. 279-287, 2005.

BOETTGER, J. **The Hall Effect Gaussmeter.** Manual of Pacific Scientific OECO, 2014.

BOZORTH, R.M.; GOLDMAN, J.E.; VAN VLECK, J.H.; ARROTT, A. et all. **Magnetic Properties of Metals and Alloys.** United States of America: American Society for Metals, 1959. 349 p.

BRAMFITT, B.L.; BENSCOTER, A.O. **Metallographer's Guide: Practice and Procedures for Irons and Steels.** United States of America: ASM International, 2002. 353 p.

BRECHER, C.; KLOCKE, F.; BRUMM, M.; HÜBNER, F. Local Simulation of the Specific Material Removal Rate for Generating Gear Grinding. In: International Gear Conference, X., 2014, Lyon Villeubanne. 2014.

BUGLIARELLO, N.; GEORGE, B.; GIESSEL, D.; McCURDY, D. et al. **Different Heat Treating Processes' as the Materials being Treated, Impart Particular Qualities in Your Gears. Allow Bodycote to Provide a Deeper Understanding of Your Options.** Gear Technology, July 2010.

CALLISTER, W.D.; RETHWISCH, D.G. **Materials Science and Engineering: An Introduction.** United States of America: John Wiley and Sons, Inc., 9th Edition, 2013. 992 p.

CEURTER, J.S.; SMITH, C.; OTT, R. **The Barkhausen Noise Inspection Method for Detection Grinding Damage in Gears.** Gear Technology, November/December 2002.

CHANG, A.M.; HALLEN, H.D.; HARRIOT, L.; HESS, H.F. et al. Scanning Hall Probe Microscopy. **Applied Physics Letters**, v. 61, n. 16, 1992.

CHEN, X.; ROWE, W.B.; McCORMACK, D.F. Analysis of the Transitional Temperature for Tensile Residual Stress in Grinding. **Journal of Materials Processing Technology**, n. 107, p. 216-221, 2000.

COMLEY, P. **Grinding Processes and their Effects on Surface Integrity**. 2005. 167 p. Thesis (School of Industrial & Manufacturing Science) – Cranfield University, Cranfield.

CULLITY, B.D. **Elements of X-Ray Diffraction.** United States of America: Addison-Wesley Publishing Company, Inc., 1956. 514 p.

DAVIS, J.R. **Gear Materials, Properties, and Manufacture.** United States of America: ASM International, 2005. 347 p.

DESVAUX, S.; DUQUENNOY, M.; GUALANDRI, J.; OURAK, M. The Evaluation of Surface Residual Stress in Aeronautic Bearings Using the Barkhausen Noise Effect. **Nondestructive Testing and Evaluation International**, n. 37, p. 9-17, 2004.

DOBMANN, G. **Non-Destructive Testing for Ageing Management of Nuclear Power Components – Control, Reliability and Human Factors**. InTech Europe, 2011. Available in: < http://www.intechopen.com/books/nuclear-power-control-reliability-and-humanfactors/ non-destructive-testing-for-ageing-management-of-nuclear-power-components>. Access in: 29.03.2017.

ERRICHELLO, R. **Measuring Residual Stress in Gears.** Gear Technology, March/April 2015.

GAO, L.; ZHOU, Y.M.; LIU, J.L.; SHEN, X.D.; REN, Z.M. Effect of Water Quenching Process on the Microstructure and Magnetic Property of Cold Rolled Dual Phase Steel. **Journal of Magnetism and Magnetic Materials**, n. 322, p. 929-933, 2010.

GAUNKAR, N.P**. Magnetic Hysteresis and Barkhausen Noise Emission Analysis of Magnetic Materials and Composites**. 2014. 68 p. Dissertation (Master Electrical and Computer Engineering) – Iowa State University, Ames

GOLDMAN, A. **Handbook of Modern Ferromagnetic Materials.** New York: Springer Science+Business Media, LLC, 1999. 646 p.

GORGELS, C.; SCHLATTMEIER, H.; KLOCKE, F. Optimization of the Gear Profile Grinding Process Utilizing an Analogy Process. **Gear Technology**, November / December 2006, p. 34 – 41.

HASHMI, M.S.J. **Comprehensive Materials Finishing – Volume 1: Finish Machining and Net-Shape Forming.** Canada: Elsevier, 2017. 414 p.

HORNBACH, D.J.; PREVÉY, P.S.; MASON, P.W. X-Ray Diffraction Characterization of the Residual Stress and Hardness Distributions in Induction Hardened Gears. In: First International Conference on Induction Hardened Gears and Critical Components, X., 1995, Indianapolis. p. 69-76.

HÜBSCHEN, G.; ALTPETER, I.; TSCHUNCKY, R.; HERRMANN, H-G. **Materials Characterization Using Nondestructive Evaluation (NDE) Methods.** United Kingdom: Woodhead Publishing, 2016. 304 p.

IKHMAYIES, S.; LI, B.; CARPENTER, J.S.; LI, J.; HWANG, J-Y. et al. **Characterization of Minerals, Metals, and Materials 2017.** United States of America: Springer International Publishing AG, 2017. 870 p.

KAMPKA, M. Manufacturing II – Fine Finishing. In Lecture for Gear and Transmission Technology, 2017, Aachen. 72p.

KARIMIAN, N.; WILSON, J.W.; PEYTON, A.J.; YIN, W.; LIU, J. et al. Differential Permeability Behavior of P9 and T22 Power Station Steels. **Journal of Magnetism and Magnetic Materials**, n. 352, p. 81-90, 2014.

KARPUSCHEWSKI, B.; BLEICHER, O.; BEUTNER, M. Surface Integrity Inspection on Gears using Barkhausen Noise Analysis. **1st CIRP Conference on Surface Integrity (CSI)**, Procedia Engineering, n. 19, p. 162-171, 2011.

KARPUSCHEWSKI, B.; KNOCHE, H.-J.; HIPKE, M. Gear Finishing by Abrasive Processes. **CIRP Annals – Manufacturing Technology**, n. 57, p. 621-640, 2008.

KAUFMANN, J.G.; CROSBY, S.R.; SIKORSKY, P.J.; SIZEK, H.W. **Electrical and Magnetic Properties of Metals.** United States of America: ASM International, 2000. 285 p.

KLOCKE, F.; SCHLATTMEIER, H. **Surface Damage Caused by Gear Profile Grinding and Its Effects on Flank Load Carrying Capacity.** Gear Technology, September/October 2004.

KLOCKE, F. **Manufacturing Processes 2: Grinding, Honing and Lapping.** Berlin: Springer, RWTHedition, 2009. 433 p.

KONOWALCZYK, P. Tooth Damages on Gears – Mechanisms and Characteristics. In Lecture for Gear and Transmission Technology, 2017, Aachen. 56p.

LIAO, Y.S.; LUO, S.Y.; YANG, T.H. A Thermal Model of the Wet Grinding Process. **Journal of Material Processing Technology**, v. 101, p. 137-145, 2000.

MAIA, A.H**. Impacts on the Surface Integrity of Titanium Milling with Minimum Quantity Lubrication and Flood of Coolant**. 2015. 120 p. Dissertation (Master Aeronautics and Mechanical Engineering) - Instituto Tecnológico de Aeronáutica, São José dos Campos.

MALKIN, S.; GUO, C. Thermal Analysis of Grinding. **CIRP Annals**, v. 56, n 2, p. 760-782, 2017.

MALKIN, S.; GUO, C. **Grinding Technology: Theory and Application of Machining with Abrasives.** Ney York: Industrial Press Inc., Second Edition, 2008. 368 p.

MAYER, J.E.; PRICE, A.H.; PURUSHOTHAMAN, G.K.; DHAYALAN, A.K. Specific Grinding Energy Causing Thermal Damage in Helicopter Gear Steel. **Journal of Manufacturing Process**, v. 4, p. 142-147, 2002.

MAZZO, N. **Engrenagens Cilíndricas – Da Concepção à Fabricação.** São Paulo: Blucher, 2013. 807 p.

MONTGOMERY, D.C. **Design and Analysis of Experiments.** Fifth Edition, United States of America: John Willey & Sons, INC, 2001. 684 p.

NESLUSAN, M.; CIZEK, J.; KOLARIK, K.; MINARIK, P. et al. Monitoring of Grinding Burn via Barkhausen Noise Emission in Case-Hardened Steel in Large-Bearing Production. **Journal of Material Processing Technology**, v. 240, p. 104-117, 2017.

NISHIZAWA, T. **Thermodynamics of Microstructures.** ASM International, The Materials Information Society, 2008. 289 p.

OPOKU, K.S**. Determining the Onset of Grinding Burn Using Magnetic Barkhausen Noise**. 2005. 110 p. Dissertation (Master Innovative Manufacturing – Advanced Automation and Design) – Cranfield School of Industrial and Manufacturing Science, Cranfield.

POPOVIC, R.S. **Hall Effect Devices: Magnetic Sensors and Characterization of Semiconductors.** London: Adam Hilger Imprint by IOP Publishing Ltd, 1991. 313 p.

POPOVIC, R.S. **Hall Effect Devices.** Second Edition, London: Institute of Physics Publishing, 2004. 426 p.

QIAO, J.; WU, Z.; WANG, T.; YAN, T. Effects of Surface Integrity on Gear Performance. In: International Conference on Power Transmissions, 2016, Chongqing, China. **Proceedings...** Chongqing, 2017. p. 353-357.

RABUNG, M.; ALTPETER, G.; DOBMANN, G.; SZIELASKO, K. Micro-Magnetic Evaluation of Micro-Residual Stresses of the IInd and IIIrd Orders. **Welding in the World**, n. 88, v. 56, p. 29-34, 2012.

RAKHIT, A.K. **Heat Treatment of Gears: A Practical Guide for Engineers.** United States of America: ASM International, 2000. 208 p.

RAMSDEN, E. **Hall-Effect Sensors: Theory and Applications.** United States of America: Elsevier Inc., 2006. 296 p.

REGO, R.R.; KLOCKE, F.; GOMES, J.O.; LÖPENHAUS, C. Assessing the Heterogeneity of Residual Stress for Complementing the Fatigue Performance Comprehension. **Journal of Strain Analysis for Engineering Design**, v. 51 (5), p. 347-357, 2016.

REGO, R.R**. Residual Stress Interaction In-Between Processes of the Gear Manufacturing Chain**. 2016. 194 p. Thesis (Doctor Aeronautics and Mechanical Engineering) - Instituto Tecnológico de Aeronáutica, São José dos Campos.

ROWE, W.B. **Principles of Modern Grinding Technology.** United States of America: Elsevier Inc., Second Edition, 2014. 437 p.

SANTA-AHO, S.; VIPPOLA, M.; SORSA, A.; LINDGREEN, M. et al. Optimized laser processing of calibration blocks for grinding burn detection wit hBarkhausen noise. **Journal of Materials and Processing Technology**, n. 212, p. 2282-2293, 2012.

SANTA-AHO, S.; VIPPOLA, M.; SORSA, A.; LINDGREEN, M. et al. Development of Barkhausen Noise Calibration Blocks for Reliable Grinding Burn Detection. **Journal of Materials and Processing Technology**, n. 212, p. 408-416, 2012.

SANTOS, C.Z**. Estudo da Tensão Residual Através de Difração de Raios X em Aço inoxidável Duplex Submetido a Diferentes Tratamentos Térmicos**. 2012. 93 p. Dissertation (Master Mechanical Engineering) – Universidade Federal do Espírito Santo, Vitória.

SHAH, S.M.A. **Prediction of Residual Stresses Due to Grinding with Phase Transformation**. 2012. 202 p. Thesis (Mecanique – Genie Mecanique) – Institut National des Sciences Appliquees de Lyon, Lyon.

SHIMIZU, M.; SAITOH, E.; MIYAJIMA, H.; MASUDA, H. Scanning Hall Probe Microscopy with High Resolution of Magnetic Field Image. **Journal of Magnetism and Magnetic Materials**, n. 282, p. 369-372, 2004.

SOSA, A.D.; ECHEVERRIA, M.D.; MONCADA, O.J.; SIKORA, J.A. Residual stresses, distortion and surface roughness produced by grinding thin wall ductile iron plates. **International Journal of Machine Tools & Manufacture**, n. 47, p. 229-235, 2007.

SUNDARRAJAN, K.D. **Study of Grinding Burn Using Design of Experiments Approach and Advanced Kaizen Methodology**. 2012. 65 p. Thesis (Doctor Manufacturing systems engineering) – University of Nebraska, Nebraska.

TAGLIARI, M.R**. Utilização de Técnicas Eletromagnéticas para Detecção de Danos Térmicos em Aço 300M Empregado em Trens de Pouso**. 2012. 75 p. Dissertation (Master Engenharia de Minas, Metalúrgica e de Materiais) – Universidade Federal do Rio Grande do Sul, Porto Alegre.

THEINER, W. A. **Structural and Residual Stress Analysis by Nondestructive Methods.** United States of America: Elsevier Science, 1997. 655 p.

TOTTEN, G.; HOWES, M.; INOUE, T. **Handbook of Residual Stress and Deformation of Steel.** United States of America: ASM International, 2002. 499 p.

WOJTAS, A.S.; SUOMINEN, B.A.; SHAW, B.A. Detection of Thermal Damage in Steel Components After Grinding Using the Magnetic Barkhausen Noise Method. In: 7th European Conference on Non-Destructive Testing, 3, 1998, Copenhagen. **Proceedings ECNDT '98**, 1998.

YIN, W.; PEYTON, A.J.; STRANGWOOD, M. Exploring the Relationship Between Ferrite Fraction and Morphology and the Electromagnetic Properties of Steel. **Journal of Material Science**, n. 322, p. 929-933, 2007.
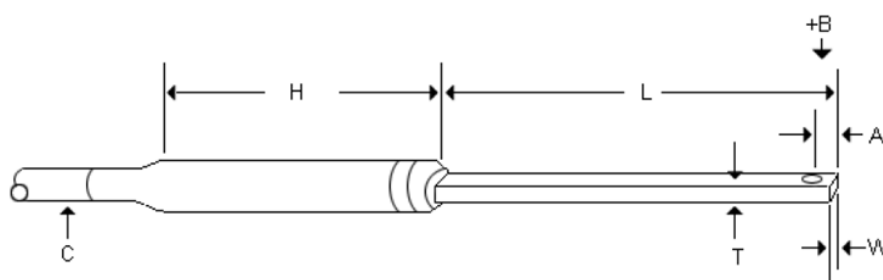
ZHOU, L.; LIU, J.; HAO, X.J.; STRANGWOOD, M.; PEYTON, A.J. et al. Quantification of the Phase Fraction in Steel Using an Electromagnetic Sensor. **Nondestructive Testing and Evaluation International**, n. 67, p. 31-35, 2014.

7 Attachments

Equipment data

Transverse Hall probe model HS-TGB5-104020 from Magnet-Physik

Transverse probes for FH 54 and FH 55

Model	HS-TGB5-104005	HS-TGB5-104010	HS-TGB5-104020
W	4.0 mm max.	4.0 mm max.	4.0 mm max.
T (max.)	1.0 mm	1.0 mm	1.0 mm
L (nom.)	55 mm	100 mm	200 mm
A	2 mm ± 0.1 mm	2 mm ± 0.1 mm	2 mm ± 0.1 mm
H (nom.)	70 mm	70 mm	70 mm
Cable length C	1.5 m	1.5 m	1.5 m
Stem material		Fiberglas epoxy	
Active area, nominal diameter	0.4 mm	0.4 mm	0.4 mm
Ranges, full scale		3 mT to 3 T	
Corrected accuracy [% of Reading, DC]	0.25 % to 3 T	0.25 % to 3 T	0.25 % to 3 T
Temperature coefficient of sensitivity (maximum)	± 0.02 %/°C (T)	± 0.02 %/°C (T)	± 0.02 %/°C (T)

(T): Probe with sensor for temperature correction.
Operating temperature range 0 °C to 75 °C.

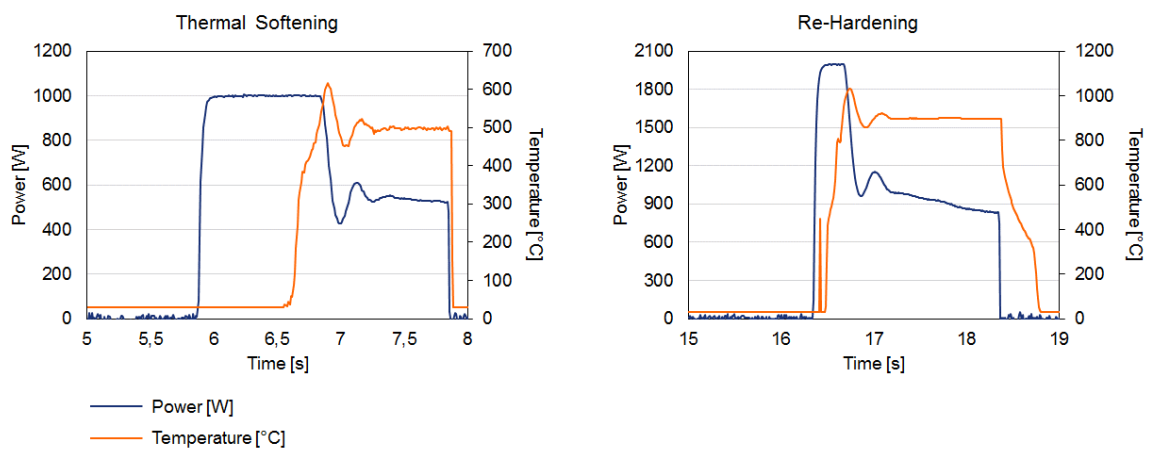Gaussmeter model FH 54 from Magnet-Physik

FH 54

- **Features**

Model	FH 54
Auto zero	✔
Auto range	✔
Relative-measurement	✔
Filter	✔
Battery status indicator	✔
Max/Min hold	Max, Min
Limit	2, ± or absolute
Peak hold	✔
Probe temperature correction	✔
Probe temperature display	✔
Probe linearity correction	✔
Analog output	✔
Computer interface	✔

- **Technical Data:**

Model	FH 54		
Display	3¾ digit (0...±2999)		
Units	Tesla, Gauss, Ampere/Meter		
Ranges	30 µT*	300 mG*	24 A/m*
	300 µT*	3 G*	240 A/m*
	3 mT	30 G	2.4 kA/m
	30 mT	300 G	24 kA/m
	300 mT	3 kG	240 kA/m
	3 T	30 kG	2.4 MA/m
	30 T*	300 kG*	24 MA/m*
	*special probes required		
Resolution (in most sensitive range)	depending on probe type		
Basic accuracy	DC: ±0.3 % (without probe) AC: ± 2%		
Frequency range	DC (with polarity display) AC approx. 20 Hz - 20 kHz (true rms)		
Peak Hold	> 150 µs		
Analog output	± 3 V, BNC connector		
Interface	RS 232, DB-9 connector		
Temperature range - Operation - Storage	+10 °C to +40 °C -40 °C to +60 °C		
Power source - Operating time	Batteries, 5 x 1.5 V size AA depending on probe type		
Accessories/Options: - Hall probes	Multiple, see probe data sheet		
- Probe connection cable - Zero field chamber - Hard case - AC adapter	Fixed to probes, different lengths available standard with meter standard with meter optional, with Euro- or US-connector recommended for continuous operation		
- Relay output for limit	optional, 2 c-form relays		
Outer dimensions	266 mm x 90 / 144 mm x 60 mm		
Weight	approx. 0.5 kg		

Power control during laser processing

Thermal Softening

Re-Hardening

FOLHA DE REGISTRO DO DOCUMENTO

[11.] RESUMO:

Gears are a key component of a transmission system, and have been widely employed in motion transmission systems. During operation, they face heavy loads conditions, low noise and long-life requirements. These functional characteristics are highly affected by the surface integrity, generated after the finishing process. In most gears manufacturing chain, finishing is performed by the process of grinding. However, the process abrasive characteristic induces an increase of temperature in the working zone, which, under non-controllable conditions, might lead to grinding burn. Grinding burn is a damage generated by high temperatures, which induces surface properties deterioration. Based on the temperature reached in the process, the damage is more or less severe, but, ultimately, it will affect the material surface integrity. Methods for grinding burn detection have been used in the industry, such as nital etching and *Barkhausen* noise. However, these methods present significant disadvantages that, at a certain extent, make them non-reliable for industrial application. Due to this technical gap, a method of magnetic surface scanning by means of Hall effect and without the use of magnetization, is proposed. For the analysis of the new method, a prototype was built. On a first phase, the influence of the prototype on the measurements is investigated, regarding the equipment positioning precision, Hall probe contact profile and environmental factors. Next, the ability of the new method to detect grinding burn is evaluated. Three degrees of thermal damage are simulated by laser process, including damages with and without phase alteration. The results for positioning precision showed that the equipment does not impact negatively on the scanning process. The Hall method scanning of damages with phase transformation shows an alteration in the remanence magnetic signal in the workpiece due to the presence of the new microstructure phases. This signal alteration highlights the position of the damage, indicating its presence in the workpiece surface; in addition, the alteration detected by the probe is in accordance with the micro-magnetic theory, which establishes a correlation between the remanence magnetic field and material hardness. The damage without phase transformation presents a change in the residual stress state, from compressive to tensile. In this case, the direction of magnetic signal alteration is not in accordance with the micro-magnetic theory, which is partially explained for the magnetization direction in favor of compressive residual stresses direction. In the end, the results show that the method is able to highlight the presence of an alteration in the residual stress state.

[12.] GRAU DE SIGILO:

(X) OSTENSIVO   ( ) RESERVADO   ( ) SECRETO